DEPARTMENT OF OCEAN ENGINEERING
MASSACHUSETTS INSTITUTE OF TECHNOLOGY
CAMBRIDGE, MASSACHUSETTS 02139

INVESTIGATION OF THE STRESS CORROSION CRACKING SUSCEPTIBILITY OF ANNEALED AND HEAT TREATED ALLOY 625 CASTINGS AND FORGINGS IN SEA WATER

by

ERIC MERWIN JONES

OCEAN ENGINEERING - COURSE XIIIA

MATERIALS SCIENCE AND ENGINEERING - COURSE III

Copy of

JUNE, 1987

INVESTIGATION OF THE STRESS CORROSION CRACKING SUSCEPTIBILITY OF ANNEALED AND HEAT TREATED ALLOY 625 CASTINGS AND FORGINGS IN SEA WATER

by

ERIC MERWIN JONES

Submitted to the Department of Ocean Engineering
on May 8, 1987 in partial fulfillment of the
requirements for Degrees of Ocean Engineer
and Master of Science in Materials Engineering

ABSTRACT

Alloy 625, the nickel based superalloy commonly called Inconel* 625, was investigated for its susceptibility to stress corrosion cracking in sea water using the slow strain rate tensile test method. Four microstructures of the alloy commonly found in end products were investigated. Bimetallic couplings with other metals were simulated with a potentiostat at plus and minus one volt with respect to a saturated standard calomel electrode (SCE). Baseline tests were conducted in air and sea water without applied potential. The response of the alloy to cathodic protection of minus three volts SCE was also investigated on the two most commonly used microstructures, "as cast" and "forged/annealed". The different microstructures developed were characterized with a scanning electron microscope (SEM). The gage lengths, fracture surfaces, and sections of test specimens were also examined with a SEM. The data from the slow strain rate tensile tests were compared with data from standard tensile tests performed on the same processed material.

The results from this investigation indicate that Alloy 625 is not susceptible to stress corrosion cracking in the normal sea water service environment where temperatures are close to ambient. However, the results indicated that Alloy 625 is susceptible to the hydrogen embrittlement form of stress corrosion cracking when subjected to potentials that produce hydrogen evolution. This embrittlement leads to intergranular cracking.

Thesis Supervisor: Dr. Regis M. Pelloux

Title: Professor of Materials Science and Engineering

* INCONEL is a registered trademark of Huntington Alloys

INVESTIGATION OF THE STRESS CORROSION CRACKING SUSCEPTIBILITY OF ANNEALED AND HEAT TREATED ALLOY 625 CASTINGS AND FORGINGS IN SEA WATER

by

ERIC MERWIN JONES

A.A. Pensacola Junior College (1974)
B.S. Mech. Eng., University of New Haven (1983)

SUBMITTED TO THE DEPARTMENT OF OCEAN ENGINEERING
IN PARTIAL FULFILLMENT OF THE REQUIREMENTS
FOR THE DEGREES OF

N00228-85-G-3262

NAVAL ENGINEER
and
MASTER OF SCIENCE IN MATERIALS ENGINEERING

at the
MASSACHUSETTS INSTITUTE OF TECHNOLOGY
June, 1987

Signature of author.....
Department of Ocean Engineering
May 8, 1987

Certified by.....R.M. Pelloux.....
Professor Regis M. Pelloux
Thesis Supervisor

Certified by.....
Professor Koichi Masubuchi
Thesis Reader

Accepted by.....A. Douglas Carmichael.....
Professor A. Douglas Carmichael, Chairman
Department Graduate Committee
Department of Ocean Engineering

Accepted by.....Samuel M. Allen.....
Professor Samuel M. Allen, Chairman
Department Committee on Graduate Students
Department of Materials Science and Engineering

ACKNOWLEDGEMENTS

Professor Pelloux's wisdom and expertise inspired me to study this intriguing field. I am grateful to him for helping me understand many of the complexities of material behavior, for sharing his perceptions, and for his thoughtful guidance throughout my studies.

This research program and all of my training in the forging field were direct results of the energy, interest, and personal encouragement of Mr. Wilford (Red) Couts, Senior Scientist for the Wyman Gordon forging company. His generous help and friendship have been of unmeasurable and unforgettable value.

Wyman Gordon Company has my gratitude for supplying the assets, material, manpower, and funds necessary to complete this study. Many staff members of the Research and Development department contributed a significant amount of their time toward this project.

I thank Mr. Steve Reichman, Director of Research and Development for Wyman Gordon Company for the opportunity to work within his department. Without his support this paper would have been much more limited in scope.

TABLE OF CONTENTS

LIST OF FIGURES

PAGE

LIST OF TABLES

1. INTRODUCTION

Alloy 625 is one of the high temperature superalloys developed for use in gas turbines and other similar service environments. It has good yield and tensile strengths up into the 1300°F range[1]. The alloy has an extensive elongation property that makes it extremely useful for designs that develop stress concentrations and for designs that need considerable cold working. It is both solution and precipitation hardenable, producing a wide range of mechanical properties. With large grains the alloy has good rupture strength and creep resistance, as long as the grain size is small compared to the section thickness[2]. Small grains, readily made through hot mechanical working, give the alloy high strength.

Alloy 625 has good weldability to itself and to other metals. This means it can also be used as a cladding material over an inexpensive material such as steel. The processes it can be welded with include shielded metal arc (SMA), gas tungsten arc (GTA), and gas metal arc (GMA)[1]. The alloy also bonds well with brazing and soldering giving the designer a wide choice of fabrication methods.

Due to its high corrosion resistance it is now being used for salt water applications. Tapping[3] stated that Alloy 625 is virtually immune to attack in sea water. However, the service environment in a shipboard system will not always be simply "pure" sea water.

2. MOTIVATION AND OBJECTIVES OF RESEARCH

Alloy 625 offers near the weight savings and corrosion resistance of titanium without giving the associated welding problems. This kind of material is needed in shipbuilding to enable designing higher density power plants and increasing payloads.

Slow strain rate testing conducted on Alloy 625 in deep sour gas well environments has shown susceptibility to hydrogen induced stress corrosion cracking. This environment includes hydrogen sulfide gas, carbon dioxide, and up to 20 percent sodium chloride (NaCl). Sea Water contains 3.5 percent NaCl and there are many sources of hydrogen in ship board sea water systems, such as a byproduct of oxygen generation.

In consideration of the high corrosion resistance reported for Alloy 625 there must be a critical level of chlorides and/or hydrogen that cause harmful damage, a point where the alloy is susceptible to their effects. Is this point ever reached in the aqueous environment in a shipboard sea water system, or is this point outside the realm of probability? Is this point fixed for all the possible microstructures of Alloy 625?

The objectives of the research effort are:

a. Determine which microstructures of Alloy 625 are commonly used in service.

b. Find out how these microstructures are produced, including the melting, remelting, mechanical working, and thermal processing.

c. Obtain or produce representative samples of these microstructures.

d. Conduct slow strain rate tests on these samples in a sea water environment under both anodic and cathodic conditions.

e. Evaluate the fractured specimens with optical and scanning electron microscopes.

f. Determine the effects on Alloy 625 from the conditions tested under.

3. BACKGROUND

Stress corrosion cracking is the failure of a material due to an environmental element(s) that only occurs when a critical tensile stress field is present. The stress may have to be in the yielding range such as found at a notch tip or weld zone. Weldment cracking can occur even without externally applied loads[4]. It is common to divide these failures into two separate divisions. When the local conditions are anodic and metal dissolution is occurring, the effect is normally termed "stress corrosion cracking". When the material is in a cathodic state and hydrogen is available for absorption, the failure is classified and "hydrogen embrittlement". One area of a component can have both anodic and cathodic regions at the same time, but the failure or cracking may be caused by only one of the reactions.

3.1 ANODIC STRESS CORROSION CRACKING

Anodic stress corrosion cracking is the failure of a material through cracks caused by a corrosive medium where the general surface may virtually be unattacked. The cracks produced from anodic metal dissolution, also called active path corrosion, can be intergranular or transgranular, particularly in nickel based alloys[5]. They may propagate through the material by different mechanisms, such as: metal dissolution along a susceptible path with the metal ions going into solution, or formation of a film that

subsequently must be broken to progress the corrosion and the crack.

3.2 HYDROGEN CRACKING

Hydrogen cracking, hydrogen embrittlement, or hydrogen induced stress corrosion cracking are all names for the same effect. Many different theories have been developed to explain the mechanism that causes this problem including hydrogen induced decohesion, void pressure, and hydride formation[6]. The fractures occurring from exposure to a hydrogen environment can vary drastically thus different mechanisms may be responsible in different materials. The fracture mode can be cleavage, quasi-cleavage, microvoid coalescence, intergranular,or topographical tearing[7]. Experimental research can be conducted on whether susceptibility to hydrogen effects exist without knowing which mechanism(s) is aggravating or causing the failures. This can be accomplished by comparing the materials reaction through changes in its mechanical behavior with and without the presence of hydrogen.

Figure 1 depicts the corrosion cell formed when an alloy is coupled with a less noble metal/alloy in an electrolyte. The less noble alloy undergoes loss of material through an anodic oxidation reaction of metal dissolution producing an excess of electrons, while a more noble alloy supports a cathodic reduction reaction transforming monotonic hydrogen into hydrogen gas, using up

the excess electrons. Either half of this system can be simulated by the application of a potential causing electron flow in the desired direction. The reduction reaction will take place, evolving hydrogen if the electron flow is into the material. The amount of hydrogen produced will be a function of the rate of electron flow. Likewise, the amount of hydrogen diffusion into the alloy will be a function of its availability.

Figure 1 Corrosion Cell Produced When Alloy 625 is Coupled With a less Noble Metal

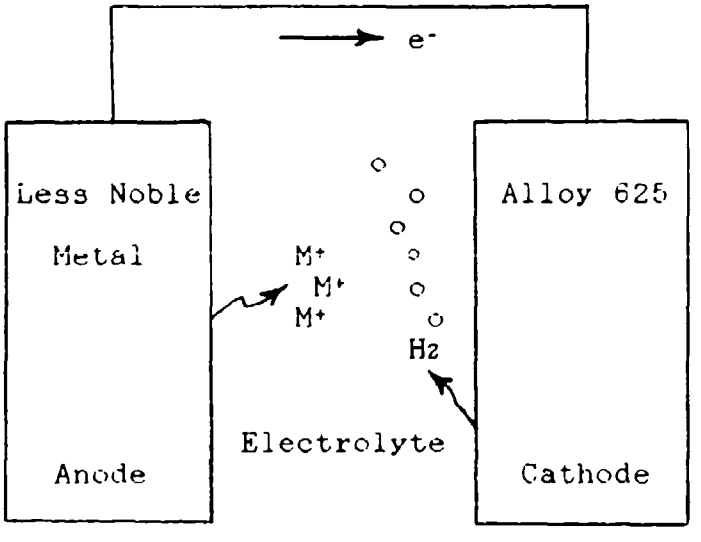

Reactions: $M \rightarrow M^+ + e^-$ $2H^+ + 2e^- \rightarrow H_2$

4. MATERIAL - ALLOY 625

Alloy 625 is a nickel based superalloy which has a face centered cubic matrix that is dispersed with carbides and nitrides. Its major constituents are about 61 percent nickel, 21.5 percent chromium, 9 percent molybdemun, 3.5 percent combined columbium and tantalum, and 2.5 percent iron. The nickel and chromium are used to resist chemical oxidation. The chromium forms a protective film of Cr_2O_3 on the exposed surfaces of the metal. The molybdemun is used for solution strengthening and resistance to pitting and crevice corrosion[1]. The columbium and tantalum are added as solution strengtheners and stabilizers against sensitization to intergranular cracking during welding. The iron is added to get back some of the ductility lost by the addition of the above strengtheners[2]. Aluminum and titanium are also added along with the columbium to form age hardening precipitates. The allowed constituents in Alloy 625 is given in the American Society for Testing and Materials specification ASTM-B564-82 as listed on Table 6.3.

4.1 CASTING METHODS

The two major methods of forming good quality Alloy 625 ingots are Vacuum Induction Melting (VIM) followed by Electro Slag Remelting (ESR) and VIM followed by Vacuum Arc Remelting (VAR). Thus the two common melting methods are normally referred to as VIM/ESR and VIM/VAR

The Vacuum Induction Melting process is where all the ingredients for the final alloy are combined together. The various ingredient materials can obtained and used in many different forms, from powder to pieces too large to manually lift. A crucible to melt the materials in is filled with the desired percentages of the components and sealed in a furnace. A vacuum is drawn on the furnace almost down to absolute, and then the furnace is induction heated to a temperature above the melting points of all the constituents. The high vacuum prevents the combination of aluminum and titanium with oxygen and nitrogen, while removing volatile metals such as lead and bismuth. The molten alloy is poured off into long cylindrical molds through a series of dams that eliminate floating slag. Once cooled, the alloy log is removed from the mold and prepared to be used as an electrode for ESR or VAR remelting. These electrodes can be in various lengths and diameters depending on the final desired ingot size. They can be over two feet wide and fifteen feet long.

Vacuum Arc Remelting is a large scale gas metal arc (GMA) welding process. The heavy electrode is suspended in a sealed cylinder twice its length. The cylinder is evacuated to a very low pressure and the walls are cooled with a flow of helium gas. The electrode is lowered to the bottom and an arc is struck by applying a potential. The lower end of the electrode melts off forming an ingot below it. The height of the electrode is controlled along with

the current to get the best processing rate. The ingredients in the alloy are not changed during the VAR process, only the relative mixing and grain size.

Electro Slag Remelting is similar to submerged arc welding. As in VAR, the heavy electrode with a potential applied is lowered down through a long cylinder that has water jacket cooling. Simultaneously a flow of powdered flux is poured onto the weld pool. The arc and weld pool stay submerged in the liquid slag. The slag has the capability of removing impurities while keeping the alloy isolated from atmospheric contaminants. A purge of the inert gas argon is also used to reduce the possibility of air contaminates. This process has cooling water vice the cooling gas flow used in VAR, thus the ingot cools faster causing a thinner solidification zone resulting in finer grains for the same diameter ingot.

4.2 MECHANICAL PROPERTIES

Alloy 625 has a wide range of mechanical properties which depend on its composition and how it was processed. Processing includes how it was melted and mechanically worked as well as its thermal history. Strength and elongation are the major trade off variables when selecting the microstructure to be used. The higher the strength desired the lower the elongation achieved.

The yield strength can vary between 32 to 90 ksi, while the ultimate tensile strength can vary between 70 and 145 ksi at ambient temperature. Elongation can vary between 20

and 65 percent at ambient temperature. At higher temperatures the strengths decrease and the elongation increases.

The lowest yield and tensile strengths are developed in semi-single crystal Alloy 625, material that is cast and then homogenized so that diffusion and grain growth eliminate most of the dendritic grain boundaries and the large segregated carbides. The strengths are on the order of 35 and 70 to 90 ksi respectively. The corresponding elongation for this microstructure is greatest at more than sixty percent.

The highest strengths and accompanying lowest elongation occur when forged material is heat treated for ten hours or more at around 1200 degrees F. These secondary phases increase the hardness and strengths while reducing elongation. The yield and tensile strengths of this form can be as high as 105 and 150 ksi respectively[8], while the elongation can drop down to as much as thirty percent.

Cast material has yield and tensile strengths on the order of 45 and 85 respectively and an elongation between 40 and 50 percent.

Forged material strengths are about 60 ksi for yield and 120 ksi for tensile. The corresponding elongation is in the 50 to 60 percent range.

The tensile elastic modulus decreases with increasing temperature and decreasing strength. At ambient temperature it is between 28 and 35 x 10^6 psi.

4.3 MICROSTRUCTURES FROM PROCESSING

Cast Alloy 625 has a grain size that is a function of its casting method. The direction and speed of the cooling determine the thickness and shape of the solidification zone which, in turn, determine the shape and size of the grain and the amount of segregation. Columnar grains are achieved by single direction cooling, whereas equiaxed grains are derived from multi-directional cooling[2]. The slower the cooling rate, the larger the grains grow and the greater the segregation problem. Large grains are beneficial for high temperature service, whereas fine grains are required for ambient temperature applications. The casting process forms large MC carbides (Cb,MO)(C,N) inner and transgranular throughout the ingot since they solidify just below the overall freezing temperature. The slower the cooling rate the larger these carbides can grow.

Homogenization at temperatures close to the MC carbide solidus will allow grain growth, dissolution of the MC carbides into the matrix, and diffusion of segregated metals from the dendritic areas. Homogenizing at lower temperatures results in the MC carbides reforming as $M_{23}C_6$ and M_6C carbides along the grain boundaries. These grain boundary carbides control grain growth in forged alloy during later heat treatments.

Hot mechanical working or forging an alloy makes fine grains and breaks up the carbides. Completing a second homogenization cycle after hot working regrows the matrix

grain structure and allows the broken up carbides to spheriodize and reform on the new grain boundaries. The finer grains with carbides intermittently spaced along them improve the yield and tensile strengths.

Heat treating/aging the 625 alloy will produce limited grain growth and the formation of many secondary phases. The phases developed depend upon what temperature the heat treatment starts at and where the temperatures are held constant. Aging in the 1200 to 1700°F range produces a body centered tetragonal (BCT) gamma double prime phase and a gamma prime phase that transforms with time into an orthorhombic Ni_3Cb phase with an abab stacking sequence. Aging closer to the high end of this band produces the orthorhombic phase, while the low end produces the BCT gamma double prime phase. Aging at an intermediate temperature produces some of both phases. Both of these phases impart high hardness and high strengths to the alloy. Aging at a higher temperature first, then in the 1300 to 1700°F range produces a grain boundary film of M_6C carbides. Around 1400°F appears to form the most continuous film.

4.4 CORROSION PERFORMANCE

Alloy 625 has exceptionally good corrosion resistance reported in the literature. The only corrosion problem documented has been from deep sour gas wells with environments high in hydrogen sulfide and chlorides. Under these adverse conditions, susceptibility to stress corrosion was reported[9].

5. MATERIAL PROCESSING FOR TESTING

The Alloy 625 that was used for testing was supplied by the forging company, Wyman Gordon, from on hand stock. Both cast and forged material were used for testing. Table 5.1 lists the specimen numbering sequences and their associated heat treatments completed after cutting into sample blanks.

5.1 CAST MATERIAL

The cast material was melted by the VIM/VAR process by Special Metals Company (SMC) as heat 9-9650. The ingot was delivered with a 30 inch diameter and weighed approximately 14,600 pounds. A test slice was removed from the end of the ingot. All test blanks were taken from the inside face of the slice at the mid-radius with their longitudinal axes in the radial direction as shown on the sample drawing in Figure 2. A drawing was made to show the location of each test specimen blank and is on file at the Wyman Gordon Company as drawing number C-2290. Each blank was numbered on the drawing. Extra coupons of material from the same areas were saved and marked with letter designations. The tensile blanks and the slow strain rate blanks each had their own numbering sequence starting from one, since they were different sizes. The blanks were divided into four groups. The first group was used as is, and labeled "as cast". The second group was homogenized at 2225-2250°F for 48 hours, then air cooled, and labeled "cast/homogenized". The third group was homogenized as above, then cooled to 2100°F and held for one hour, followed by air cooling, and

labeled 'cast/air'. The fourth group was given the same treatment as the third, followed by the hardening heat treatment listed for the second group of forging samples below. This group was labeled 'cast/heat treated'. These last two groups were not used for the slow strain rate testing due to a metal dusting corrosion problem that occurred during their heat treatment. All samples were machined to proper size as tensile and slow strain rate specimens after their thermal treatments were complete.

5.2 FORGED MATERIAL

The forged material was melted by the VIM/ESR process by Allvac as heat number W823. It started as a 34 inch diameter ingot weighting 14,658 pounds. It was initially cogged to a 29 inch diameter, then given two upset and drawing cycles to end at a 25 inch diameter, all at around 2000°F. The billet then was homogenized at 2225°F for 48 hours followed by a 2000°F upset to a 36 inch diameter. Cogging to a 25 inch diameter at 2000°F was the final mechanical working of the billet.

A four inch slice was removed from the end of the billet. A drawing was made to show the location of each test specimen blank and is on file at the Wyman Gordon Company as drawing number D-1410. Each blank was numbered on the drawing. The tensile blanks and the slow strain rate blanks each had their own numbering sequence starting from nine and seventy-three respectively. All test specimen blanks were taken from the mid-radius of the inside face of

this slice with their longitudinal axes in the radial direction as shown on the sample drawing in Figure 2. Extra coupons of material from the same areas were saved and marked with letter designations. The blanks were divided into two groups. One group was annealed for six hours at 1700°F and was labeled "forged/annealed". The other group was heat treated to get the hardest form this alloy can have, a Rockwell C hardness greater than 35. To achieve this the group was heated to 1800°F, held for one hour, water quenched, reheated to 1450°F, held for one hour, air cooled, reheated to 1200°F and held for seventy hours followed by air cooling to ambient. After all heat treatments were completed, the blanks were machined to size as tensile test and slow strain rate specimens.

Table 5.1 Heat Treatment For Alloy 625

Slow Strain Rate and Tensile Test Specimens

Category	Specimen Label	Heat Treatment
1. Cast	#1-#18 small #1 and #2 large "G" chunk	None
2. Cast Forged	#19-#36 small #3 and #4 large "A" chunk	Homogenize at 2225-2250 degF for 48 hours, air cool
3. Cast	#37-#54 small #5 and #6 "B" chunk	Homogenize at 2225-2250 degF for 48 hours, cool to 2100 degF, hold for 1 hour, air cool
4. Cast	#55-#72 small #7 and #8 large "C" chunk	Same as #3 and: a. Heat to 1800 degF, 1 hour, water quench b. Heat to 1450 degF, 1 hour, air cool c. Heat to 1200 degF, hold for 70 hours, air cool
5. Forged	#73-#90 small #9 and #10 large "D" chunk	Heat to 1700 degF, hold for 6 hours, air cool
6. Forged	#91-#108 small #11 and #12 "E" chunk	Same as steps a, b, and c in #4
7. Forged	"F1" chunk	Heat to 1400°F, hold for 16 hours, water quench
8. Forged	"F4" chunk	Heat to 1500°F, hold for 16 hours, water quench
9. Forged	"F5" chunk	Heat to 1600°F, hold for 16 hours, water quench

* Temperatures are plus and minus 15 degrees

** Small specimen dimensions are 2.0" x 0.3" square

*** Large specimen dimensions are 2 3/4" x 1/2" square

Figure 2 : Typical Test Specimen Location

Section of Alloy 625 Billet/Ingot

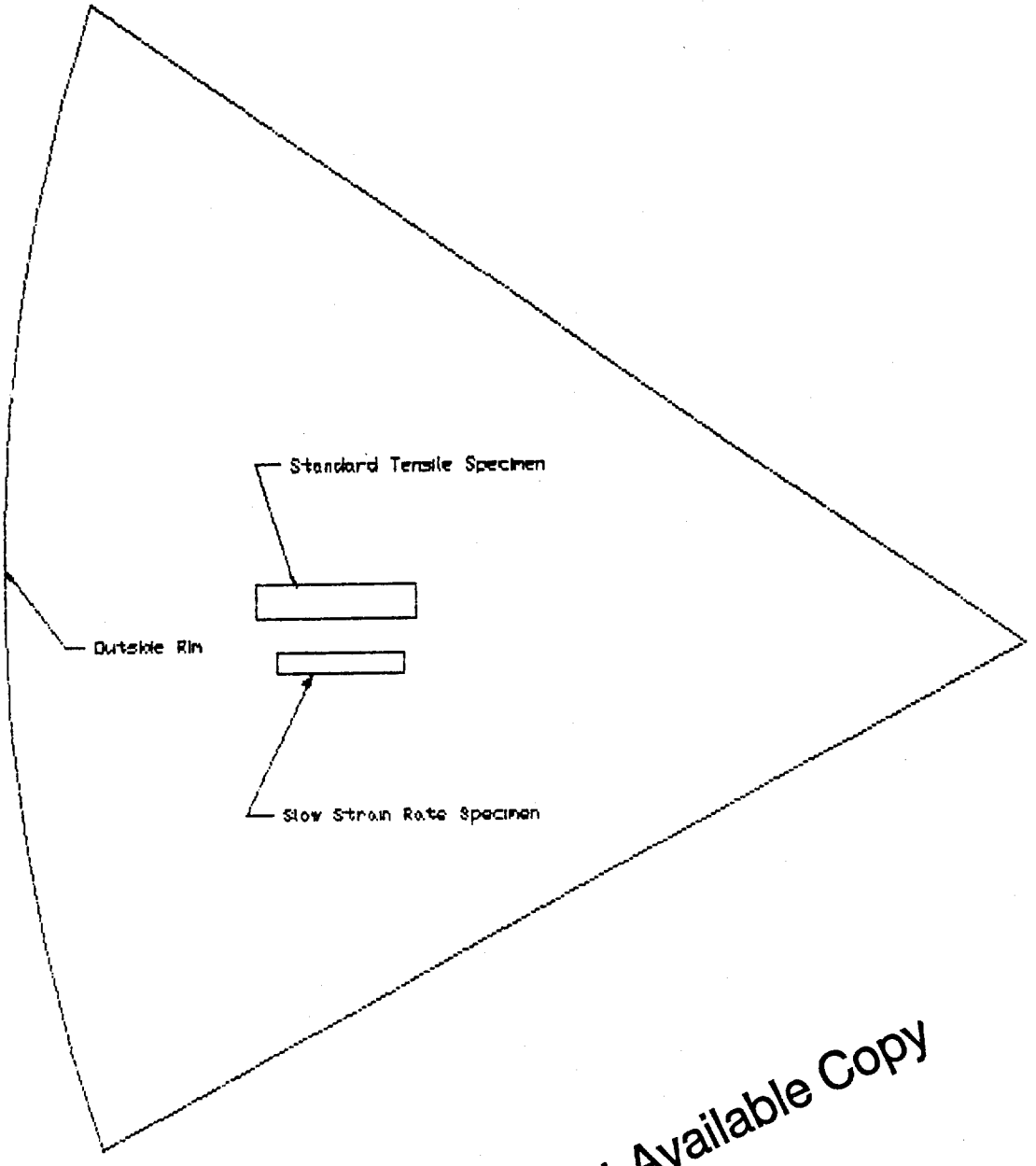

6. VERIFICATION OF COMPOSITION AND MICROSTRUCTURE

The microstructure and mechanical properties were determined by tensile testing, hardness testing, chemical analysis, and scanning electron microscope microanalysis. These tests were completed on all six microstructures even though only four were used for the slow strain rate tests.

6.1 TENSILE TESTING

The tensile tests specimens were taken from the same areas of the casting and forging slices and had the same orientation as the slow strain rate specimens, gage lengths radial to the billet/ingot with casting grain perpendicular to the gage length. The half inch square, two and three quarters inch long blanks were all heat processed along with the slow strain rate blanks. The specimens from the four microstructures in which slow strain rate tests were also conducted, were all machined to the standard gage diameter of approximately .252 inches. The specimens for the other two microstructures, that developed a metal dusting corrosion problem during heat treatment, were machined to a gage diameter of approximately .179 inches.

The tensile tests results are listed on Table 6.1 and displayed in Figure 3. They show the variations in mechanical properties that were achieved between the different microstructures.

The yield strengths are around 50 KSI lower than the ultimate strengths in all but the cast/homogenized/heat treated material. This form has its yield and ultimate

strengths only a few KSI apart, implying fracture should occur without much yielding. The corresponding elongation and reduction in area support this as they are both about 11 percent, while the others are all greater than 29 percent. The semi-single crystal cast/homogenized form has the highest elongation, greater than 60 percent. This microstructure also has the unique feature of having a corner at the yield point on its stress strain diagram. That is, once the yield point is reached, the material yields without any increase in stress. This effect only lasts for approximately one percent elongation, then work hardening intervenes.

Table 6.1 Standard Tensile Test Results

Sample #	Type Test	Yield KSI	UTS KSI	% El	% RA	Dia Start inch	Dia Finish inch
1	C	52.7	100.6	42.0	41.3	0.2513	0.1930
2	C	52.3	95.0	38.5	42.6	0.2521	0.1910
3	CH	34.3	72.6	65.5	40.9	0.2518	0.1935
6	CHair	36.5	76.5	61.5	42.5	0.1787	0.1355
7	CHT	72.0	76.8	11.0	11.3	0.1785	0.1680
9	FA	83.9	120.8	45.5	39.1	0.2517	0.1965
11	FHT	93.2	142.5	30.0	29.6	0.2521	0.2115
12	FHT	90.4	141.0	35.0	35.3	0.2518	0.2025

C = As Cast

CH = Cast/Homogenized

CHair = Cast/Homogenized/cooled to 2100 deg F for 1 hour

FA = Forged/Annealed

FHT = Forged/Heat Treated

See Table 5.1 for specific heat treatments

See Section 5 for total material history

Figure 3 Graph of Tensile Test Results

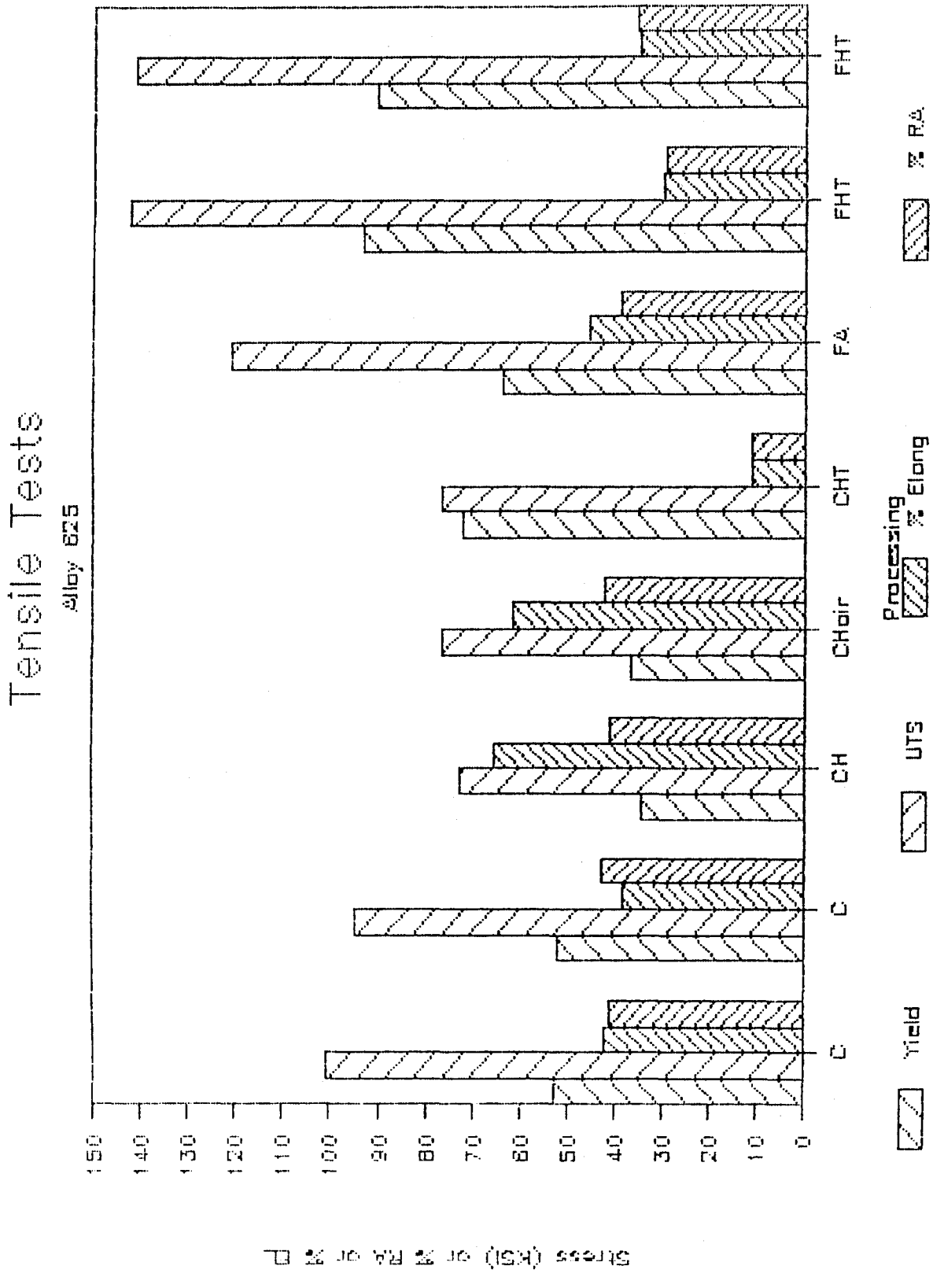

Stress (KSI) or % RA or % EL

Best Available Copy

6.2 HARDNESS TESTING

Hardness tests were conducted on all six of the microstructures with a Rockwell hardness testing machine. Both B and C ranges were used for the hardest microstructures since their hardnesses were near the limit of the B scale capability. The results of these tests, listed on Table 6.2, show the wide range of hardness that can occur with this alloy. Hardness follows the variations of the strengths and the elongations. It increases with strength and decreases with elongation.

Approximately 12.5 percent of the hardness value was lost by the homogenization process, even though segregation was eliminated. This effect is probably due to the large segregation free crystal formation causing a reduction in the yield stress and "easy glide" at the yield point, since hardness is a function of yield stress and work hardening ability.

Heat treating the homogenized alloy increased its hardness value by 33 percent, or an increase of 16.4 percent over the original "as cast" hardness value. This is due to the new phases and grain boundry carbide film formed during the heat treatment.

The increase in hardness between the heat treated cast and forged microstructures shows the effect of multiple grain boundries on the hardness.

Table 6.2 Hardness Test Results

As Cast	R_B	84.7		
Cast/Homogenized	R_B	74.2		
Cast/Homogenized/1hr@2100°F	R_B	73.3		
Cast/Heat Treated	R_B	98.6	Rc	21.3
Forged/Annealed	R_B	92.8		
Forged/Heat Treated	R_B	99.8	Rc	25.6

6.3 CHEMICAL ANALYSIS

The chemical analysis of the ESR (forged) and VAR (cast) material are given on Table 6.3. The chemistry of each melt is within the ASTM-B564-82 specification, also listed on Table 6.3. The only two significant differences in the materials are the carbon and phosphorus percentages. The carbon in the ESR alloy is twice that in the VAR alloy. Phosphorus is opposite with over twice as much in the VAR alloy.

Table 6.3 Alloy 625 Specification and Chemistry Analysis

Alloy 625 Chemistry Analysis in Weight Percent

Element	Specification ASTM B564-82	VIM/ESR Allvac S2230 Heat W823-1	VIM/VAR SMC S2183 Heat 9-9650
Nickel + Colbalt	58.0 min	60.87	60.10
Chromium	20.0-23.0	22.01	21.80
Molybdenum	8.0-10.0	8.42	8.85
Iron	5.0 max	3.77	4.46
Niobium + Tantalum	3.15-4.15	3.74	3.70
Colbalt	1.0 max	0.10	0.20
Manganese	0.5 max	0.25	0.28
Silicon	0.5 max	0.30	0.24
Aluminum	0.4 max	0.28	0.24
Titanium	0.4 max	0.30	0.29
Carbon	0.1 max	0.056	0.027
Sulfur	0.015 max	0.001	0.001
Phosphorus	0.015 max	0.004	0.010

6.4 SEM MICROANALYSIS

Each of the six microstructures was examined with a scanning electron microscope in the as polished, acid etched, and electro-chemical etched condition. Photo micrographs were taken in each condition at various magnifications. This series of micrographs is included in Figures 4 through 9.

The "as cast" material, shown in Figure 4, has large grains, copious carbides, and excessive segregation. The alloy in the upper left photomicrograph was lightly etched to show the grains. The average grain size is about .020 inches. The photomicrograph on the upper right shows some of the secondary platelet phases that were formed during solidification. The material in the lower photomicrographs was heavily etched and show the high percent segregation and the dendritic structure of the cast material.

The photomicrographs in Figure 5 show the enormous grains that grew during homogenization. The MC carbides have spheroidized in the matrix and a fine film of either $M_{23}C_6$ or M_6C carbides was formed along the grain boundaries. The segregation and dendritic structure was completely eliminated by using such a high temperature (2225-2250°F) for homogenization.

The material shown in Figure 6 was cast/homogenized and then held at 2100°F for 1 hour. Its grain boundaries appear to be filled with a thick layer of cellular $M_{23}C_6$ carbides.

The appearance of more MC carbides in the matrix is probably due to a longer etching time than the above microstructure.

Heat treating the cast material in Figure 7 caused what appears to be globular or blocky $M_{23}C_6$ carbides on the grain boundaries. The bottom photomicrographs show dislocation slip bands throughout the matrix and heavy growth along the grain boundaries.

Figure 8 shows the results of forging and annealing Alloy 625. The grain size is about an ASTM 6. There are discontinuous blocky carbides along the grain boundaries. The bottom right photomicrograph shows a secondary phase precipitated out from the grain boundaries that appears to be gammma prime. There is still a high percentage of blocky spheroidized MC carbides dispersed throughout the matrix.

Heat treating the forged material caused some grain growth and enlargement of the grain boundary carbides as shown in Figure 9. Again the heat treatment caused dislocation slip bands to appear throughout the matrix.

Figure 4 Photomicrographs of "As Cast" Alloy 625

Top Left: 100X
Bottom Left: 50X

Top Right: 1000X
Bottom Right: 200X

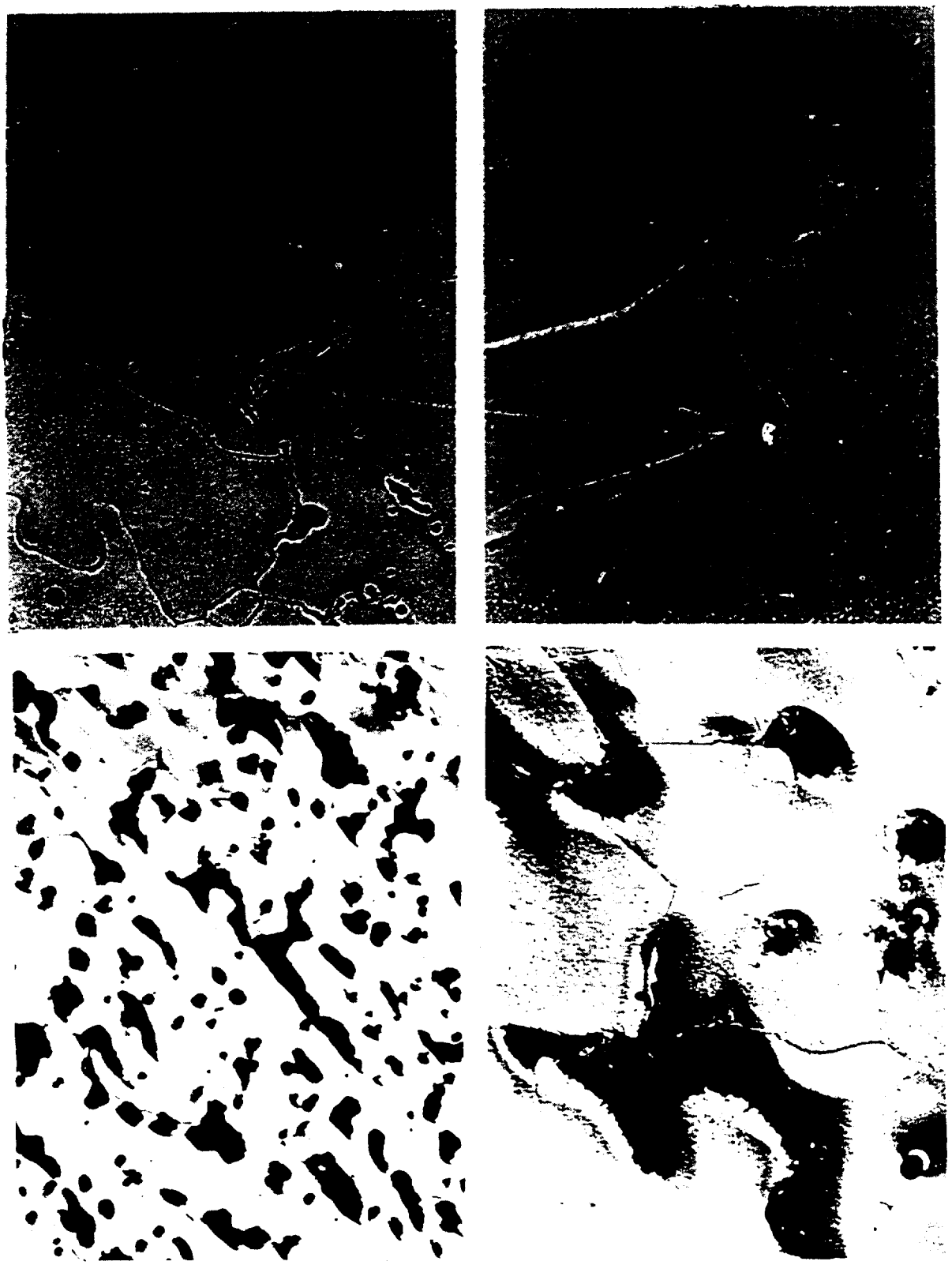

Figure 5 Photomicrographs of "Cast/Homogenized" Alloy 625

Top Left: 100X
Top Right: 1000X
Bottom Left: 50X
Bottom Right: 1000X

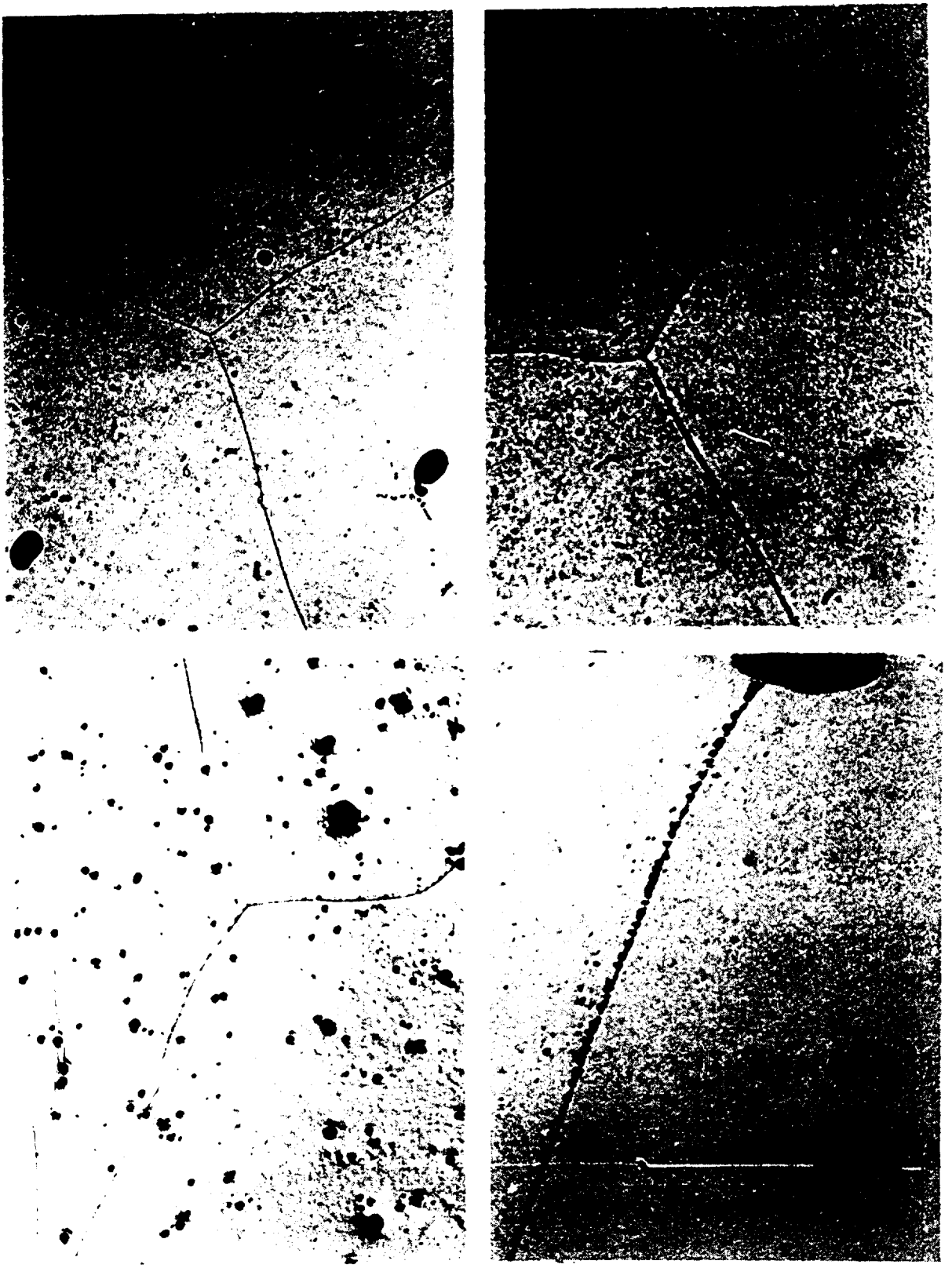

Figure 6 Photomicrographs of "Cast/Homogenized/2100°F" Alloy 625

Top Left: 100X
Top Right: 1000X
Bottom Left: 50X
Bottom Right: 1000X

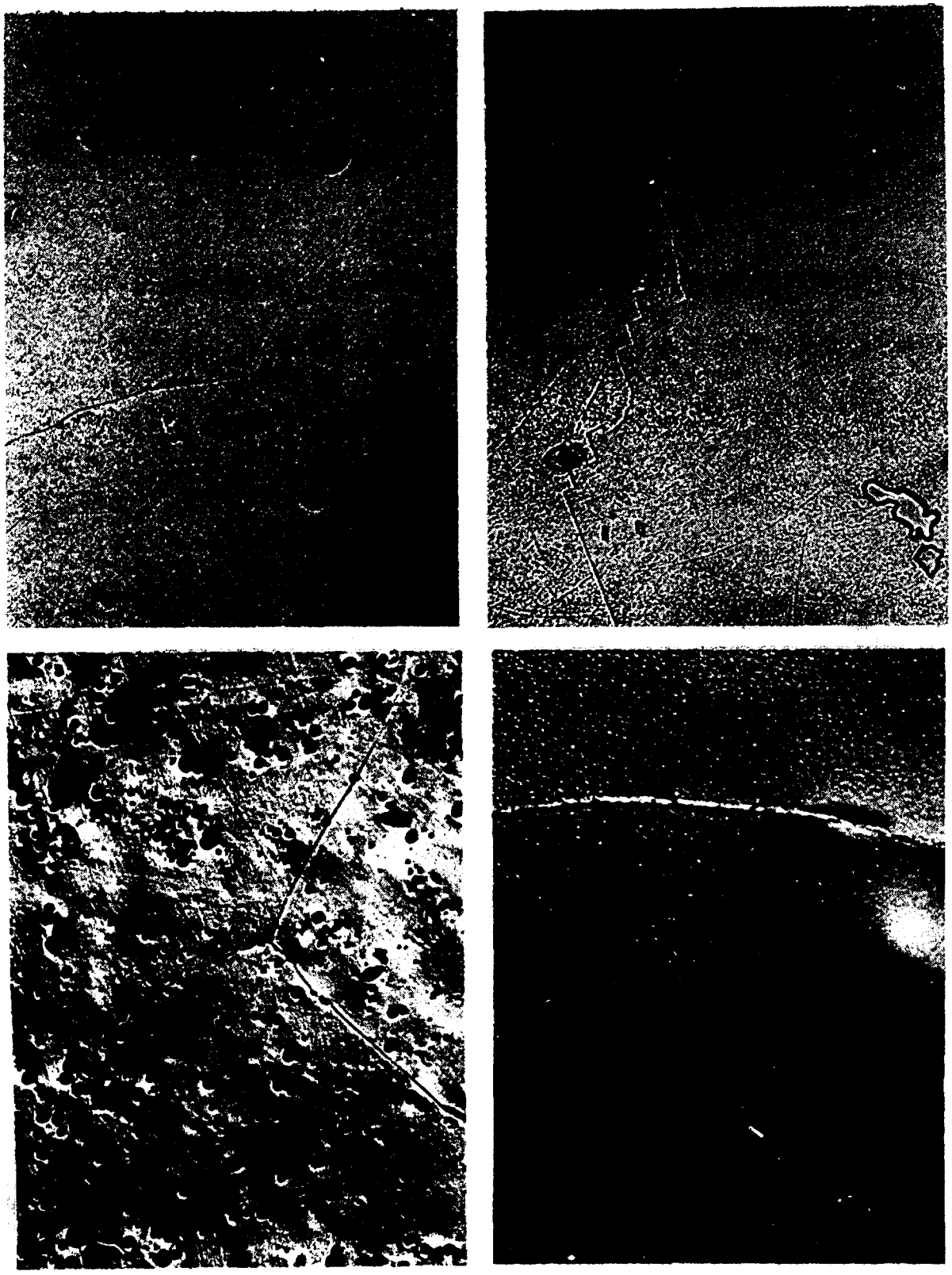

Figure 7 Photomicrographs of "Cast/Heat Treated" Alloy 625

Top Left: 100X
Top Right: 1000X
Bottom Left: 50X
Bottom Right: 1000X

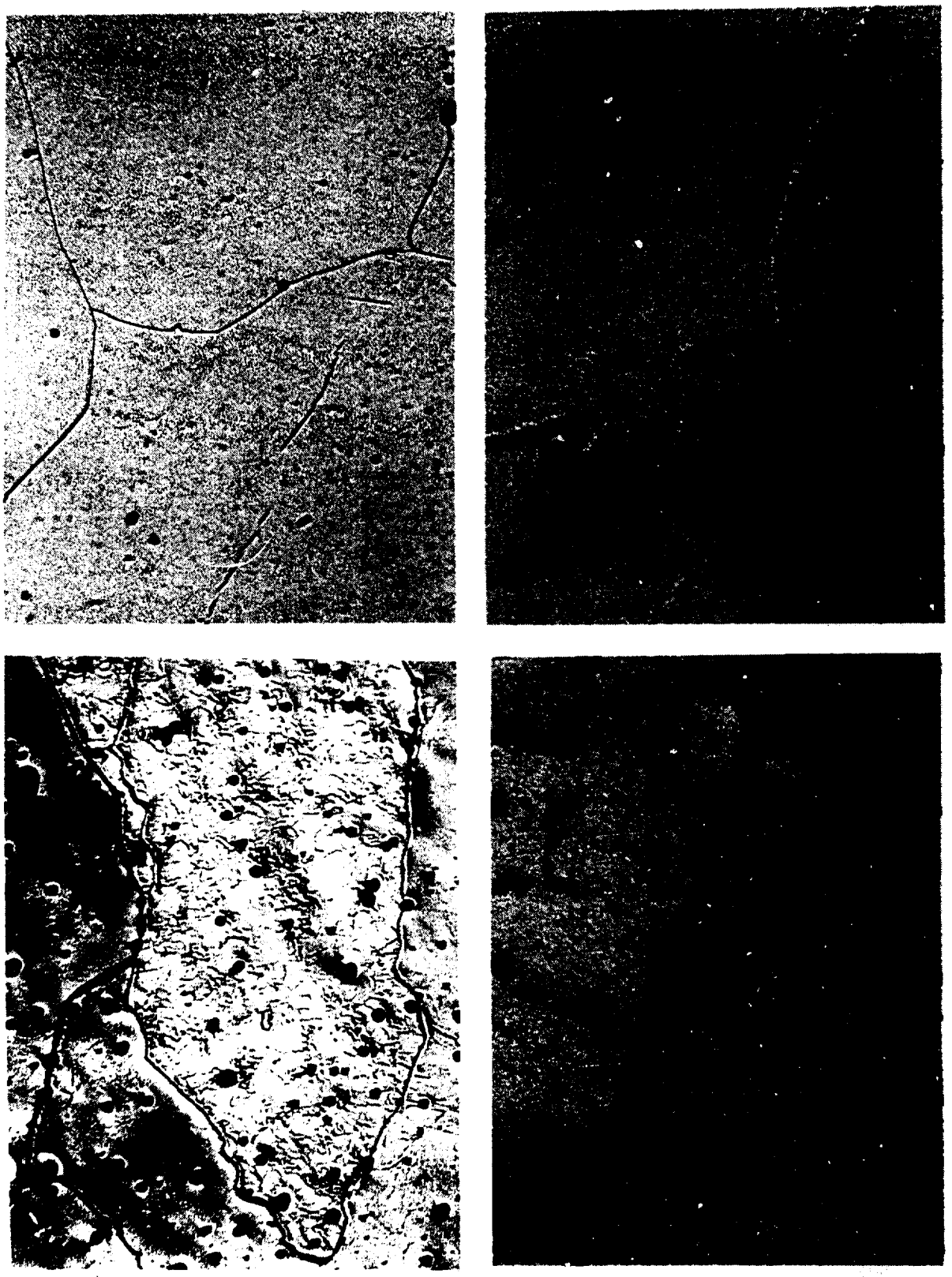

Figure 8 Photomicrographs of "Forged/Annealed" Alloy 625

Top Left: 100X
Top Right: 1000X
Bottom Left: 50X
Bottom Right: 1000X

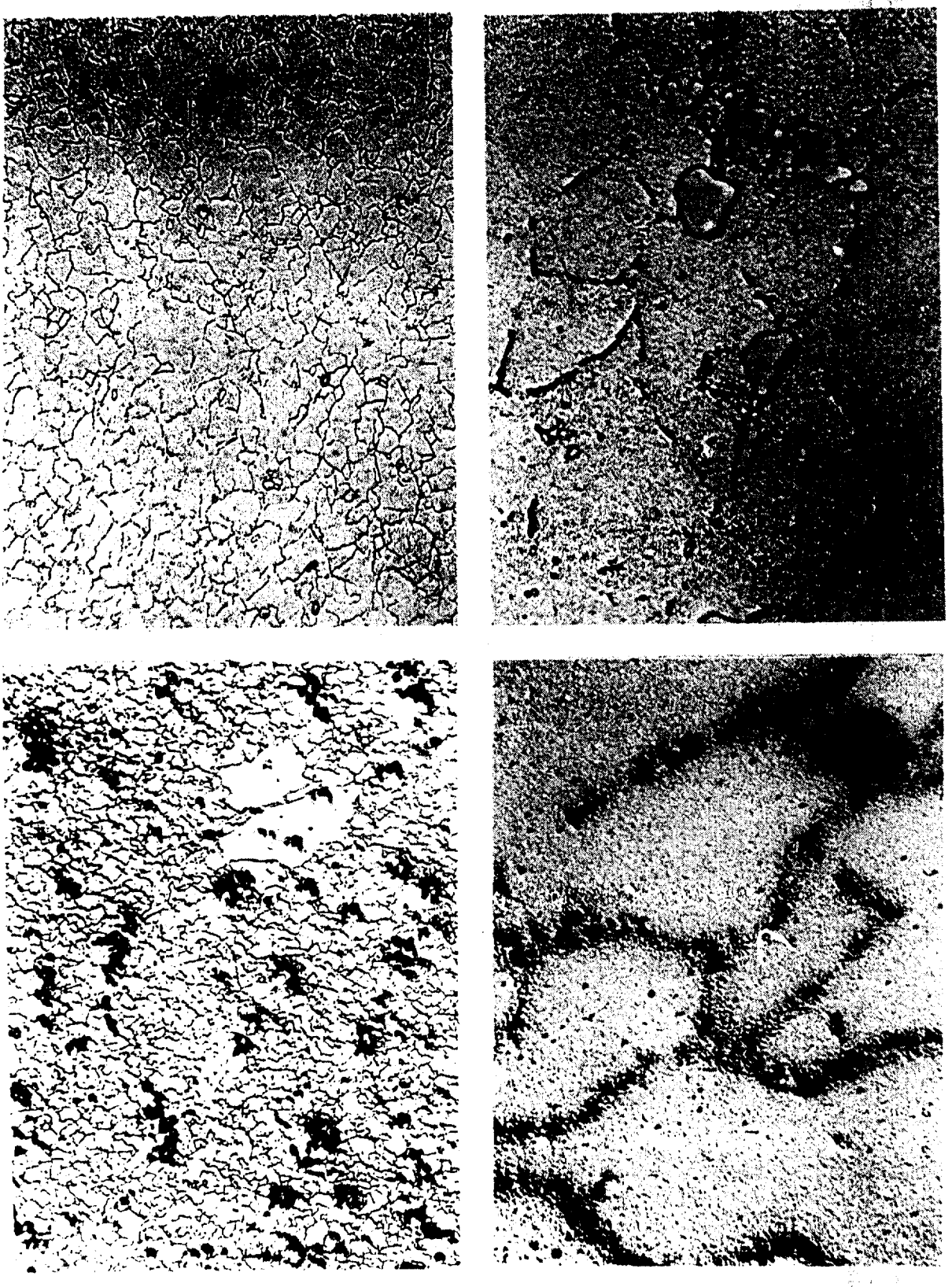

Figure 9 Photomicrographs of "Forged/Heat Treated" Alloy 625

Top Left: 100X
Bottom Left: 50X
Top Right: 1000X
Bottom Right: 1000X

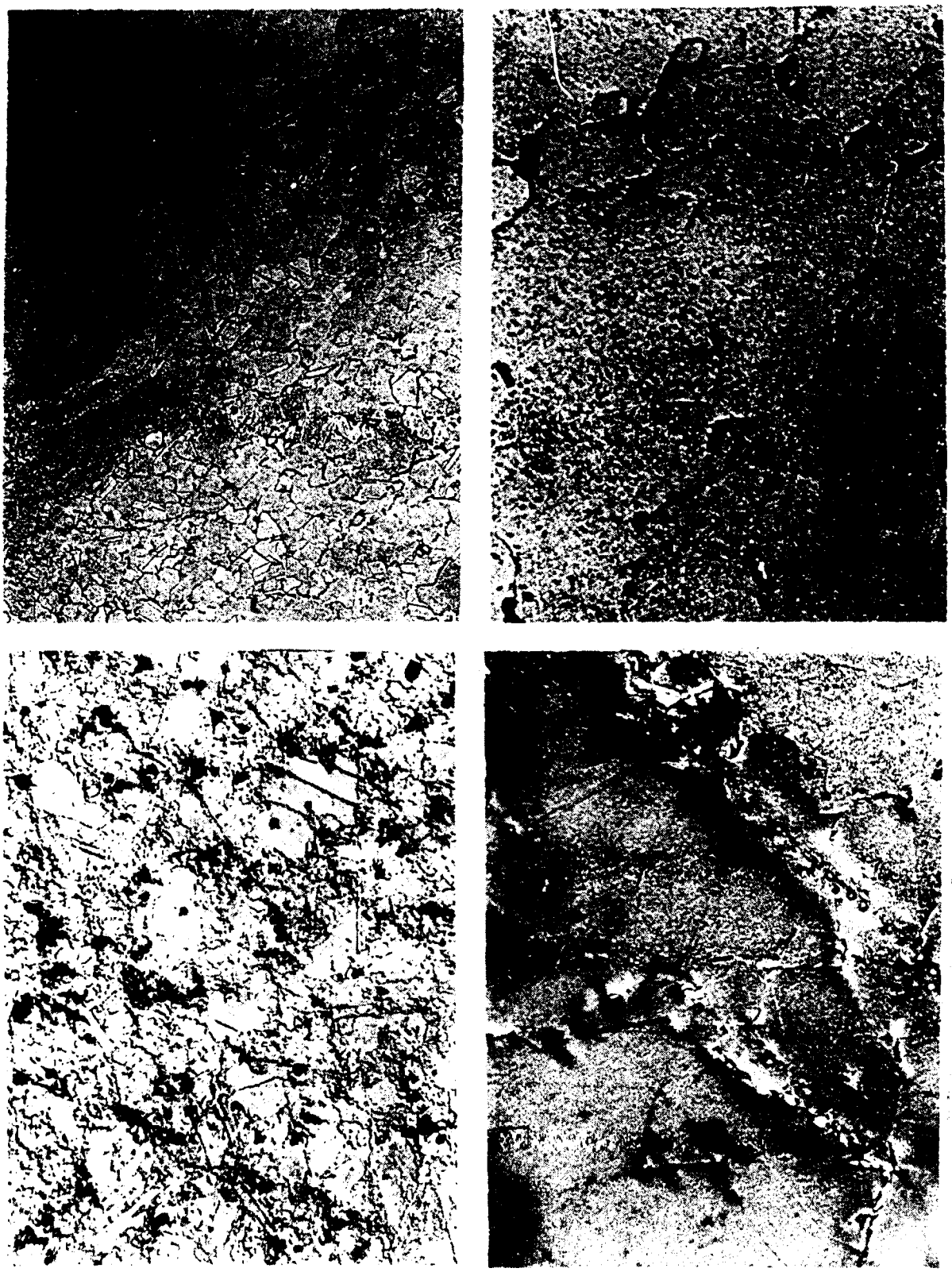

7. PROCEDURES AND APPARATUS FOR LABORATORY TESTING

The object of this testing program was to determine if Alloy 625 can withstand the environmental condition found in a submarine sea water system. Laboratory testing should be as close to the expected conditions as possible, but it is most beneficial to set up the worst conditions. The sea water was simulated with "substitute ocean water" without heavy metals. It was mixed in accordance with ASTM standard specifications D-1141 and E-200. Stagnated or pocketed sea water was felt to be the worst condition since local changes in chemistry (such as pH) can occur, thus a "flow through" system was not employed. Air was bubbled into the sea water to cause localized circulation, to have a constant oxygen level for all tests, and to set up the poor condition of high air saturation (since a submarine main ballast tank blow system readily adds air to the sea water systems). The sea water was changed and all equipment was cleaned for each test.

Baseline tests were run using the same equipment but no sea water. This was followed by a series of tests in sea water allowing free corrosion (no applied potential). This gave a bimetallic coupling with the bottom steel grip. The final tests were accomplished with potential applied to emulate other bimetallic couplings, a hydrogen environment, and stray potentials that could be developed from sources such as rotating shafts, chlorination units, or cathodic/anodic protection systems. The potentials used on

all four of the tested microstructures were +1.0 volts SCE for anodic charging and -1.0 volts SCE for cathodic charging. Further testing with cathodic charging at -2.0 and -3.0 volts SCE was conducted on the forged/annealed material and -3.0 volts SCE on the "as cast" material. Equipment problems precluded further testing at these more negative potentials

7.1 SLOW STRAIN RATE TESTING

7.1.1 BACKGROUND

The slow strain rate test is designed to give a "quick look" at how a material reacts to a set of conditions. The material is pulled apart slowly, constantly exposing new surfaces either by cracking the previous surface (film rupture) or by slip planes piercing the surface exposing their sides. As such, an oxide film cannot passivate the metal. However, the rate of strain has to be slow enough to allow chemical and electrolytic reactions and diffusion to occur. Diffusion effects are both across the Helmholts plane to alloy surface gap and into the material.

7.1.2 SAMPLE PREPARATION

The fully heat processed .30 inch square, 2 inch long specimen blanks were machined in accordance with Figure 10. The gage length was offset to one end of the specimen to allow the waterline to be maintained between the upper grip and the gage length during elongation. This minimized the coupling with the grips but kept the gage length submerged in the test environment. The final finish on the specimen

was made by polishing the gage length along its longitudinal axis to eliminate any circumferential scratches. The approximate dimensions of the finished gage diameters and gage lengths were .080 inches and .6 inches respectively. The gage diameters were all measured with a dial caliper just prior to testing.

Figure 10 : SLOW STRAIN RATE TEST SPECIMEN

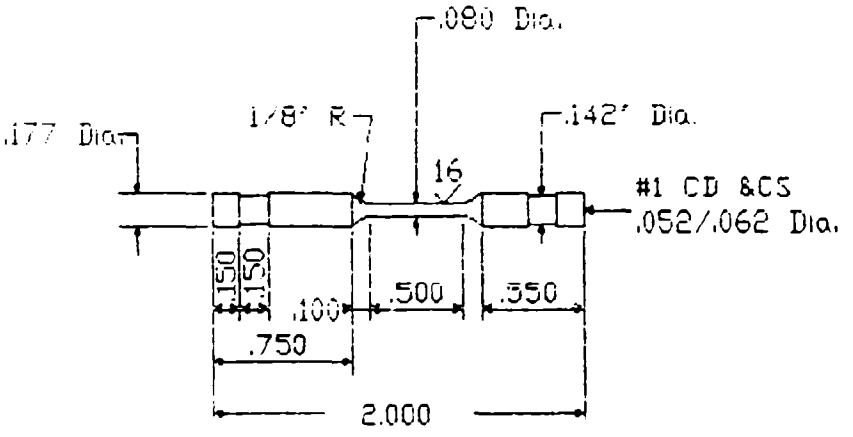

All dimensions in inches

Tolerances: +/-.002 inches on diameters

+/- .010 inches on lengths

Diameters concentric within .0005" FIR

Slight taper to center of gage length permitted

Surface Finish:

16 RA on gage length with longitudinal scratches only

32 RA on other surfaces with transverse scratches

7.1.3 TEST APPARATUS

All testing was accomplished on an Instron constant speed, screw driven, tensile testing machine at a crosshead speed of .002 inches per minute. This gave a starting strain rate of 5.6×10^{-5} per second, that decreased with time since the specimen gage diameter was constantly decreasing. Using the signal from the load cell a load versus displacement graph was made on the chart recorder installed on the Instron. The chart recorder was calibrated with the load cell and standard weights prior to each set of test runs.

The specimen was held between two steel slip ring grips attached to pull rods and surrounded by a plexiglass environment box. A drawing of the test gear as used is shown in Figure 11. The steel grips were taped over to minimize their contact with the sea water and hold the slip rings in place. The box had a removable split lid with four penetrations for services and a sliding "O" ring seal around the upper pull rod. The lower pull rod was threaded into the bottom of the box through an "O" ring seal.

A small air pump was used to supply air to the sea water. The air flow was controlled by a needle valve in the tygon hose supply line and discharged through a glass dispersion filter submerged in the sea water.

A saturated calomel electrode (SCE) was coupled with the sea water through a Luggin capillary probe and a salt bridge to act as a reference electrode. A one inch square

platinum sheet was used as an auxiliary electrode. It was submerged in the liquid less than a half inch away and level with the gage length. The two electrodes and a wire from the upper pull rod were connected to an E & EG model 273 potentiostat. A voltage sensing jumper was installed on the cable connection box to the potentiostat since the currents in use were less than 100 milliamps. For each test run the Luggin probe was filled with sea water from the cell by drawing a vacuum through a valve in the probe connection line, then dumped after the test run.

The potentiostat was used to read the voltage and current before potential was applied. The potentiostat was programed to turn its cell on at the beginning of the test at zero voltage, then ramp increase the voltage at ten volts per minute up to the preset test voltage. The ramp increase was used to allow time to analyze the current development and take corrective action, such as reselecting the current scale. Current was monitored and logged on the chart recorder paper periodically throughout the test. After the specimen fractured, the cell was turned off and the static voltage and current were again read once they were stabilized.

Fresh sea water was mixed just before each set of test runs. The pH of the sea water was checked before testing to insure it was the required 8.2. After each test was completed part of the sea water from that test was saved in a sealable bottle to enable later analysis. Conductivity

and pH were checked immediately after test completion on several of the samples.

After fracturing, the sample was removed from the gear and thoroughly flushed to remove the salt water and any loose corrosion. The sample pieces were examined immediately with an optical microscope, then taped side by side together and sealed in a plastic tube to prevent mechanical damage before SEM examination.

Figure 1: Test apparatus used for Slow Strain Rate Testing

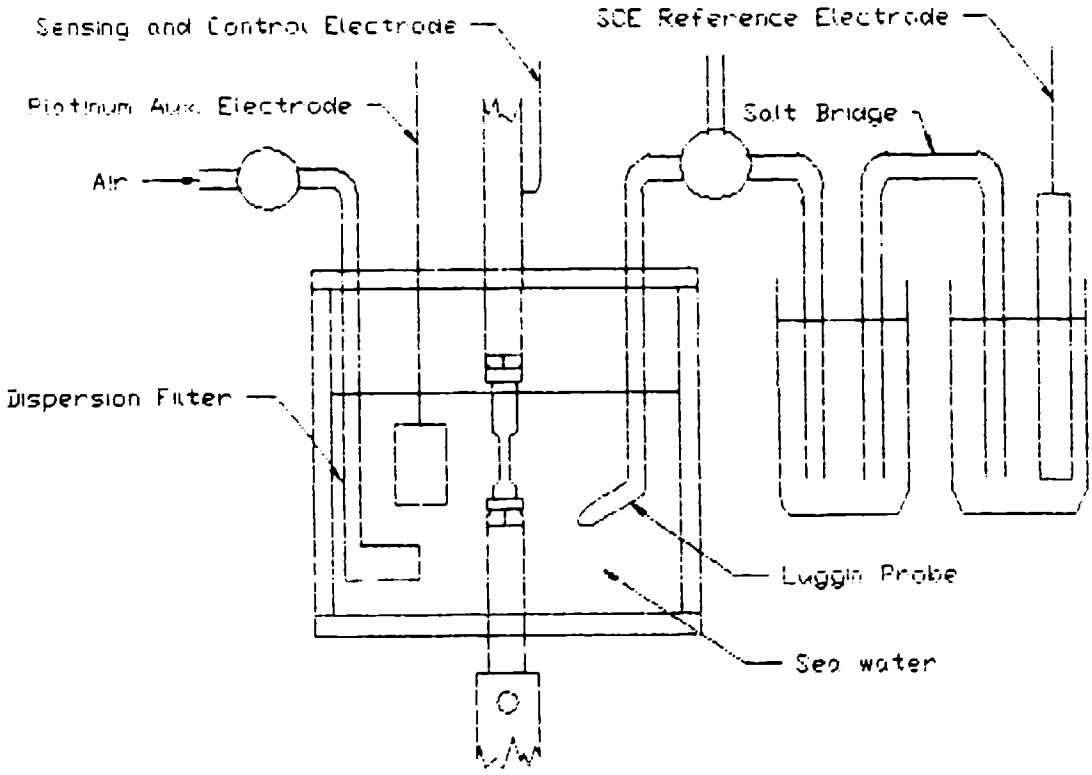

8. RESULTS OF EXPERIMENTAL RESEARCH

8.1 SLOW STRAIN RATE TESTS

The data from the slow strain rate tests were in the form of the tensile load on the test specimens versus crosshead position with respect to time as a plot on a strip chart, or a load versus displacement graph. From these charts the following data were extracted; point two percent (0.2%) yield load, ultimate tensile load, fracture load, and time to fracture (difference in time from (0.2%) yield and fracture). The specimen gage diameters were also recorded. This raw data is presented on Table 8.1. The sample numbers are the original numbers assigned to the specimens when the positions of the blanks were laid out on the billet and ingot slices.

Table 8.2 and Figures 13 through 20 present the reduced data. The categories of the reduced data are; yield stress, ultimate strength (UTS), fracture load percentage of UTS load, percent elongation, and yield work energy. The first two were calculated by dividing the respective loads by the original cross sectional area of the center of gage section (based on the measured gage diameter). The third is the fracture load divided by the UTS load times 100. The percent elongation was calculated by dividing the crosshead movement time between the (0.2%) yield point and fracture, by the original gage length, then multiplying by 100. The effective original gage length measured at 0.60 inches on a sampling of the specimens, then assumed to be a constant on

all specimens. The yield work energy was an integration of the area under the curve on the chart between the 0.2% yield point and the point of fracture. This is "work per specimen" vice "work per unit area" since the cross sectional area was constantly decreasing without a viable way to measure it.

The fracture load percentage of ultimate tensile load was used to appreciate the level of load to which the material holds together after reaching UTS. A high percentage means that the material separated almost immediately after reaching UTS, while a low percentage indicates that the material held together for some time while localized elongation or slippage continued.

The current produced from the applied potential followed a pattern on all the samples. It started high at the beginning of the tests, dropped by at least a factor of ten before the yield point was reached, then slowly reduced over the elongation range until fracture occurred. The average of the current readings for all the tests at about the five percent elongation point are shown on Table 8.3 and displayed in Figure 12. This gives a quasi passivation curve for Alloy 625. It is somewhat artificial since; the material is constantly being stretched exposing new surfaces, it is in discrete increments, and it is per submerged surface area of the sample. Note that the units are "current" not "current per unit area".

When pulling the samples in sea water at +1.0 volt the water tinted yellow by the time the yield point was reached. Before test completion the water was so clouded with yellow precipitate the specimen could not be seen. The pH of the sea water for these samples went from 8.2 to 6.3.

The specimens tested in sea water without potential and at -1.0 volt had a few small bubbles develop on their surfaces that stayed attached. The pH for the -1.0 volt tests also dropped some, ranging from a pH of 6.95 to 8.18.

The conductivity readings did not vary between tests more then the accuracy of the meter used to read it.

During the elongation process of the "as cast" and "cast/homogenized" material the cross section flattened and visual bands or "orange peeling" appeared on the gage area. These bands were symmetrical and angled across the flat sides. The bands appear to be preferred slip planes sliding in large crystals. The FCC structure of Alloy 625 has the {111} planes as its preferred slip planes. Thus the slip systems must be orthogonal or in parallel planes. The latter would give an appearance of an offset stack of disks, as was seen on the cast specimens.

The forged microstructures did not "band" as the cast ones did. They maintained their overall roundness, but the surfaces became irregular as each of the small grains distorted in different directions.

Figures 13 and 14 show the "as cast test results. The placement of the tests across the graphs correlate with the

vertical placement of the tests on Tables 8.1 and 8.2. The first specimen was pulled in less than a minute which could distort its results, such as high yield and high load at fracture. This also precluded integration of the area under the curve. The third sample curve was not integrated due to a slipping recorder clutch producing a discontinuous curve. The fracture loads at failure on the +1.0 and -3.0 volt samples were exceptional low. The significant deviations that correlate are the reduced elongation and reduced yield work energy for the -3.0 volt cathodic test. They were decreases of 41 and 23 percent respectively from the average air tests results.

Figures 15 and 16 show the "cast/homogenized" test results. There is no significant variation across the range of tests for any of the indices.

Figures 17 and 18 show the "forged/annealed" test results. The results are consistent except for the cathodic potentials of -2.0 and -3.0 volts where the fracture load percentage, the elongation, and the yield work energy all were low. They dropped below the average values for the air tests by 25, 27, and 31 percent for the -2.0 volt tests and 33, 33, and 42 percent for the -3.0 volt tests respectively. The last test for this microstructure, specimen number 84 on Tables 8.1 and 8.2, is not shown in the figures. It was conducted in demineralized water in an attempt to eliminate the chlorides from the test environment. The test was unsuccessful in that the current level was in the

nanoamphere range due to the high resistivity of the water and the 6 volt limitation of the potentiostat. The results of this test fell in line with the air tests results.

Figures 19 and 20 show the "forged/heat treated" test results. Like the other tests where no high cathodic potentials were used, these tests had no significant variations.

In summary, across the spectrum of the microstructures there was no statistical difference in the results between the air tests, the anodic potential tests and the -1.0 volt cathodic tests. Only at the higher cathodic potentials where hydrogen was being produced was there any change in results. Even then the yield strength was not affected.

The cast material tests had considerable data scatter which should be expected when the grain size is on the order of, or greater than, the specimen gage diameter.

Table 8 1 Raw Data From Slow Strain Rate Tests

Sample #	Diameter inches	Yield Load Lbf	UTS Load Lbf	Fracture Load Lbf	Time min
		Cast Microstructure			
2	0.0817	310	440	400	0.9
3	0.0800	269	428	155	92
4	0.0800	230	443	225	115
5	0.0800	248	480	147	115
6	0.0803	253	453	280	98.5
7	0.0815	252	421	47	91
8	0.0808	247	407	175	89
9	0.0812	262	372	0	63
Ave =	0.0805	252	429	147	95
AveAir (except sample #2)	0.0800	249	450	176	107
		Cast/Homogenized Microstructure			
25	0.0794	150	338	5	164
26	0.0794	173	393	5	157.5
27	0.0808	160	327	5	177.5
29	0.0805	163	324	3	149
28	0.0809	168	385	25	156
Ave =	0.0802	163	353	9	161
AveAir	0.0794	162	366	5	161
		Forged/Annealed Microstructure			
76	0.0802	293	603	525	103
77	0.0806	298	611	580	123
78	0.0802	300	592	510	114.5
81	0.0806	320	605	552	115
82	0.0809	312	573	520	100
83	0.0811	300	598	550	122
87	0.0811	330	582	400	83
85	0.0812	323	559	340	76
84	0.0804	312	603	580	109
Ave =	0.0807	310	592	506	105
AveAir	0.0804	296	607	553	113
		Forged/Heat Treated Microstructure			
97	0.0800	460	710	685	96
98	0.0800	438	698	670	94
99	0.0800	440	705	670	99
101	0.0800	453	698	630	89
100	0.0800	452	703	670	91.5
Ave =	0.0800	449	703	665	94
AveAir	0.0800	449	704	678	95

Table 8.2 Reduced Data From Slow Strain Rate Tests

Sample Number	Type Test	Yield Str KSI	UTS KSI	Fract Ld/ UTS Load Percent	Elongation	Yield Energy in-lbf
		Cast Microstructure				
2	Air	59.1	83.9	90.9	30.00	N/A
3	Air	53.5	85.1	36.2	30.67	65
4	Air	45.8	88.1	50.8	38.33	N/A
5	Air	49.3	95.5	30.6	38.33	89.2
6	SW	50.0	89.4	61.8	32.83	74.3
7	+1V	48.3	80.7	11.2	30.33	63.1
8	-1V	48.2	79.4	43.0	29.67	60.4
9	-3V	50.6	71.8	0.0	21.00	39.8
Average =		49.4	84.3	34.3	31.6	65.3
Ave Air =		49.5	89.6	39.0	35.8	77.1
(except sample #2)						
		Cast/Homogenized Microstructure				
25	Air	30.3	68.3	1.5	54.67	76.2
26	Air	34.9	79.4	1.3	52.50	92.6
27	SW	31.2	63.8	1.5	59.17	86.4
29	+1.0V	32.0	63.7	0.9	49.67	72.8
28	-1.0V	32.7	74.9	6.5	52.00	89.5
Average =		32.2	70.0	2.4	53.6	83.5
Ave Air =		32.6	73.8	1.4	53.6	84.4
		Forged/Annealed Microstructure				
76	Air	58.0	119.4	87.1	34.33	113.6
77	Air	58.4	119.8	94.9	41.00	125.7
78	SW	59.4	117.2	86.1	38.17	113.8
81	+1V	62.7	118.6	91.2	38.33	119.7
82	+.5V	60.7	111.5	90.8	33.33	96.9
83	-1V	58.1	115.8	92.0	40.67	129.6
87	-2V	63.9	112.7	68.7	27.67	82.6
85	-3V	62.4	107.9	60.8	25.33	70.0
84	-6VDI	61.5	118.8	96.2	36.33	111.2
Average =		60.6	115.7	85.6	35.0	107.0
Ave Air =		58.2	119.6	91.0	37.7	119.7
		Forged/Heat Treated Microstructure				
97	Air	91.5	141.2	96.5	32.00	115.3
98	Air	87.1	138.9	96.0	31.33	115.8
99	SW	87.5	140.3	95.0	33.00	122.4
101	+1V	90.1	138.9	90.5	29.67	116.2
100	-1V	89.9	139.9	95.3	30.50	118.8
Average =		89.2	139.5	94.5	31.5	116.9
Ave Air =		89.3	140.1	95.2	31.7	116.6

Table 8.3 Passivation of Alloy 625 in the Yield Region

Voltage applied to Slow Strain Rate Tensile Test specimens by E & EG potentiostat. Electrolyte in use was synthetic ASTM sea water without heavy metals. Current measured at approximate 5 percent elongation after yield.

Voltage Applied (Volts SCE)	Current (Amps)	Log of Current
+1.0	0.0095	-2.022
+0.5	0.0050	-2.301
-0.5	$2.0x1^{-11}$	-10.699
-1.0	$5.0x10^{-6}$	-5.280
-2.0	0.237	-0.625
-3.0	0.435	-0.314

Figure 12 **Passivation of Alloy 625 in Yield Region**

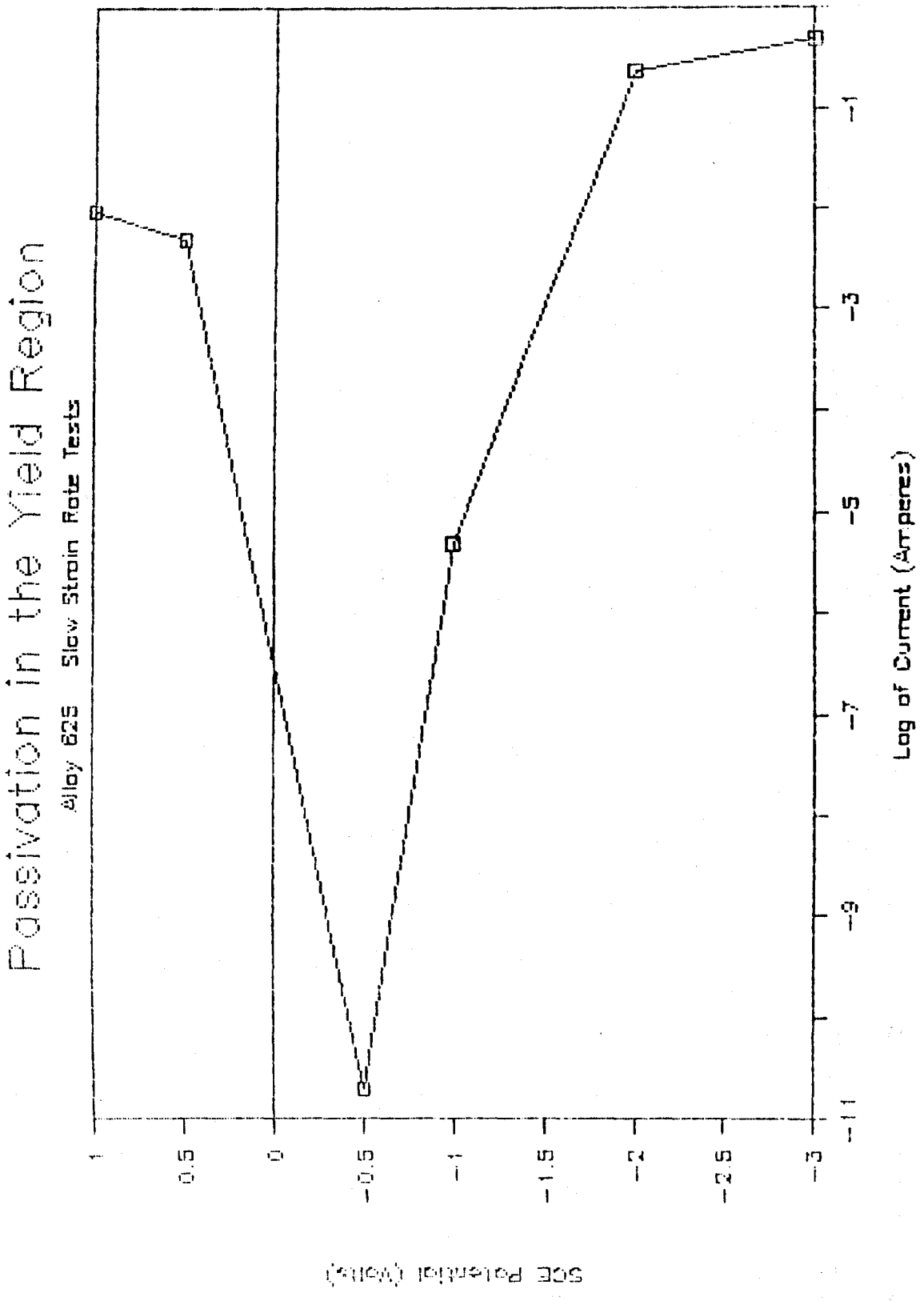

Figure 13 Graph of Slow Strain Rate Test Results for "As Cast" Alloy 625 - Test Condition versus Yield Stress, Ultimate Stress, and Percent Fracture Load of UTS Load

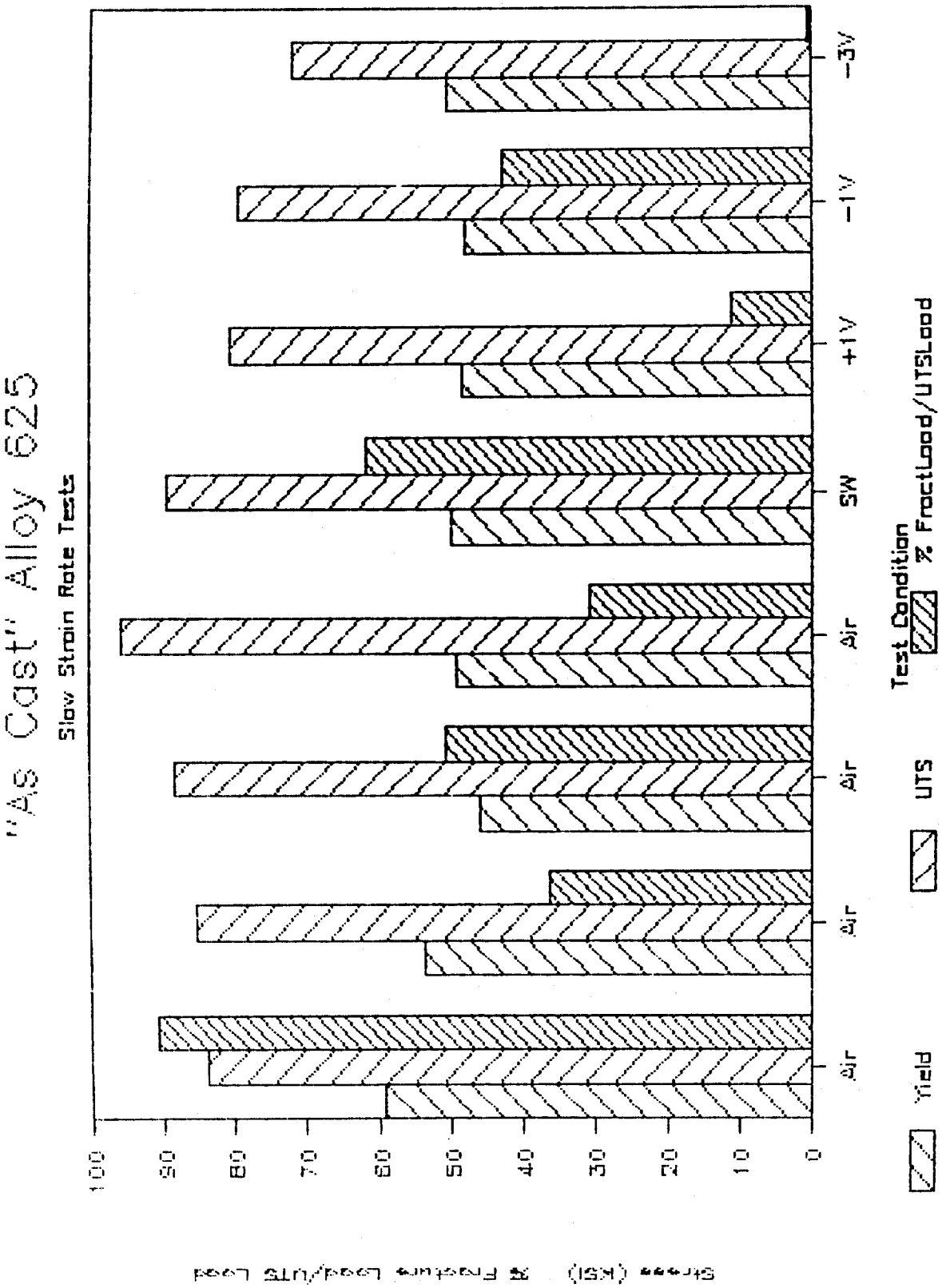

Figure 14 Graph of Slow Strain Rate Test Results for "As Cast" Alloy 625 - Test Condition versus Percent Elongation and Yield Work Energy

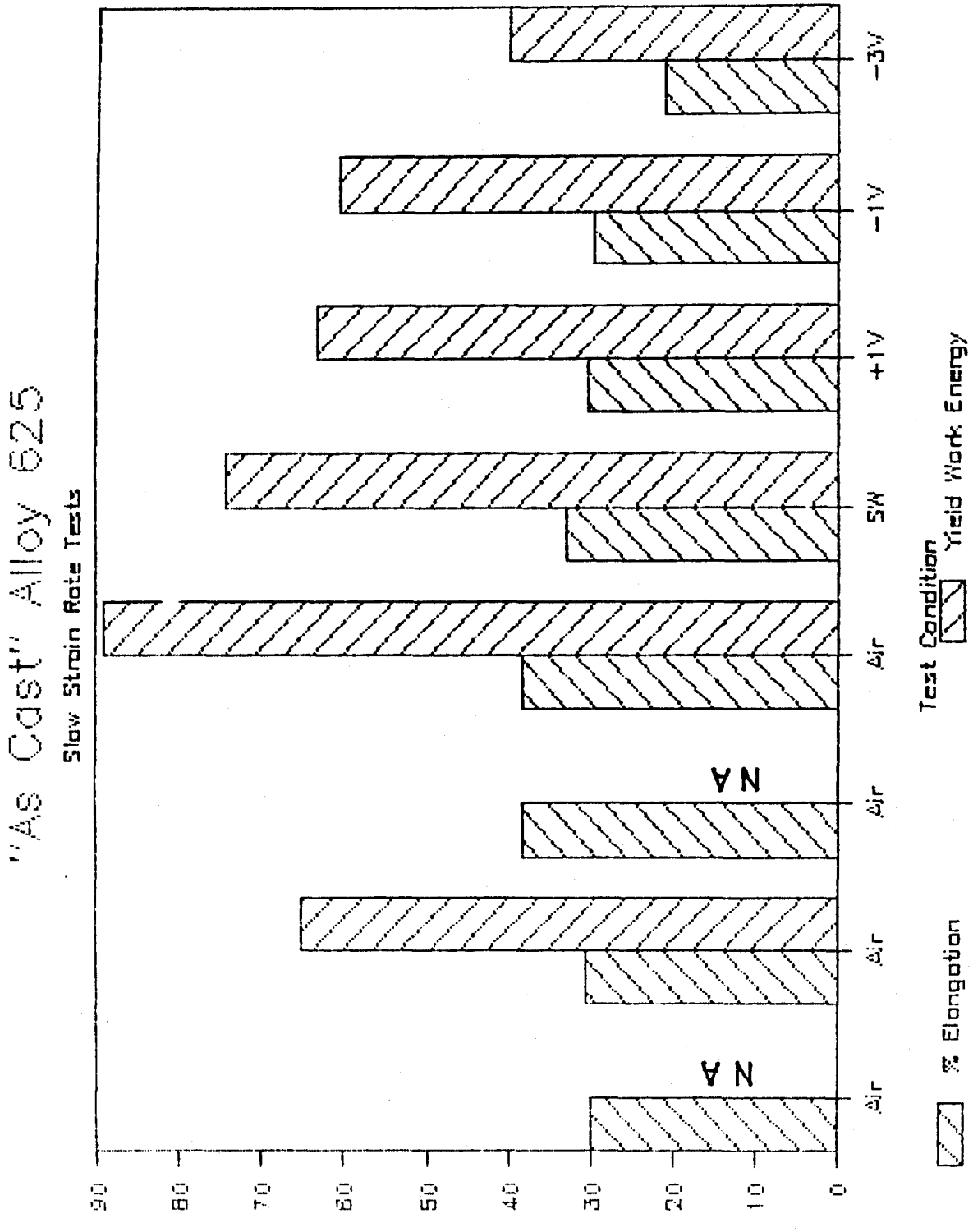

Yield Energy (in-lbf) and % Elongation

Figure 15 Graph of Slow Strain Rate Test Results for "Cast/Homogenized" Alloy 625 - Test Condition versus Yield Stress, Ultimate Stress, and Percent Fracture Load of UTS Load

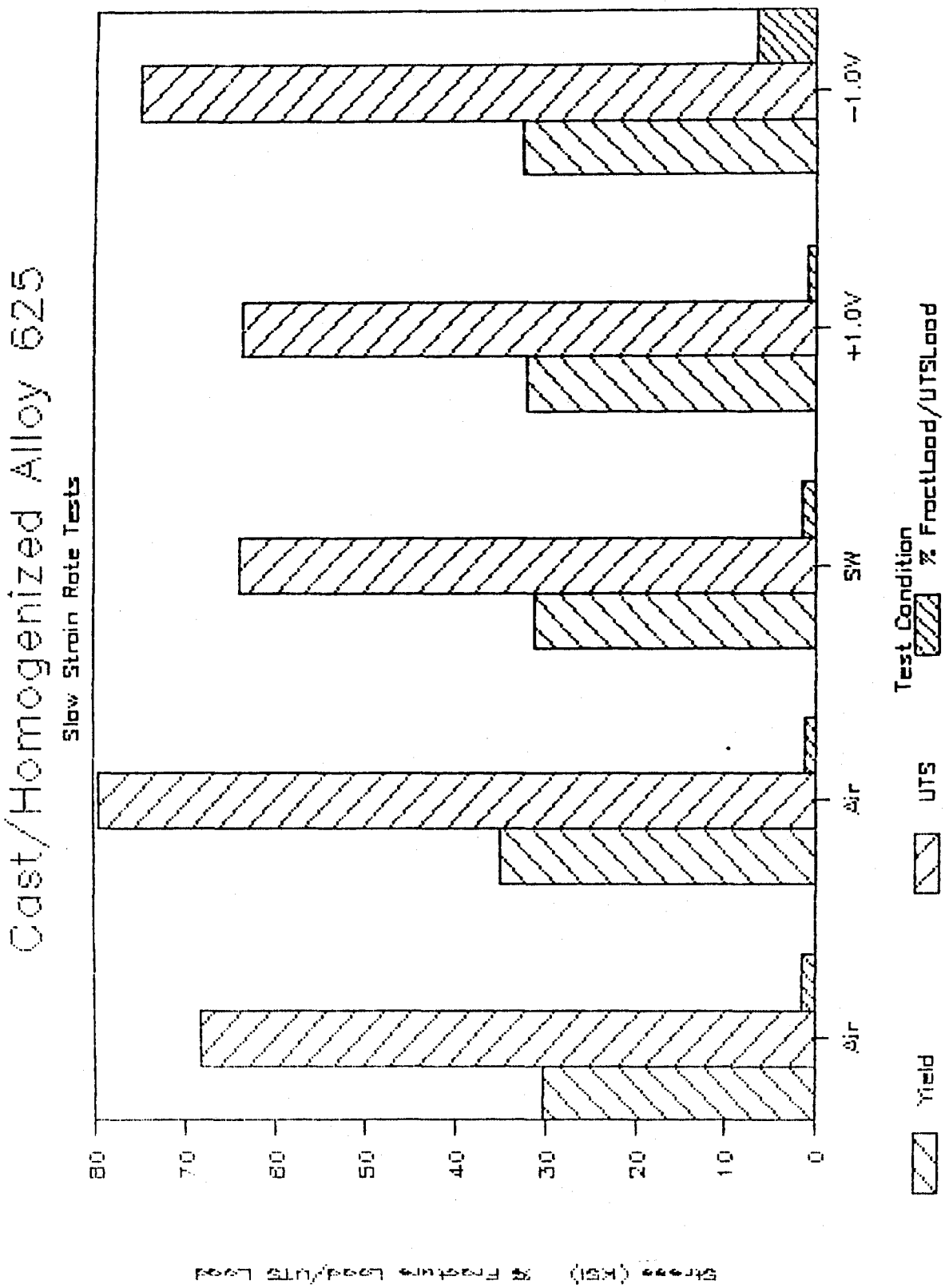

Figure 16 **Graph of Slow Strain Rate Test Results for "Cast/Homogenized" Alloy 625 - Test Condition versus Percent Elongation and Yield Work Energy**

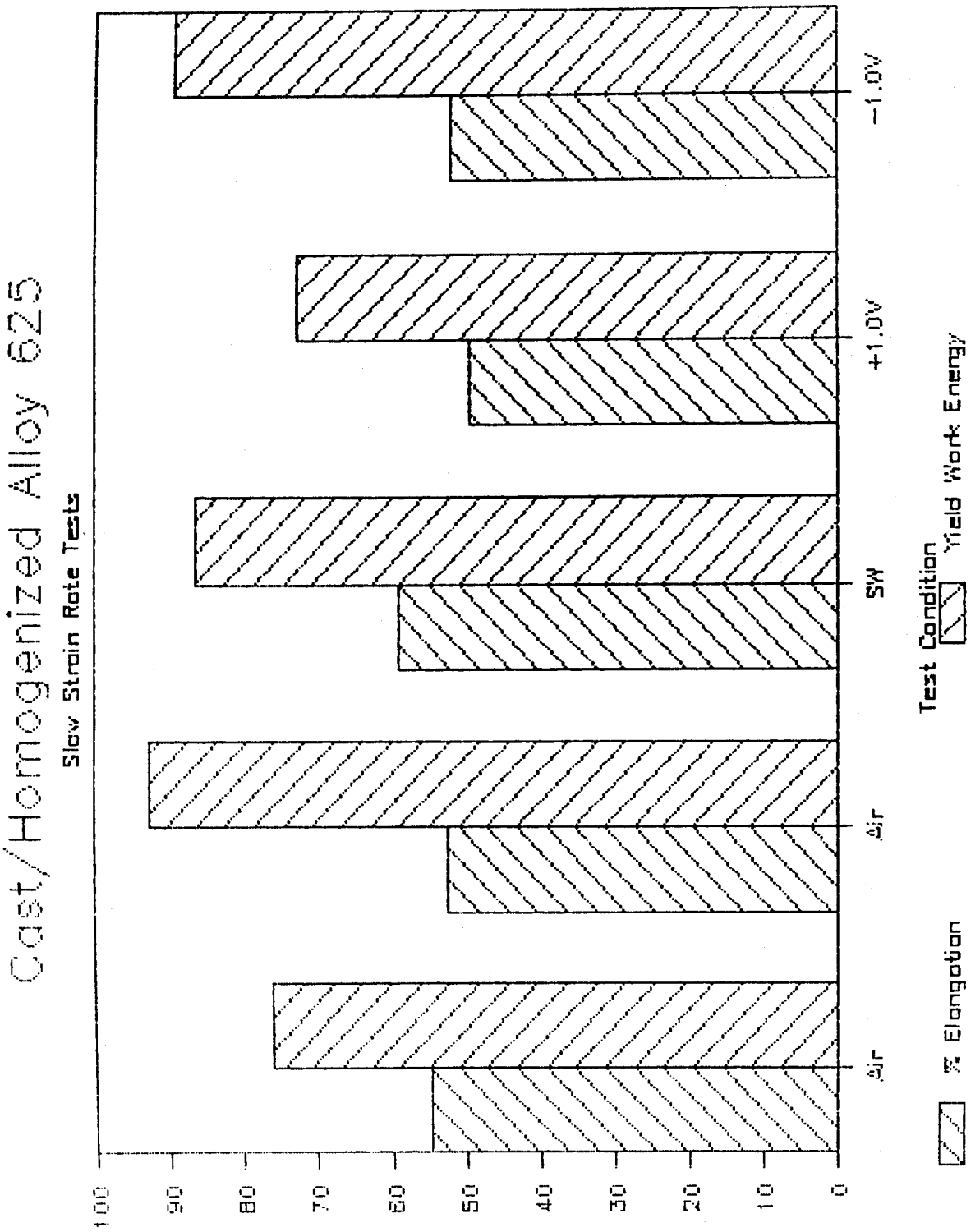

Figure 17 Graph of Slow Strain Rate Test Results for "Forged/Annealed" Alloy 625 - Test Condition versus Yield Stress, Ultimate Stress, and Percent Fracture Load of UTS Load

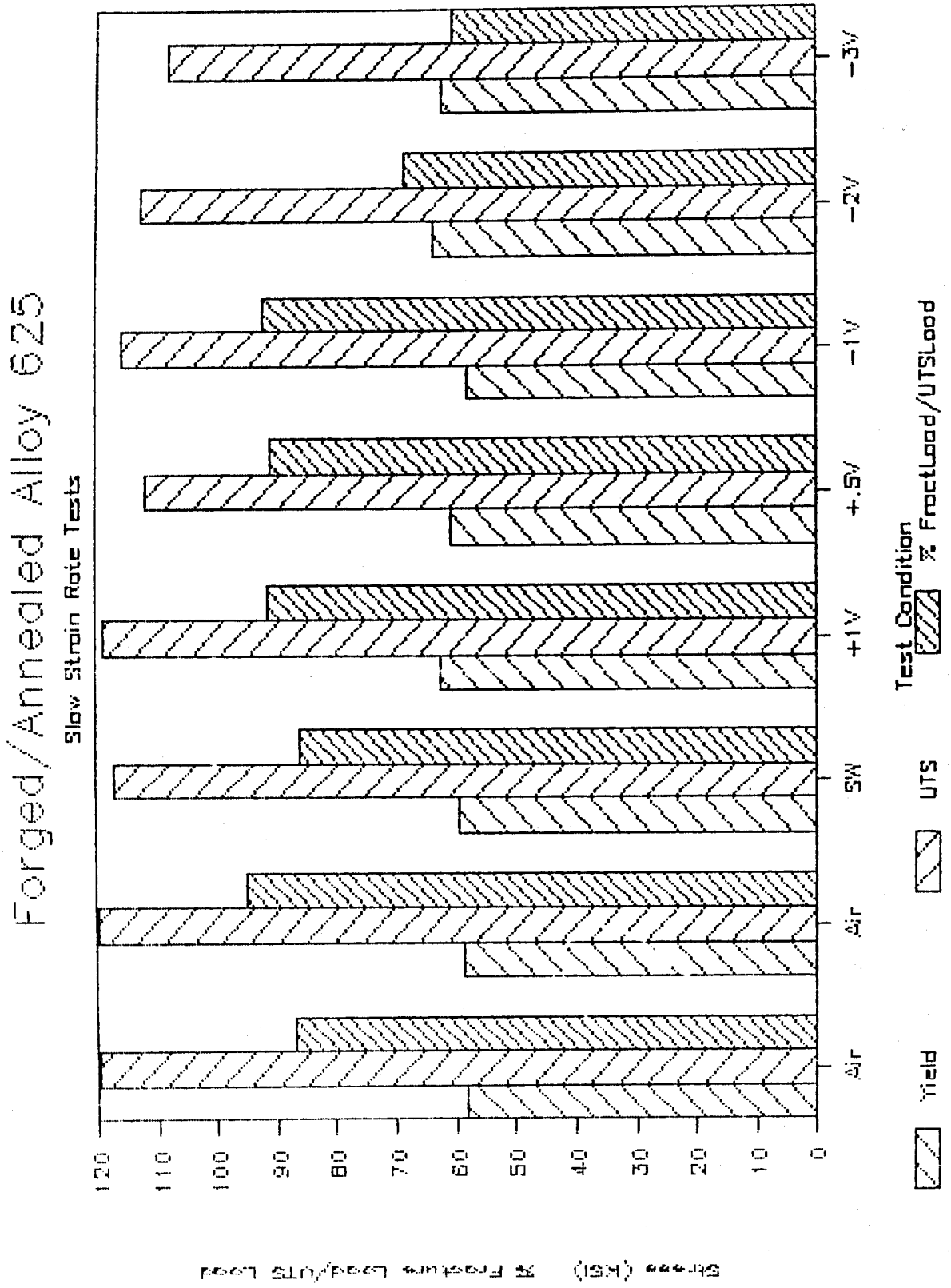

Figure 18 **Graph of Slow Strain Rate Test Results for "Forged/Annealed" Alloy 625 - Test Condition versus Percent Elongation and Yield Work Energy**

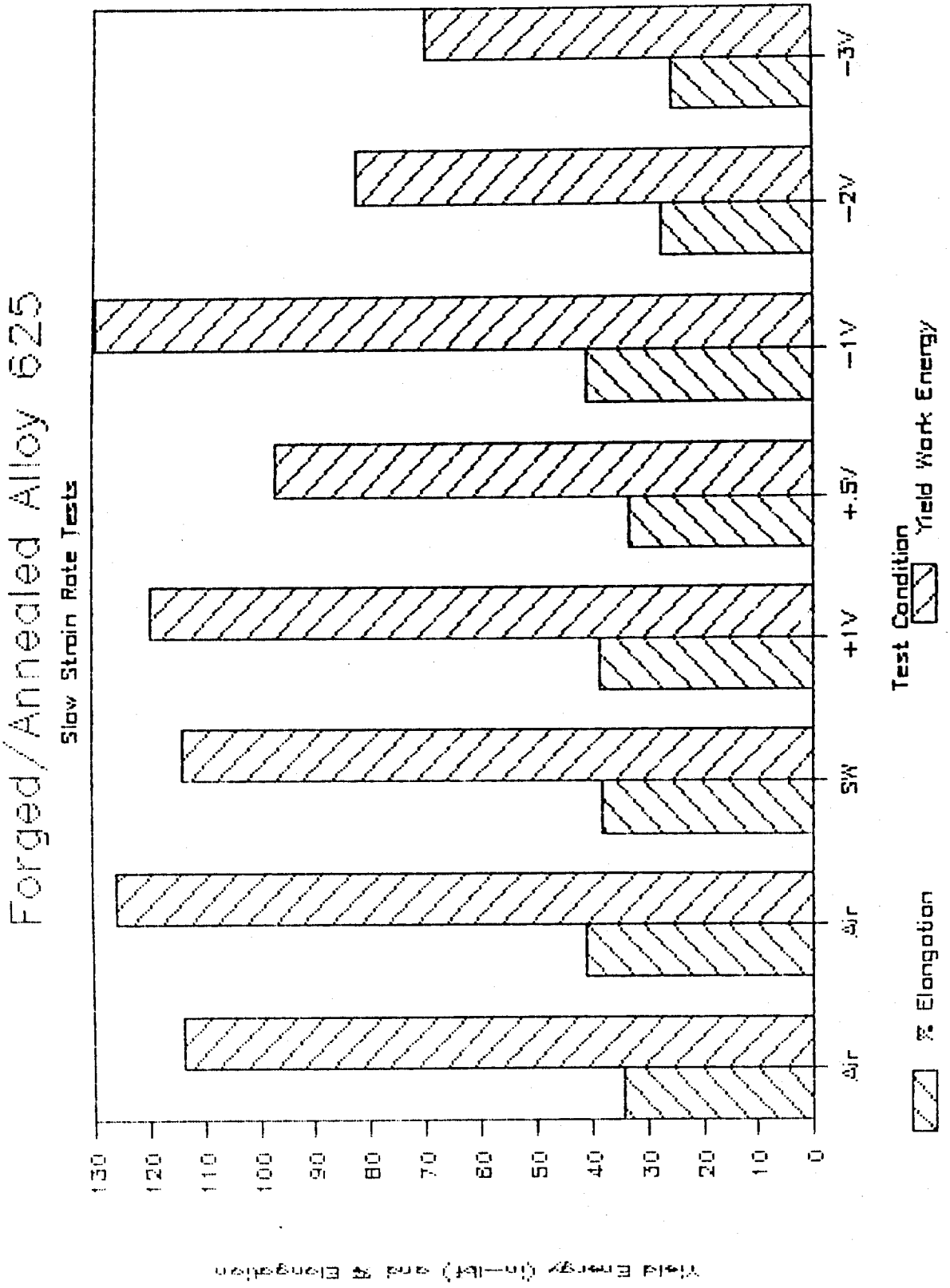

Figure 19 Graph of Slow Strain Rate Test Results for "Forged/Heat Treated" Alloy 625 - Test Condition versus Yield Stress, Ultimate Stress, and Percent Fracture Load of UTS Load

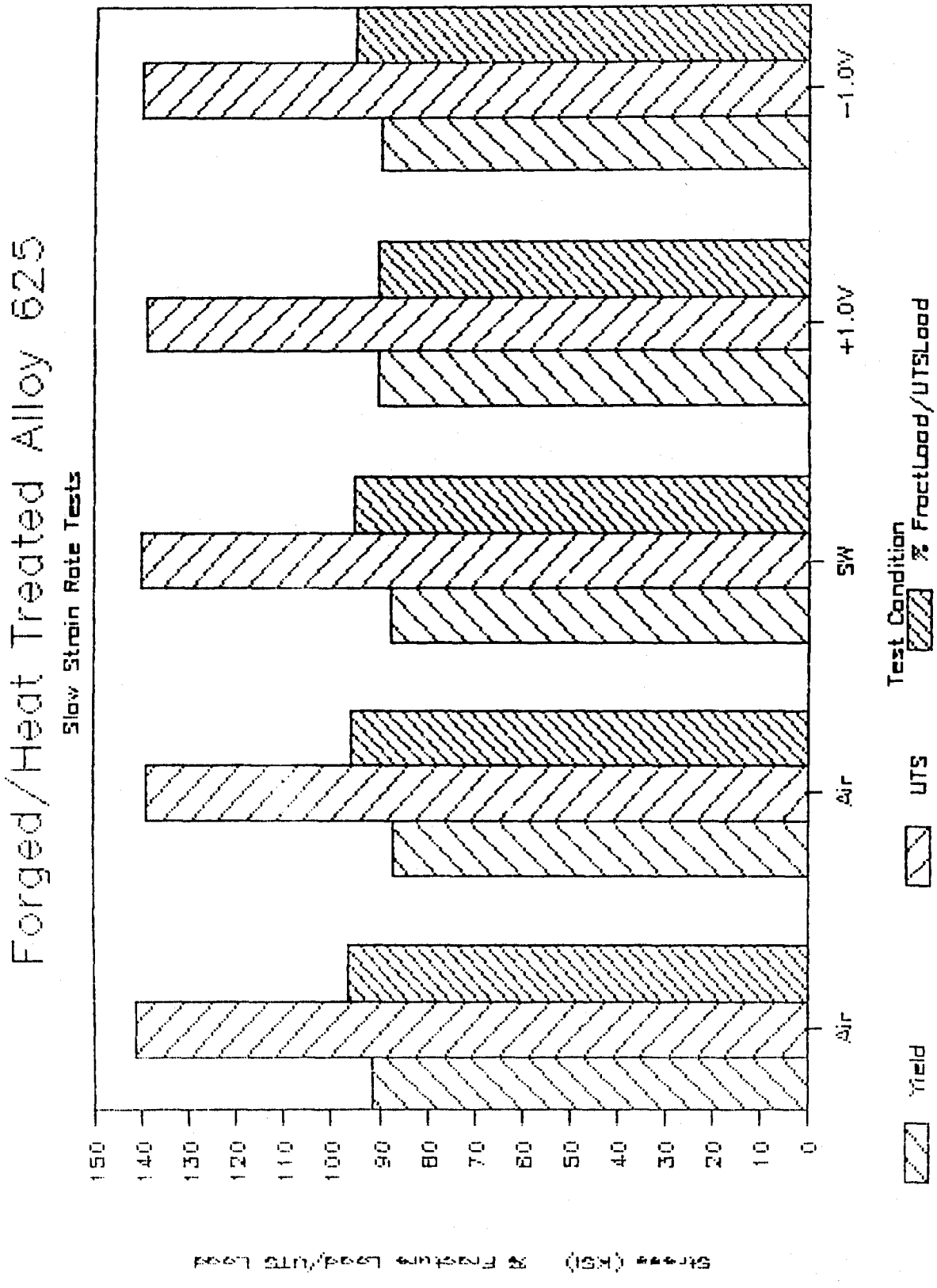

Figure 20 Graph of Slow Strain Rate Test Results for "Forged/Heat Treated" Alloy 625 - Test Condition versus Percent Elongation and Yield Work Energy

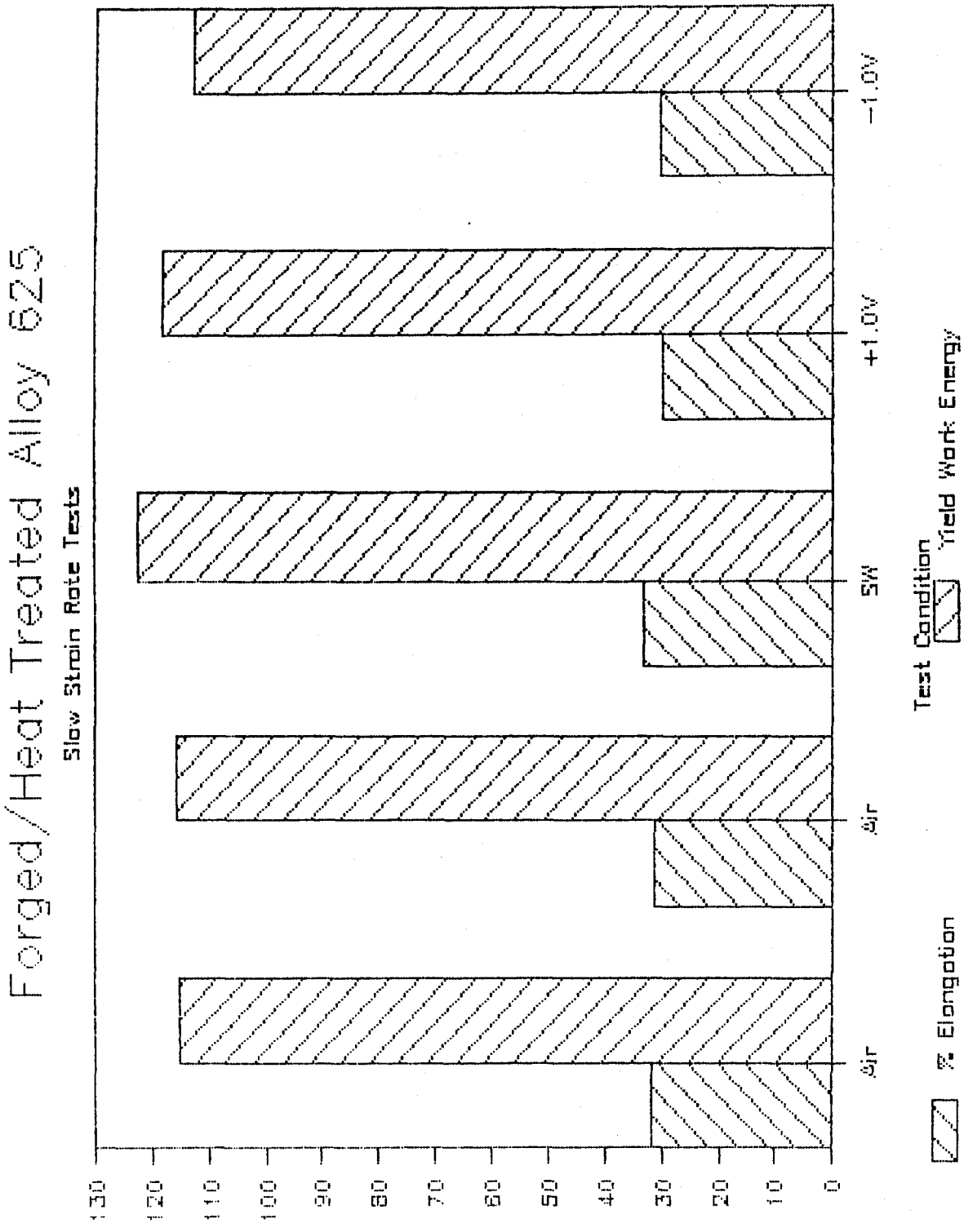

8.2 MICROANALYSIS OF TESTED SPECIMENS

The fractured slow strain rate test specimens were analyzed with optical and scanning electron microscopes (JOEL JXA 840 and Amray 1200B) on their fracture surfaces, elongated gage lengths, and sectioned gage lengths.

Before viewing, the specimens were ultrasonicly cleaned in acetone, rinsed with alcohol, and air jet dried. A series of photomicrographs were taken of the gage lengths and fracture surfaces. The gage lengths are shown in Figures 21 through 27. The fracture surfaces are shown in Figures 28 through 36. The numbers in the lower left hand corners of the pictures are the specimen numbers as listed on Table 8.1.

All microstructures tested at anodic potentials had general surface film corrosion that was shattered during the elongation process. This surface of "mud cracking" was microprobed to determine its major metal constituents. They were 43% Ni, 27% Mo, 21% Cr, 7% Fe, 1% Cb, and 1% Ti. The shoulder of the specimen was also microprobed for a comparison. It had 65% NI, 8% Mo, 23% Cr, 4% FE, and .4% Ti in its composition. The high molybdenum content in the former surface indicates corrosion took place. A high level of this element would also enhance the "mud cracking" effect. The fracture surfaces of these anodically tested specimens matched the fracture surfaces of the respective microstructures tested in air and sea water without potential.

The secondary cracking on the gage surfaces of samples tested in air, sea water without potential, and at anodic potentials was very limited and appeared to be only large carbides shattered on or slightly below the surface. See Figures 21 and 24.

The -1.0 volt specimen surfaces had a larger percentage of cracks, but they again appeared to be caused by large carbides on or near the surface. However, the cracks tended to be much larger than the initiating carbides. See Figures 25 and 27.

The -2.0 and -3.0 volt specimen surfaces had many more secondary cracks that did not all appear to contain shattered carbides. These cracks were longer than cracks formed in other test conditions for the same microstructures. Cracks also developed in the higher stressed plastic regions of the crack tips. See Figures 22 and 26.

The top photomicrographs in Figure 25 show a testing problem that was encountered. The photomicrograph on the left matches the lower of the two on the right. The upper right one is from the other half of the specimen. The difference is that only one end of the specimen was connected to the potentiostat. This allowed uncontrolled corrosion of the other end for the short time after fracture before the potential from the potentiostat was secured. This became apparent at the completion of one of the -1.0 volt tests, when the specimen surface which had only a few

small stationary bubbles attached suddenly became enveloped in a flow of bubbles.

The fracture surfaces of the specimens varied between microstructures and between the high cathodic voltage tests and all the other tests on the same microstructure.

Figure 28 shows the fracture surface of the "as cast" material that was tested at -1.0 volt. It is representative of the other test conditions except for the -3.0 volts condition. The fracture was based on large void formations that were initiated at large MC carbide inclusion sites.

The fracture surface of the "as cast" -3.0 volt test is shown in Figure 29. This surface has quasi cleavage along its outer radial areas indicating the hydrogen environment affected its fracture mechanisms.

The "cast/homogenized" specimens, shown in the photomicrographs of Figure 30 underwent a unique fracture mechanism of localized shear slip with steps at inclusions. This was the result of preferred slip plane sliding in a large crystal. The specimen in Figure 31 was unable to fail in the same way since it had a large fault or grain boundary preventing the slip system from progressing. Thus it underwent void coalescence until the slip systems were again able to operate.

The air test and -1.0 volt test samples of the "forged/annealed" material in Figure 32 and 33 failed through microvoid coalescence. Whereas the -2.0 and -3.0 volts samples, shown in Figures 34 through 36, failed

through at least the three mechanisms of microvoid coalescence, quasi cleavage and intergranular cracking. Again the hydrogen appears to have affected the fracture.

To view the cross section of the specimens they were mounted in plastic, ground down to their midsection, and polished. The surfaces were examined optically then etched with 5 percent nital and reexamined. To obtain better resolution the specimens were reground and polished to a 0.05 micron finish, then electrolytically etched with a 10 percent hydrochloric-methanol solution for 15 seconds at 9-10 volts. A scanning electron microscope was employed to take the photomicrographs shown in Figures 37 and 38 at 500X.

Figure 37 shows some of the secondary cracks formed in the "as cast" alloy. The top two photomicrographs have cracks formed at shattered carbides, while the bottom one clearly displays intergranular cracking. This latter one was tested at the cathodic potential of -3.0 volts.

Figure 38, photomicrographs of the "forged/annealed" microstructure, again indicates the same behavior.

Figures 37 and 38 also show the size and population of the carbides, along with how they shatter when stressed in tension. These shattered carbides are nucleation sites for void formations and intergranular cracks.

8.3 CORRELATION OF TENSILE TESTS

The data obtained from the tensile tests conducted on the same material, with the same heat treatment and

mechanical working history as the slow strain rate tests were compared to the mechanical properties obtained from the slow strain rate tests. Figures 39 through 42 display the results for both style tests combined together for each microstructure. These results show no statistically significant differences between the tensile tests and the slow strain rate tests for air, sea water, +1.0 volt, and -1.0 volt, even though the gage diameters and strain rates were different.

Figure 21 Photomicrographs of "As Cast" Alloy 625 Elongated Gage Length for Air and +1.0 Volt Test Conditions - Specimens 4 and 7

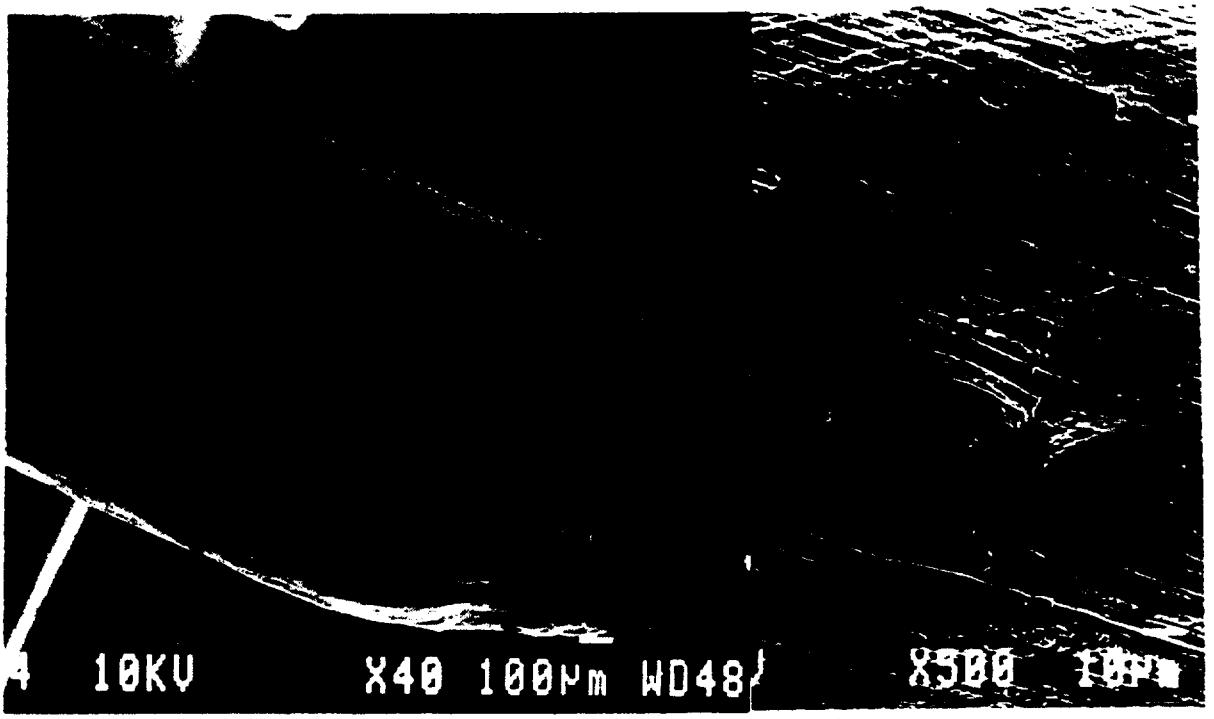

Figure 22 Photomicrographs of "As Cast" Alloy 625 Elongated Gage Length for -1.0 and -3.0 Volts Test Conditions - Specimens 8 and 9

Figure 23 Photomicrographs of "Cast/Homogenized" Alloy 625 Elongated Gage Length for Air and -1.0 Volt Test Conditions - Specimens 25 and 28

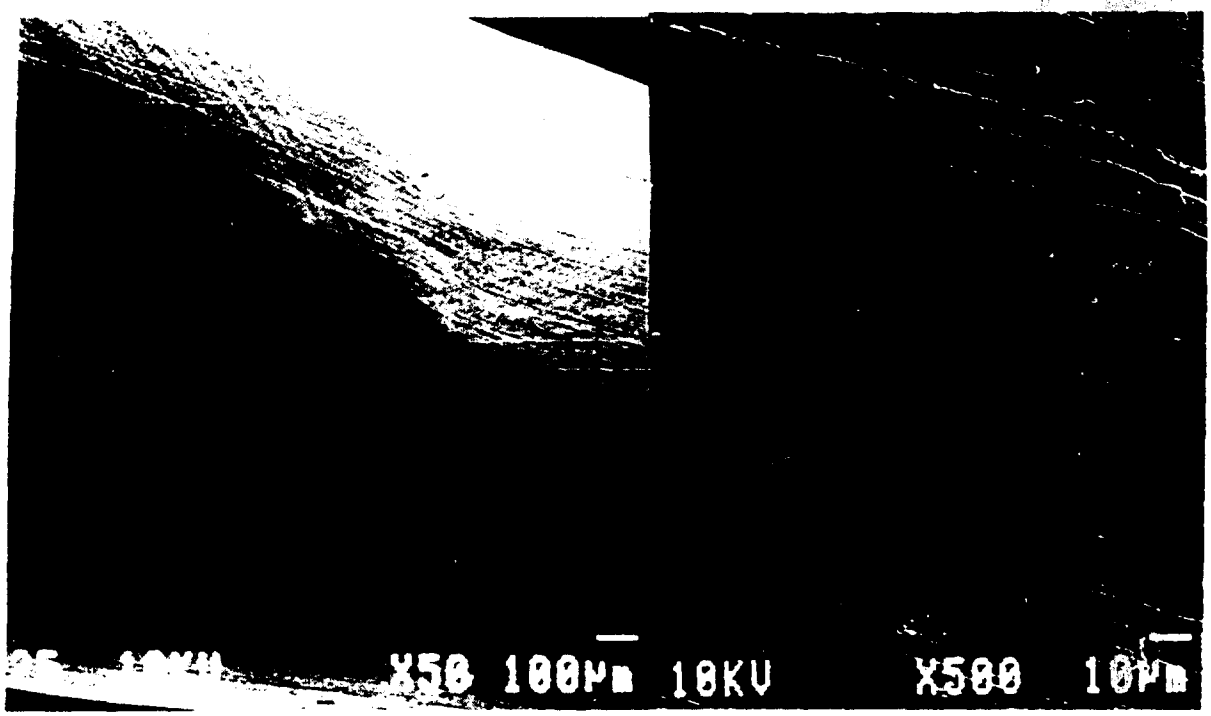

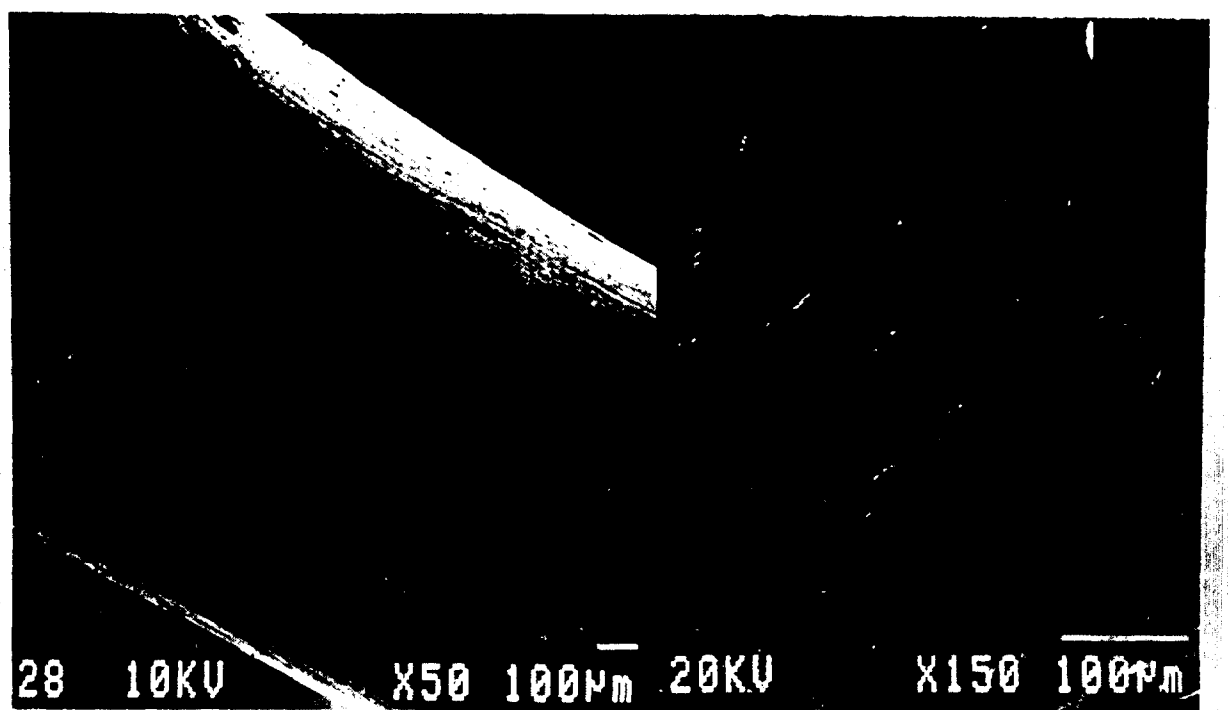

Figure 24 Photomicrographs of "Forged/Annealed" Alloy 625 Elongated Gage Length for Air and Sea Water Test Conditions - Specimens 76 and 78

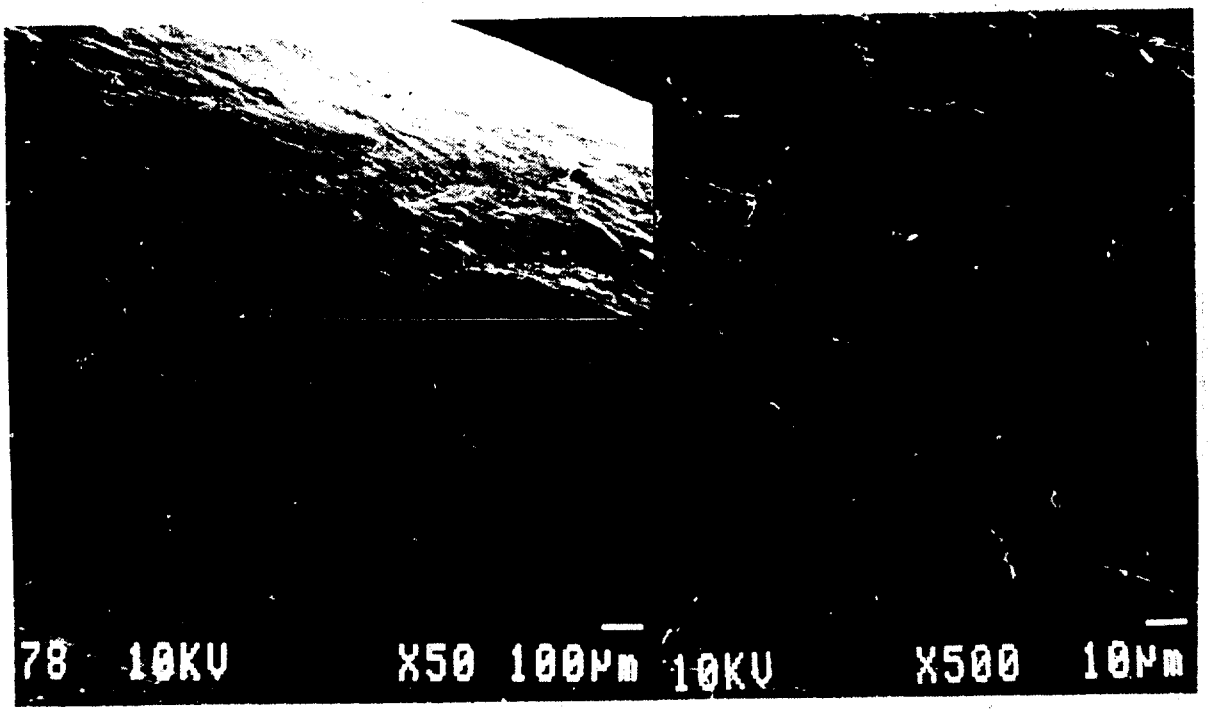

Figure 25 Photomicrographs of "Forged/Annealed" Alloy 625 Elongated Gage Length for +1.0 and -1.0 Volts Test Conditions - Specimens 81 and 83

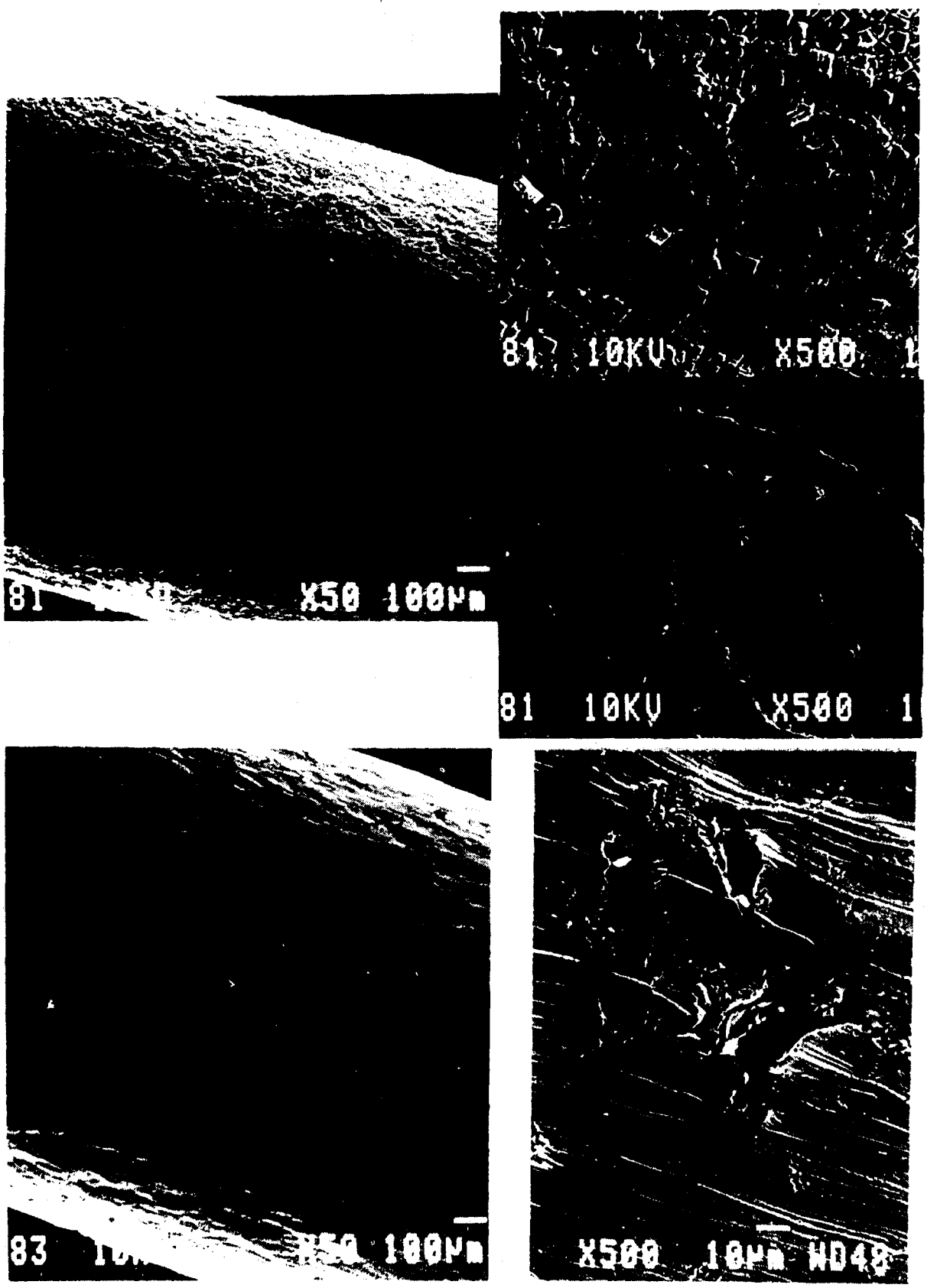

Figure 26 Photomicrographs of "Forged/Annealed" Alloy 625 Elongated Gage Length for -3.0 and -2.0 Volts Test Conditions - Specimens 85 and 87

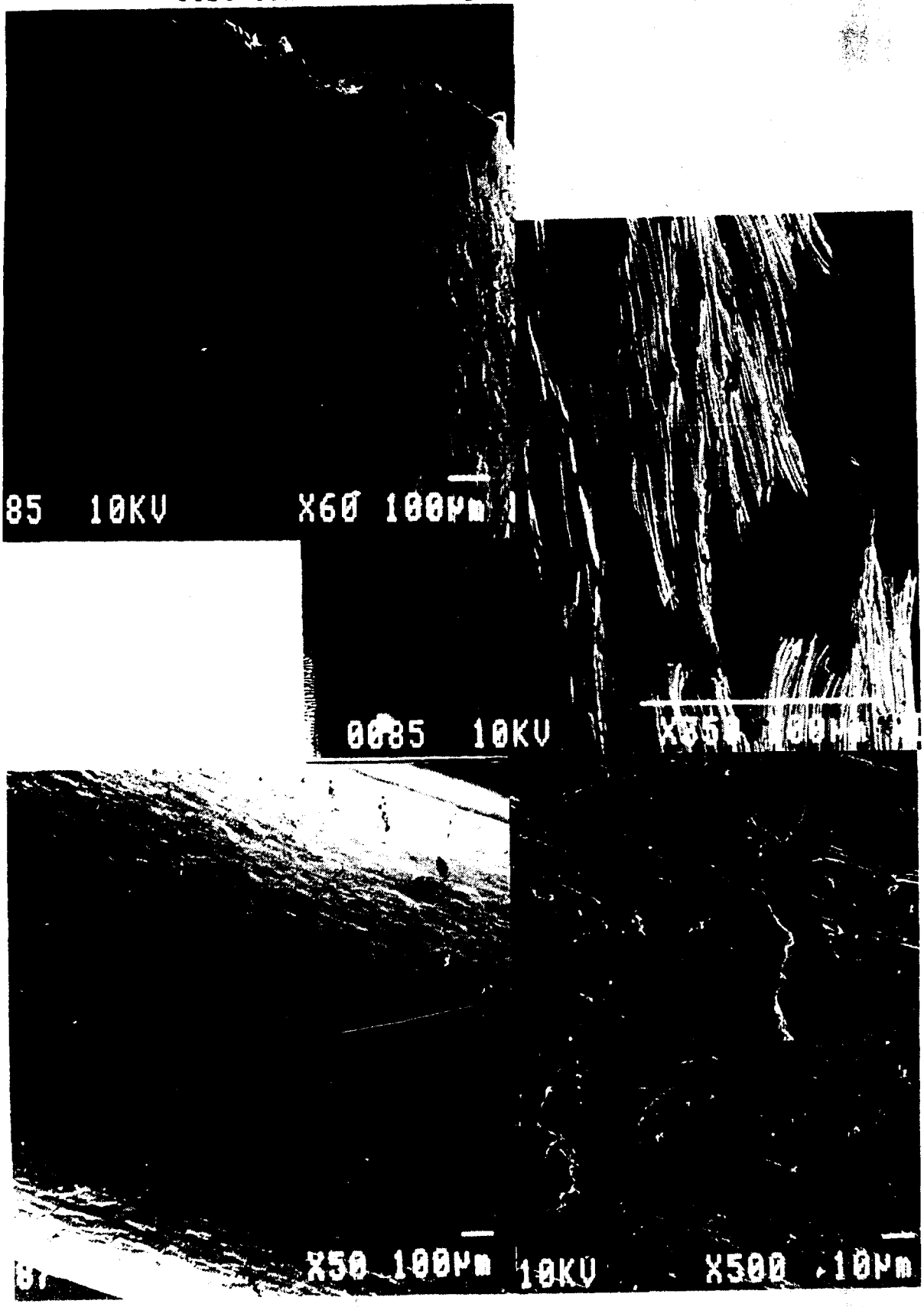

Figure 27 Photomicrographs of "Forged/Heat Treated" Alloy 625
Elongated Gage Length for -1.0 and +1.0 Volts
Test Conditions - Specimens 100 and 101

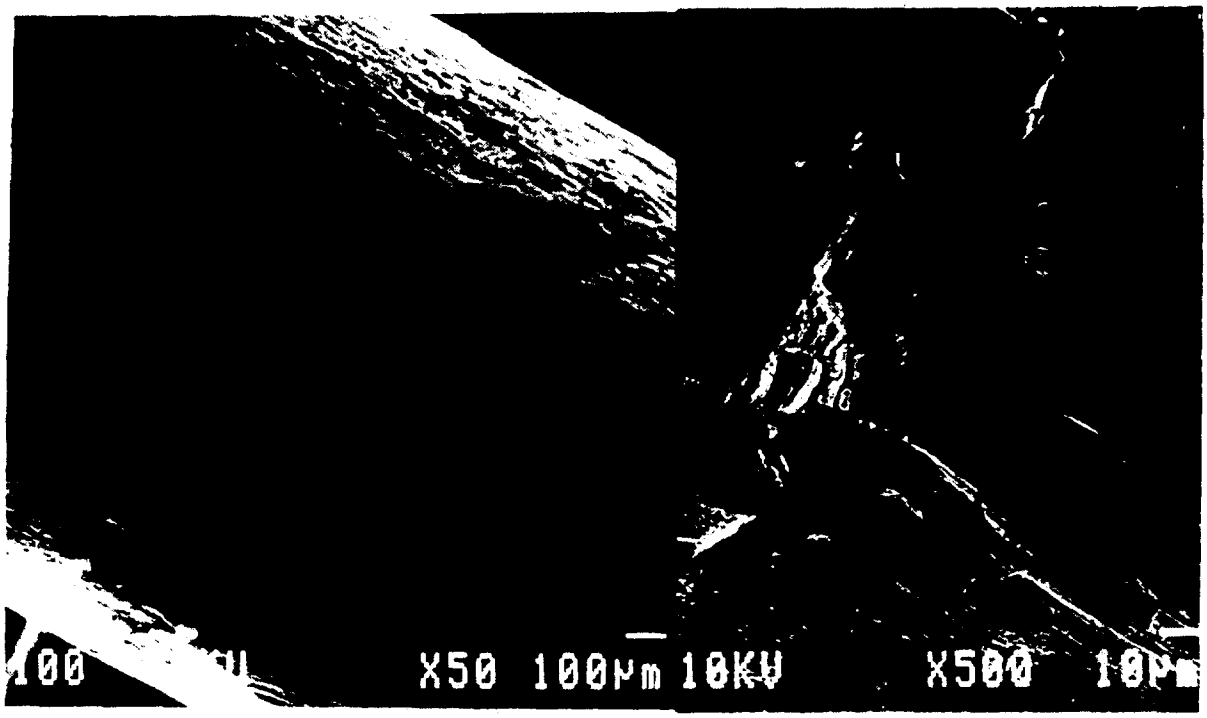

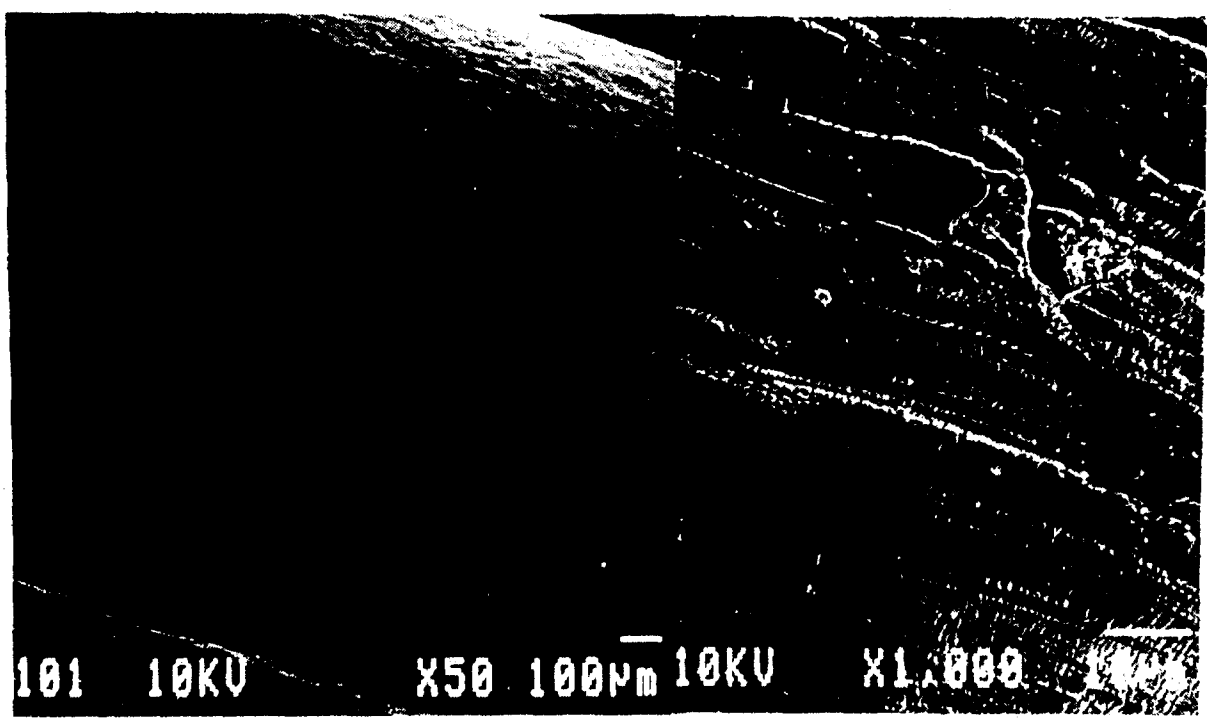

Figure 28 Photomicrographs of "As Cast" Alloy 625 Fracture Surface for -1.0 Volt Test Condition Specimen 8

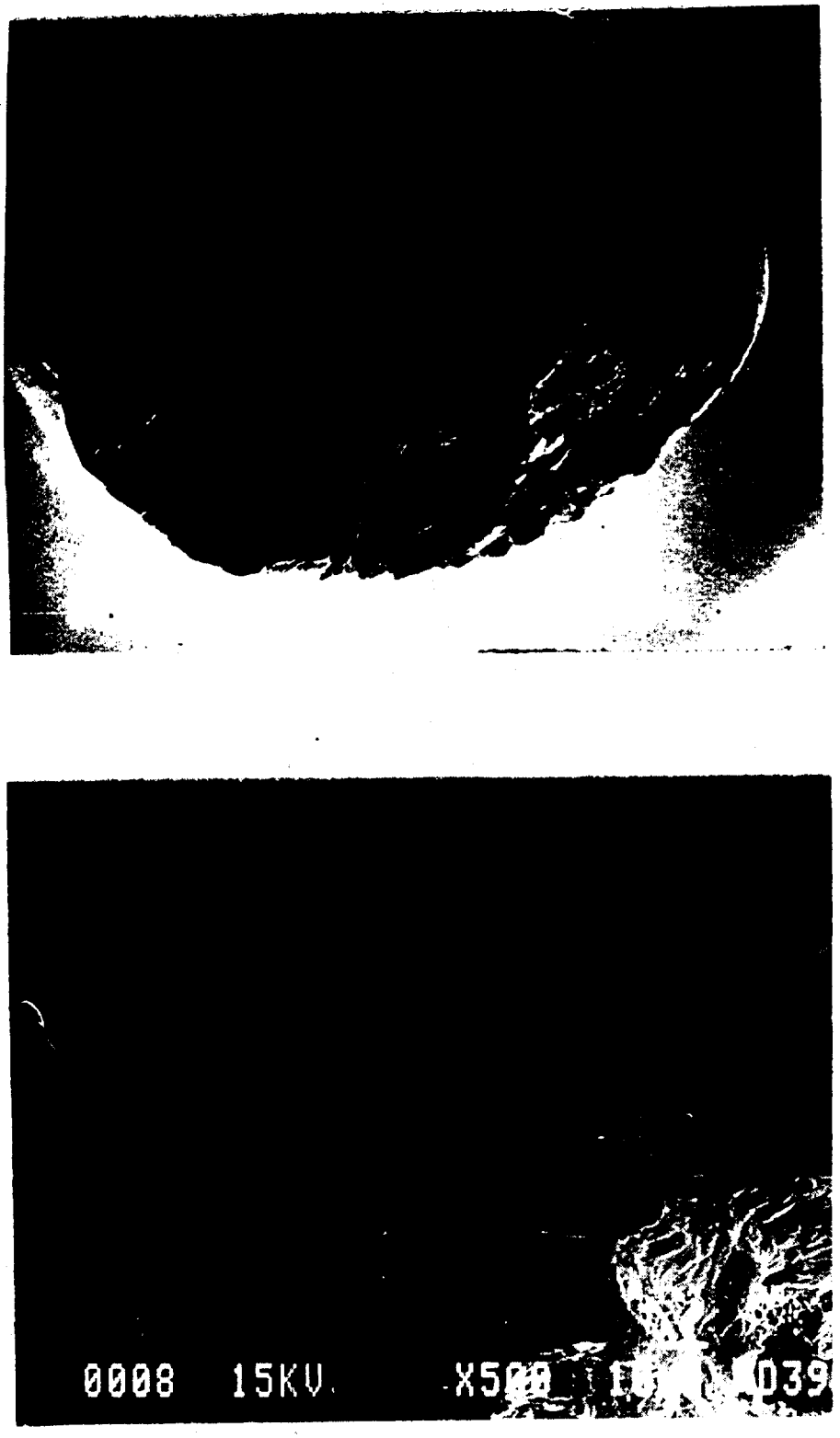

Figure 29 Photomicrographs of "As Cast" Alloy 625 Fracture Surface for -3.0 Volts Test Condition Specimen 9

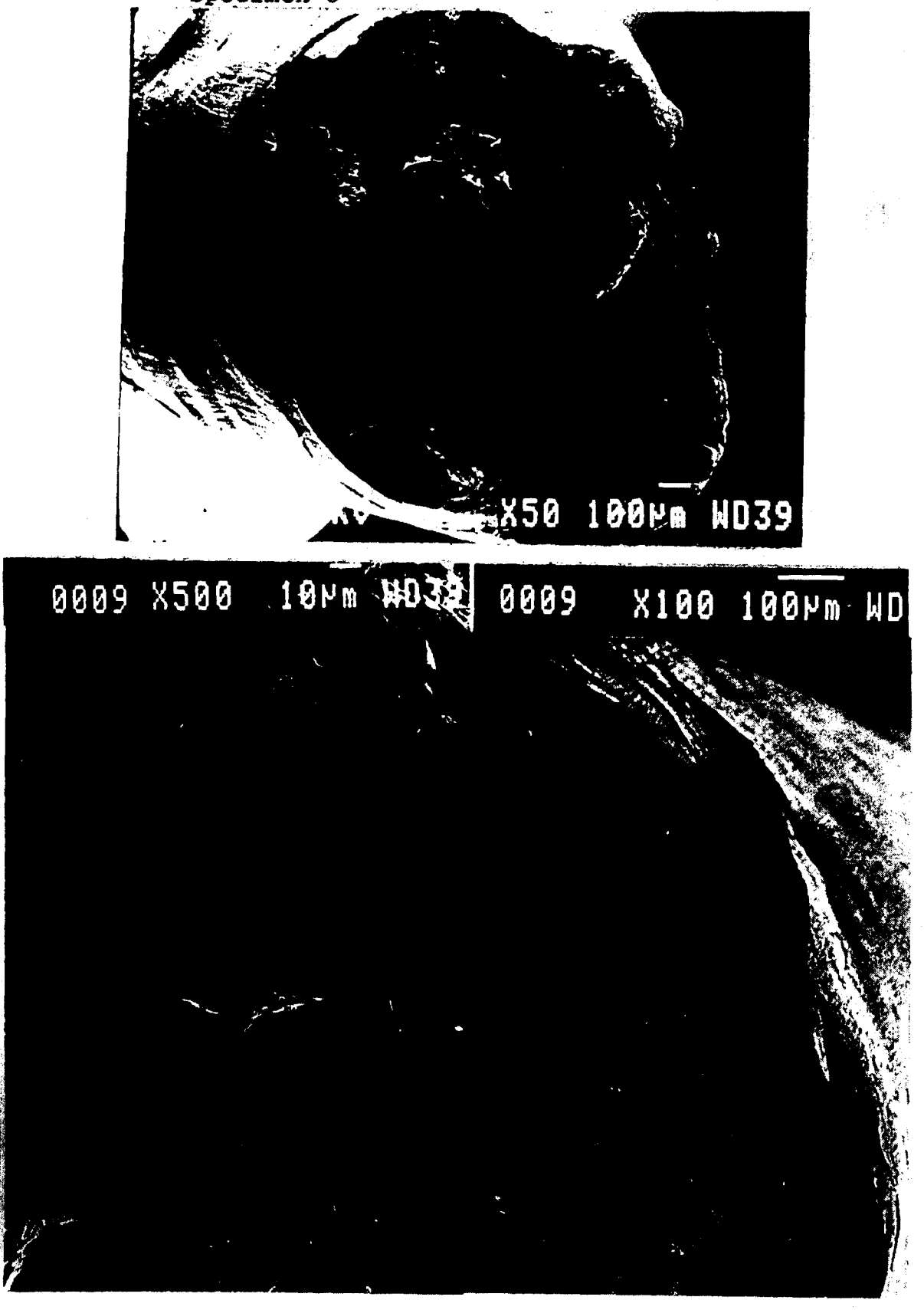

Figure 30 Photomicrographs of "Cast/Homogenized" Alloy 625 Fracture Surface for Air and +1.0 Volt Test Conditions - Specimens 25 and 29

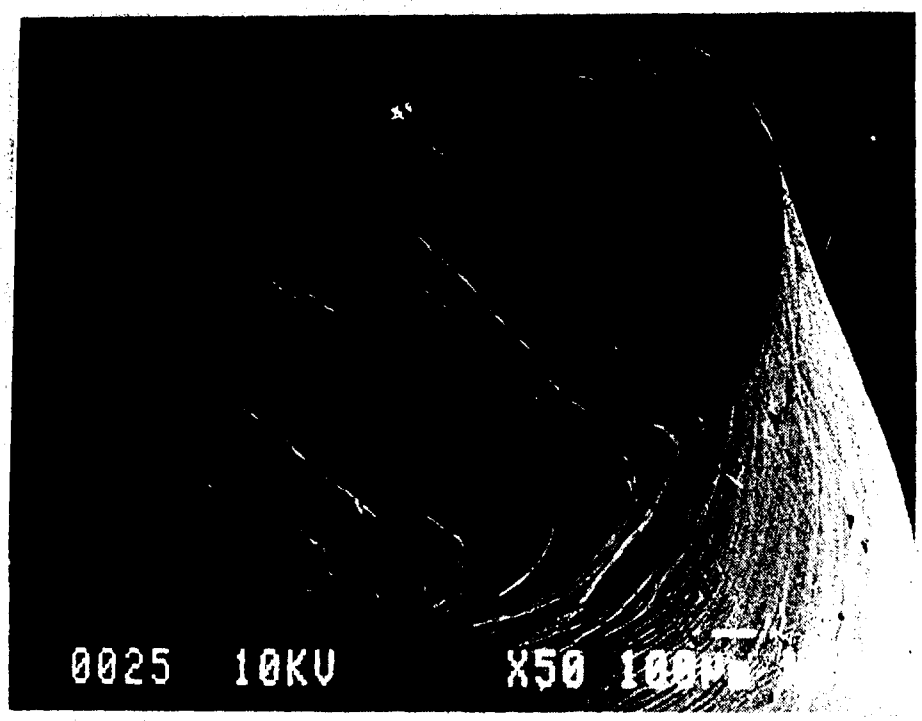

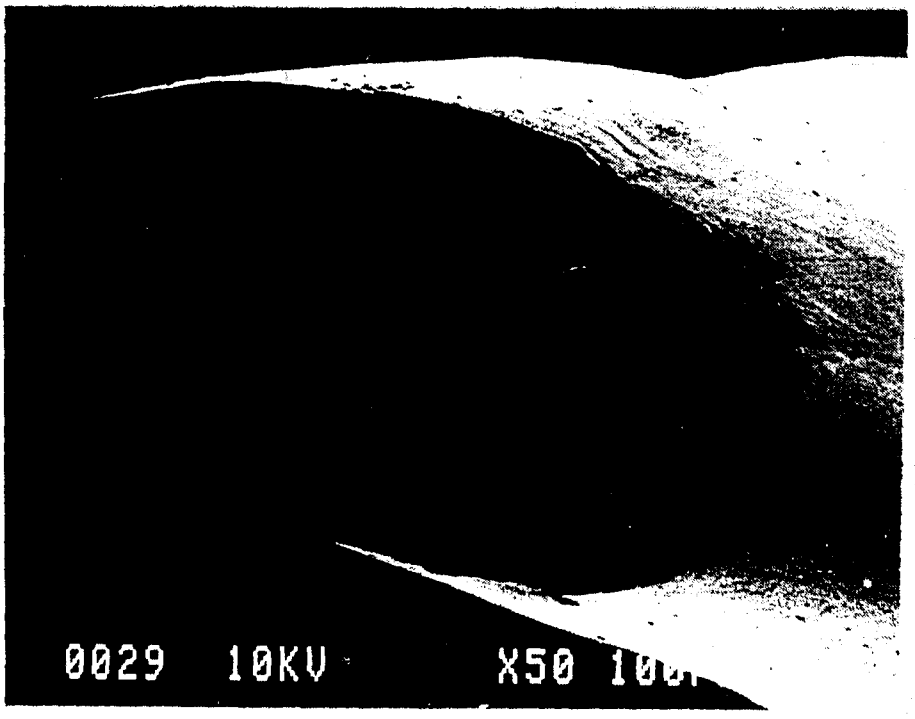

Figure 31 Photomicrographs of "Cast/Homogenized" Alloy 625 Fracture Surface for -1.0 Volt Test Condition - Specimen 28

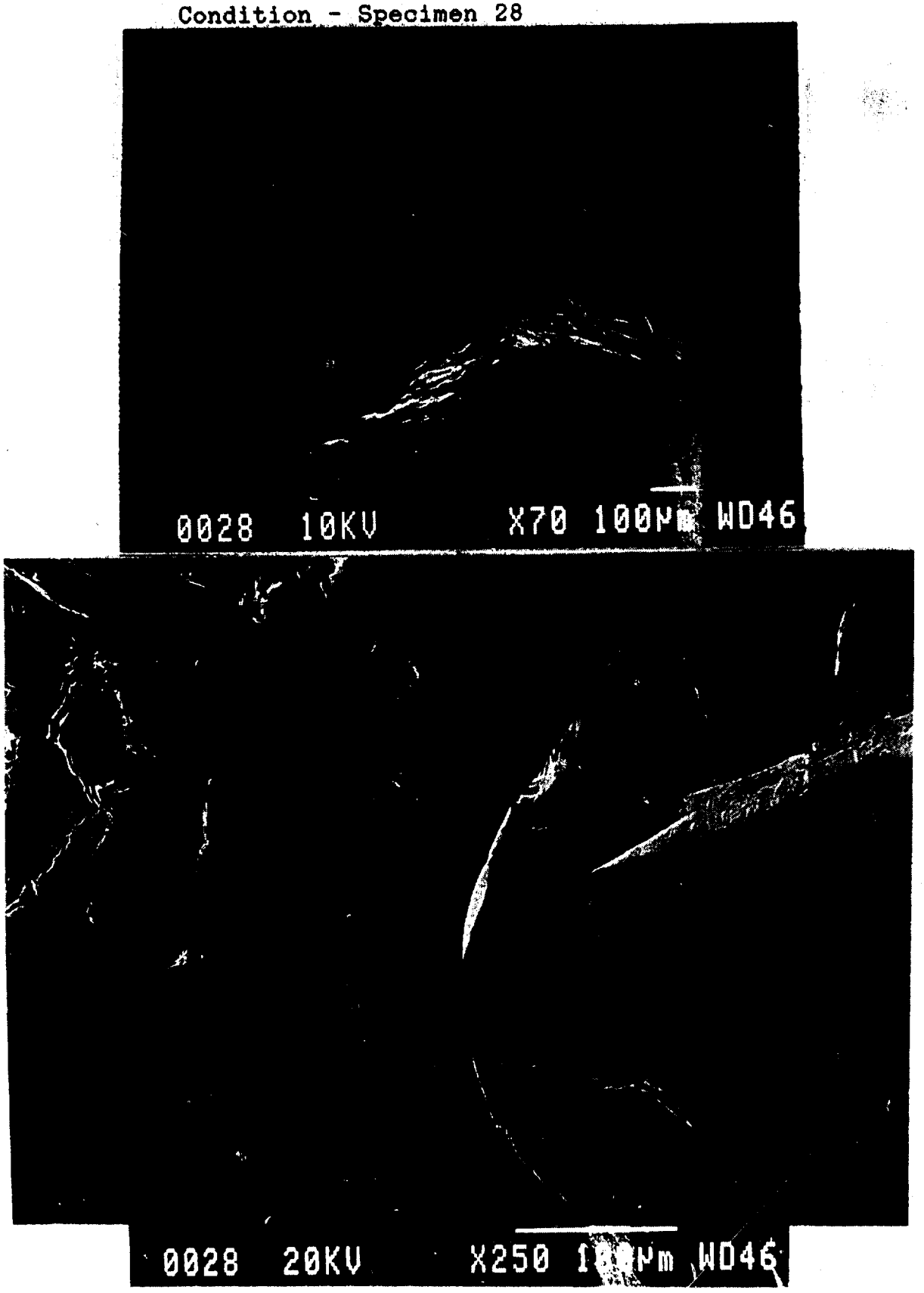

Figure 32 Photomicrographs of "Forged/Annealed" Alloy 625 Fracture Surface for Air Test Condition Specimen 76

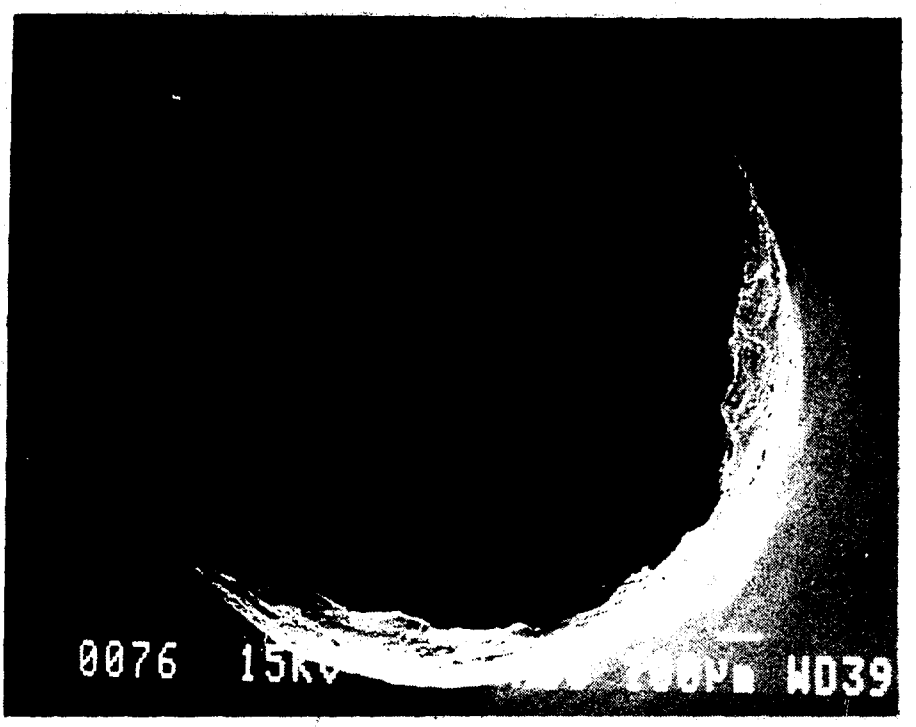

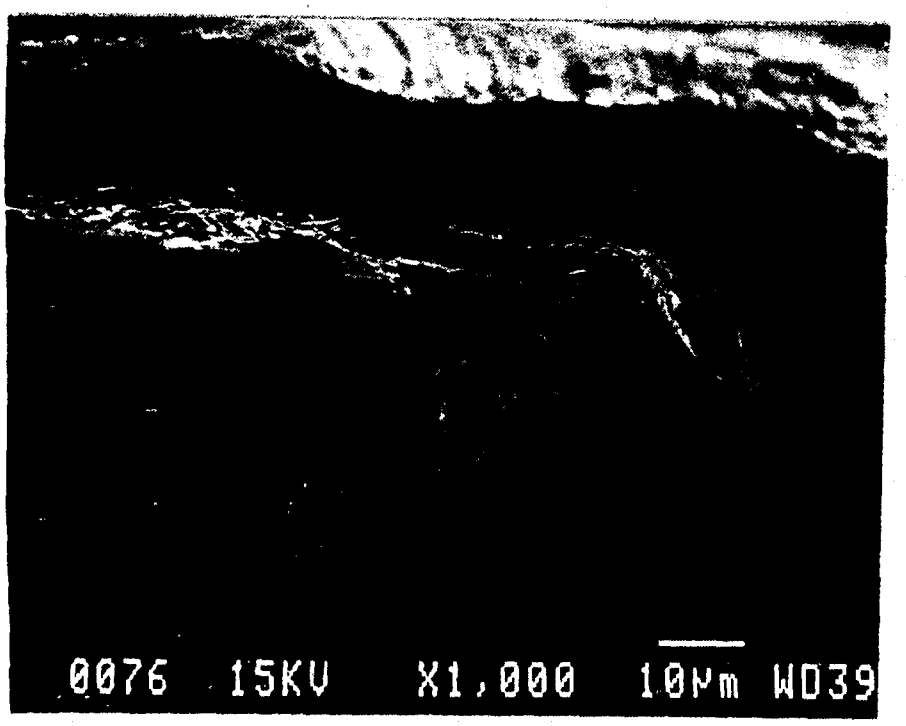

Figure 33 Photomicrographs of "Forged/Annealed" Alloy 625 Fracture Surface for -1.0 Volt Test Condition Specimen 83

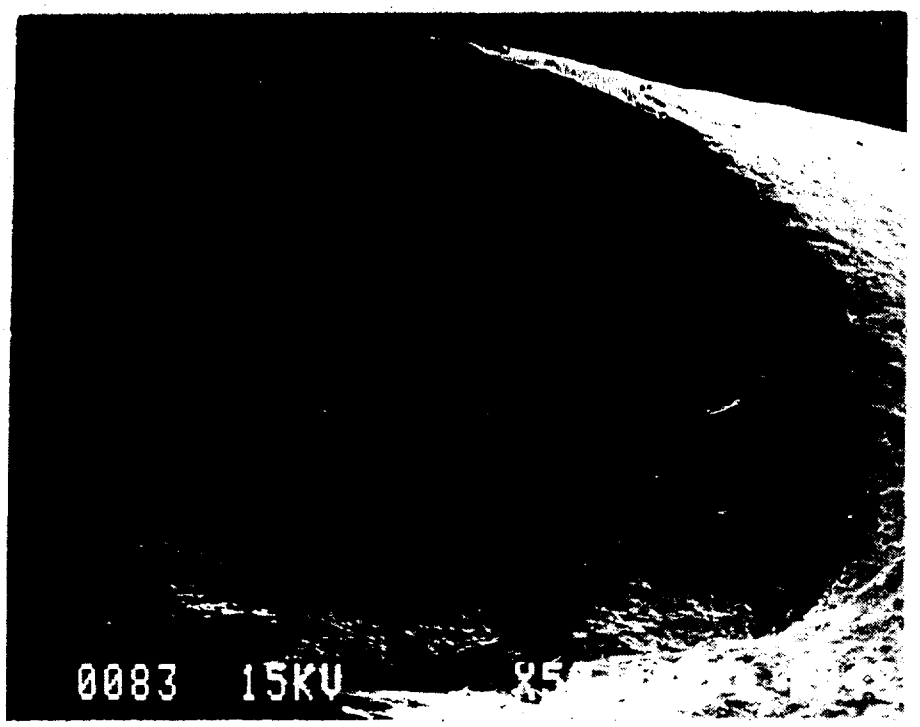

Figure 34 Photomicrographs of "Forged/Annealed" Alloy 625 Fracture Surface for -2.0 Volts Test Condition Specimen 87

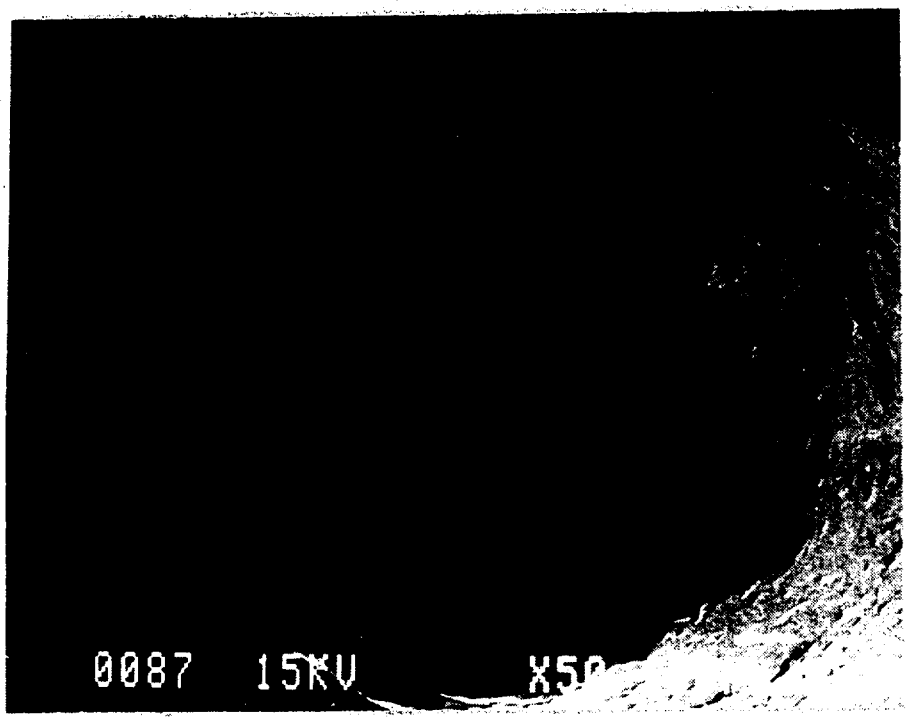

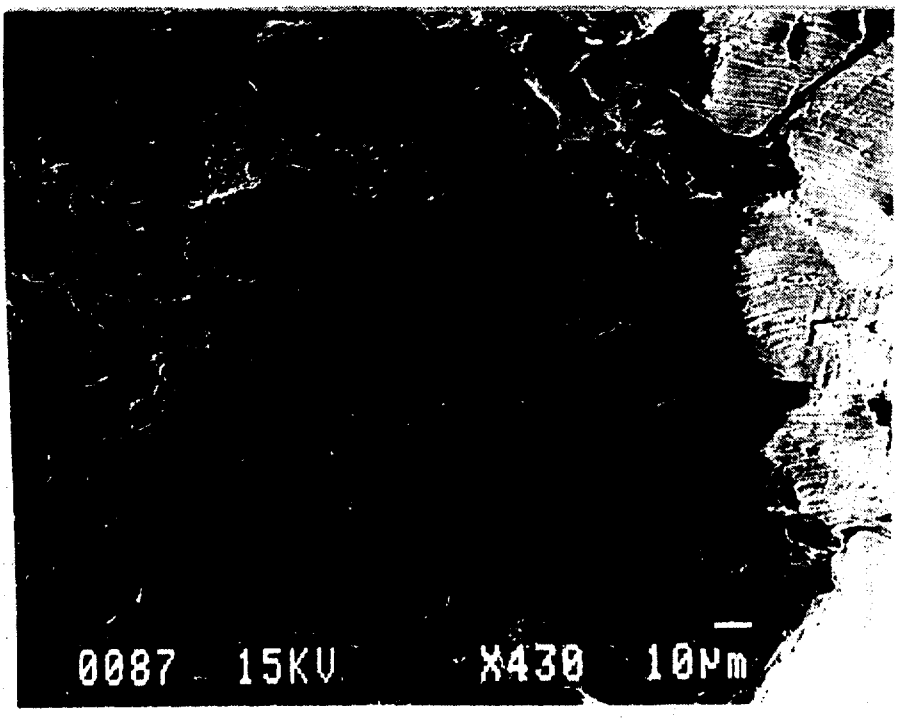

Figure 35 Photomicrographs of "Forged/Annealed" Alloy 625 Fracture Surface for -3.0 Volts Test Condition Specimen 85

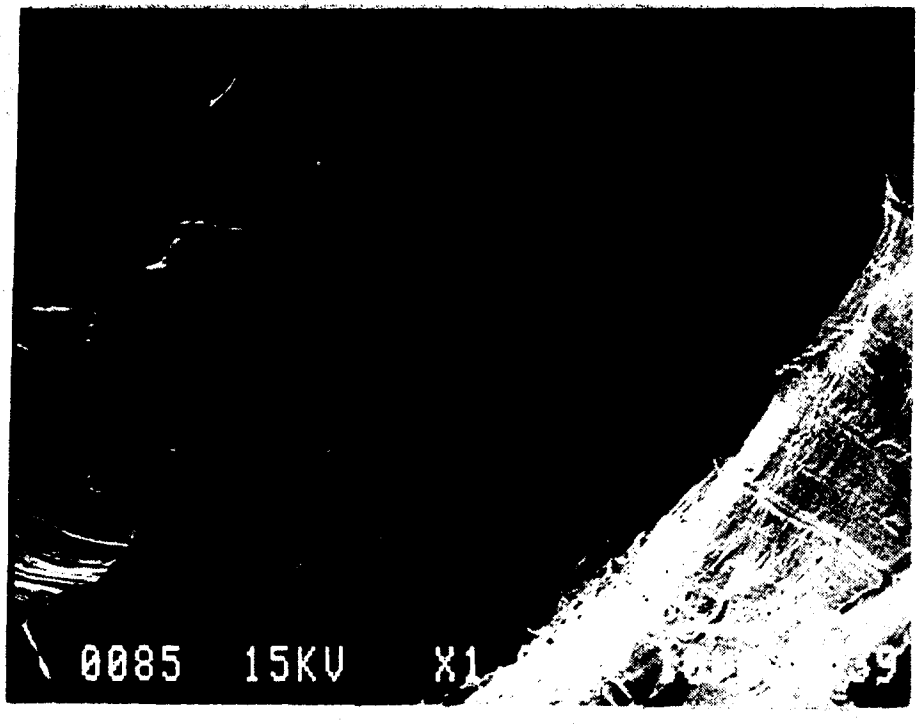

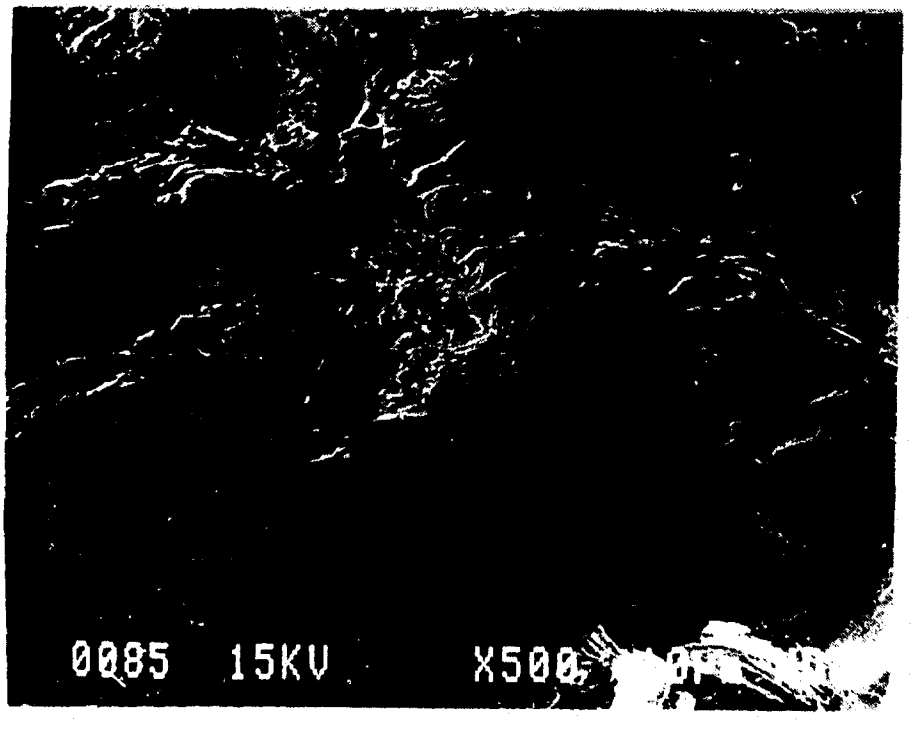

Figure 36 Photomicrographs of "Forged/Annealed" Alloy 625 Fracture Surface for -3.0 Volts Test Condition Specimen 85

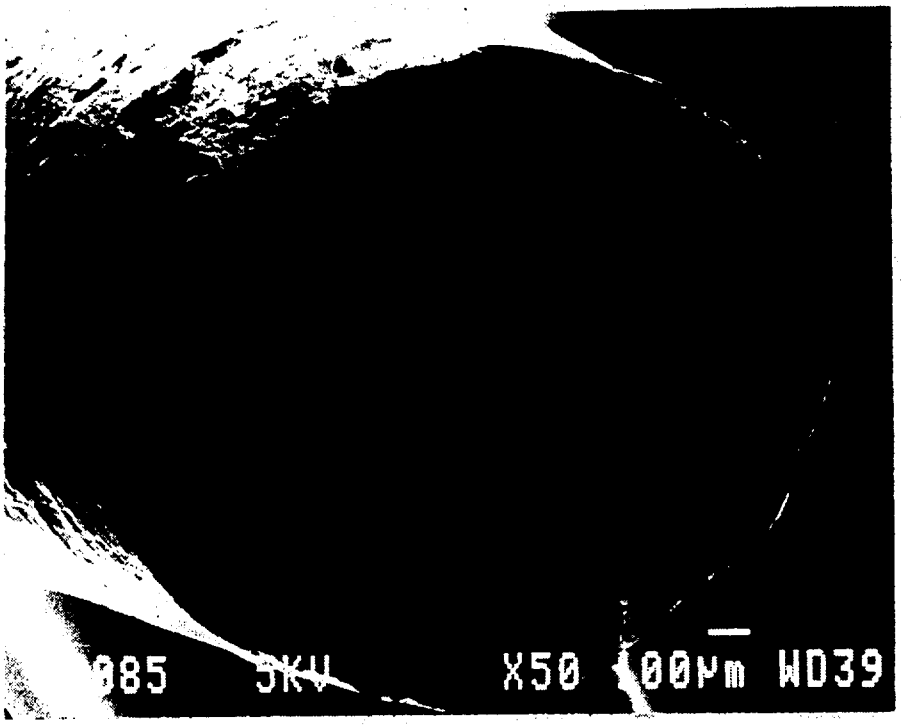

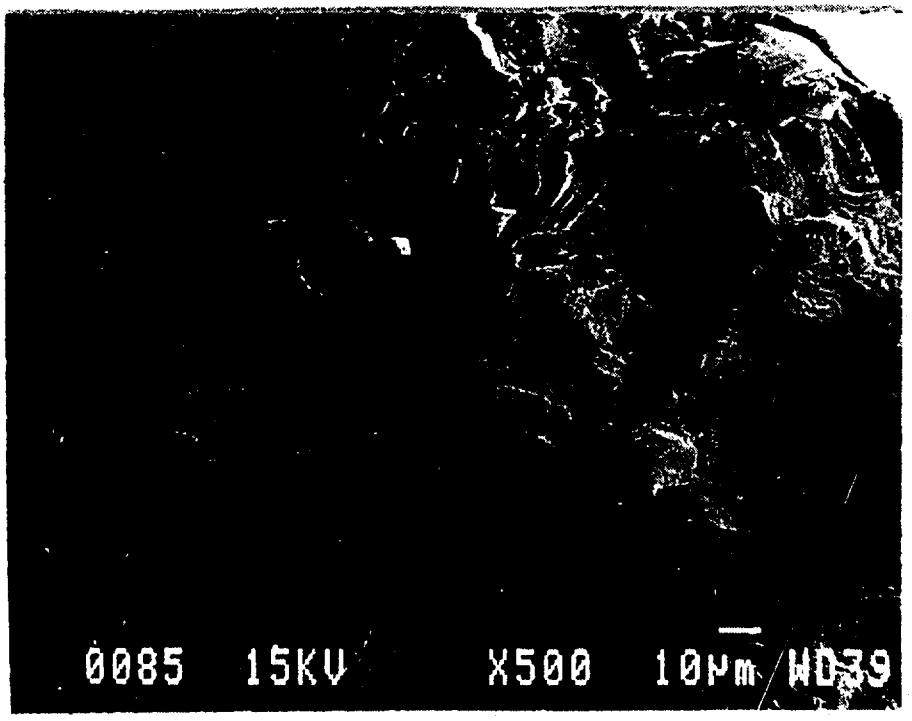

Figure 37 Photomicrographs of "As Cast" Alloy 625 Sectioned Gage Lengths for Air, -1.0, and -3.0 Volts Test Conditions - Specimens 4, 8, and 9 Top, Middle, and Bottom respectively

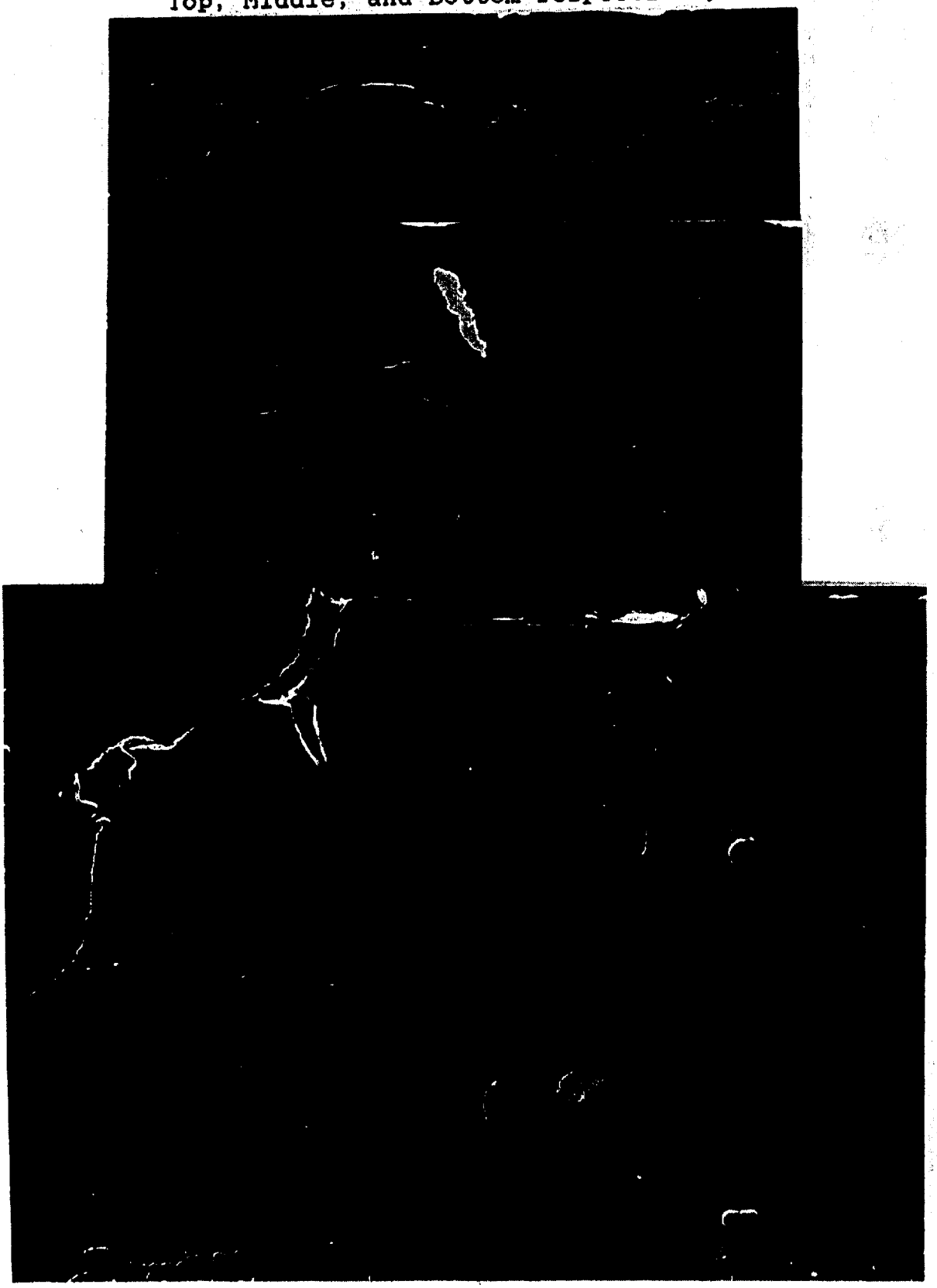

Figure 38 Photomicrographs of "Forged/Annealed" Alloy 625 Sectioned Gage Lengths for Air, -1.0 and -3.0 Volts Test Conditions - Specimens 76, 83, and 85 Top, Middle, and Bottom respectively, all at 500X

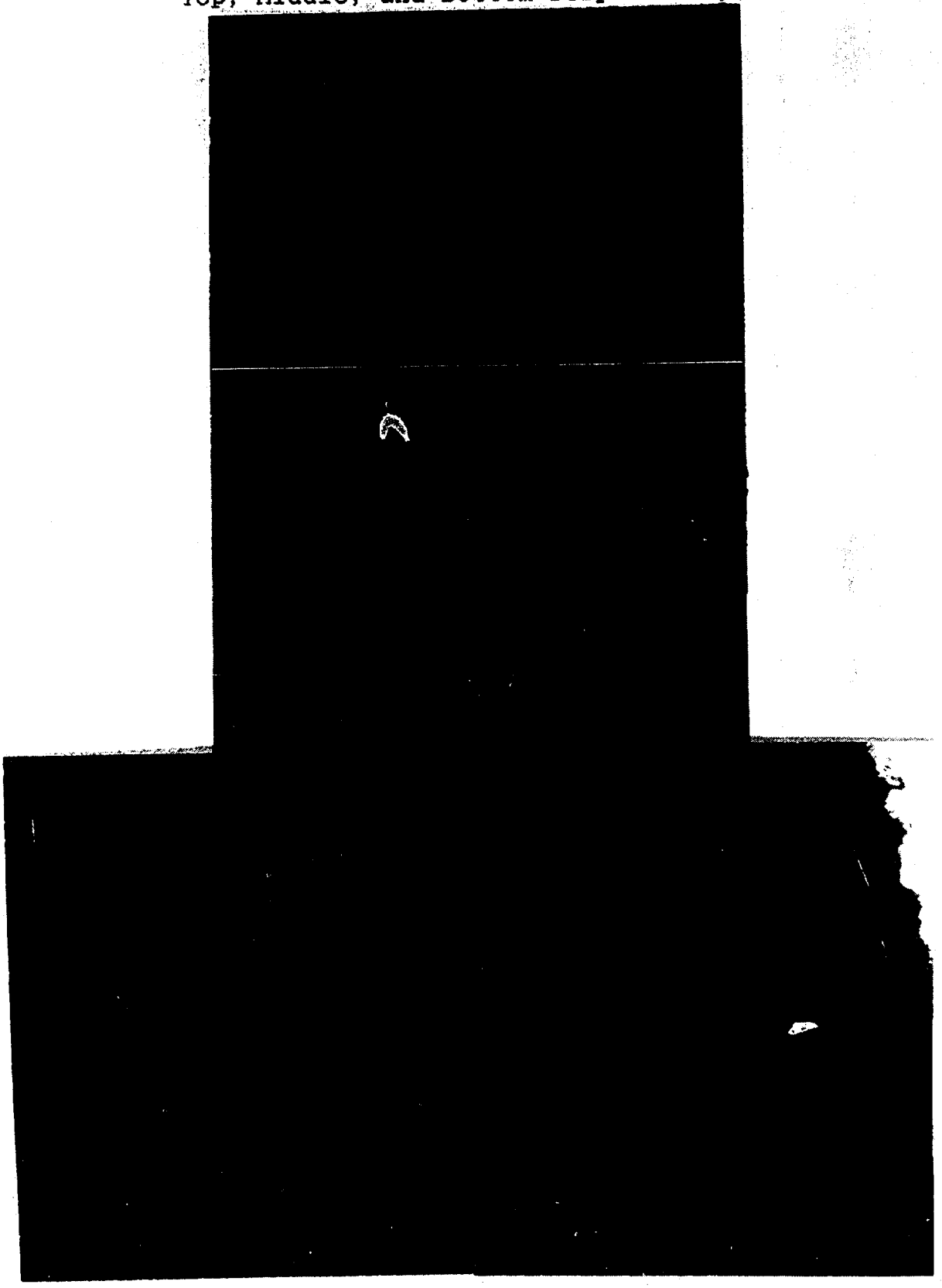

Figure 39 **Graph of Tensile and Slow Strain Rate Tests for "as cast" Alloy 625 - Test Type versus Yield Stress, Ultimate Stress, and Percent Elongation**

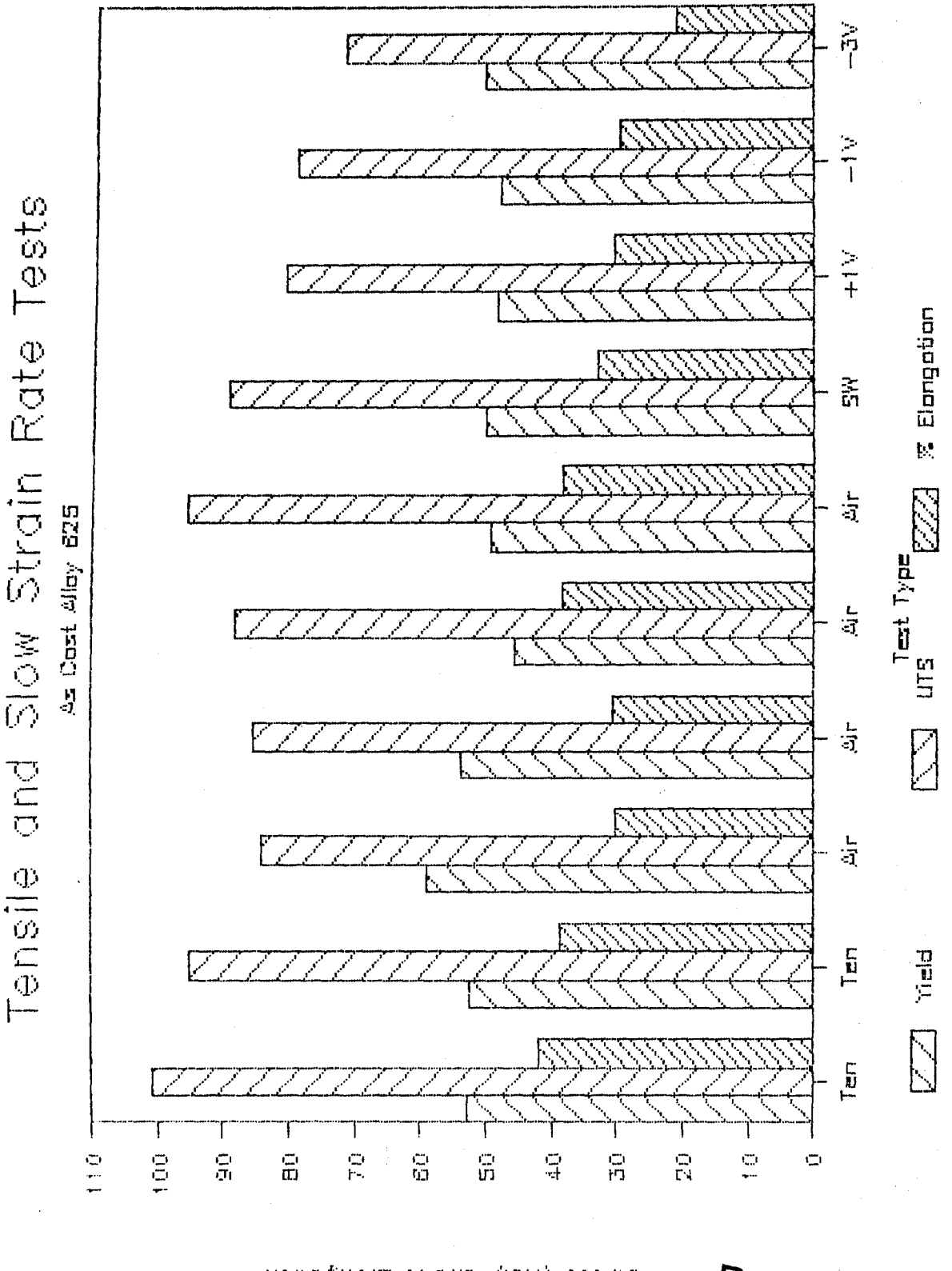

Figure 40 Graph of Tensile and Slow Strain Rate Tests for "Cast/Homogenized" Alloy 625 - Test Type versus Yield Stress, Ultimate Stress, and Percent Elongation

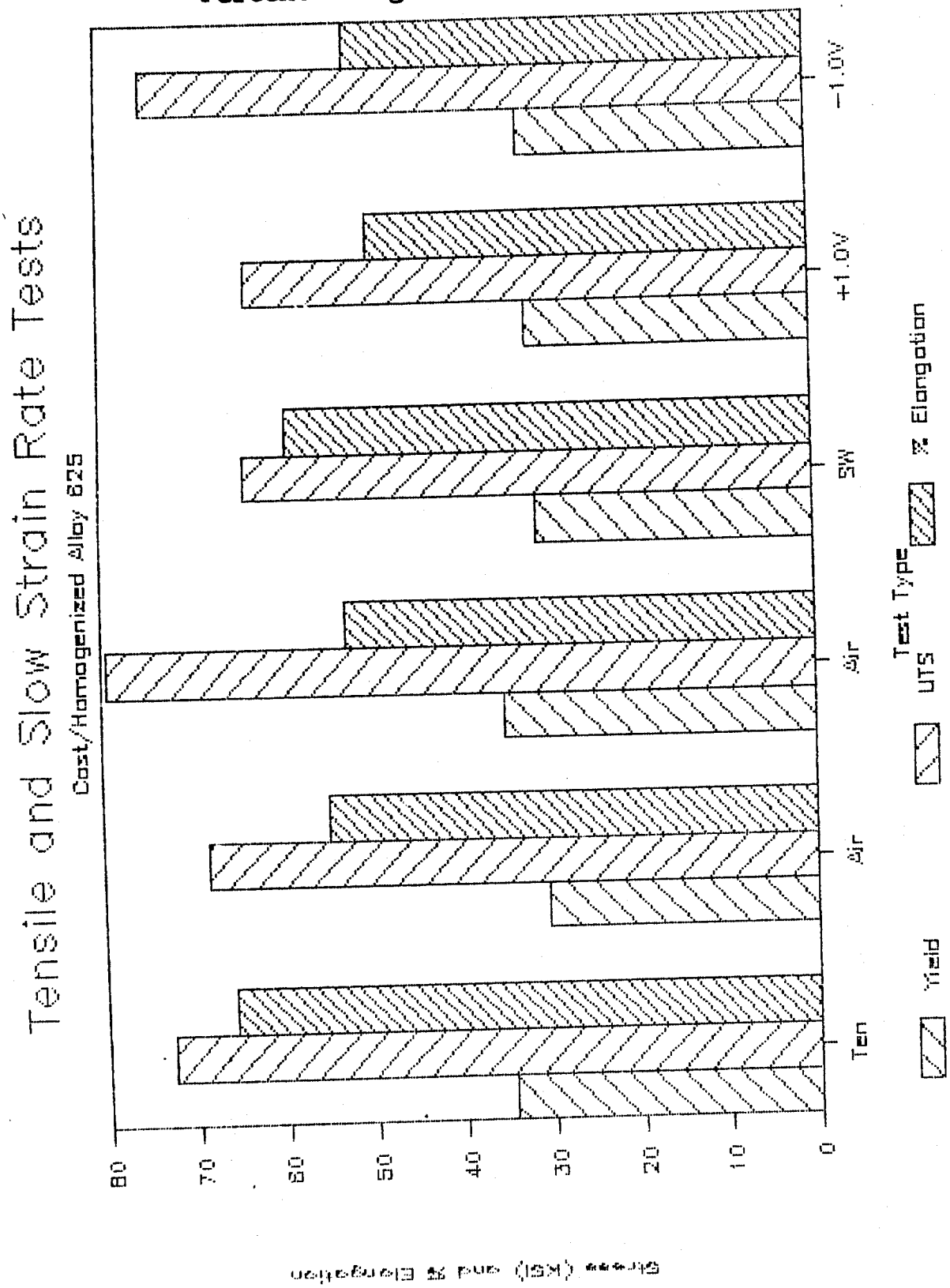

Figure 41 Graph of Tensile and Slow Strain Rate Tests for "Forged/Annealed" Alloy 625 - Test Type versus Yield Stress, Ultimate Stress, and Percent Elongation

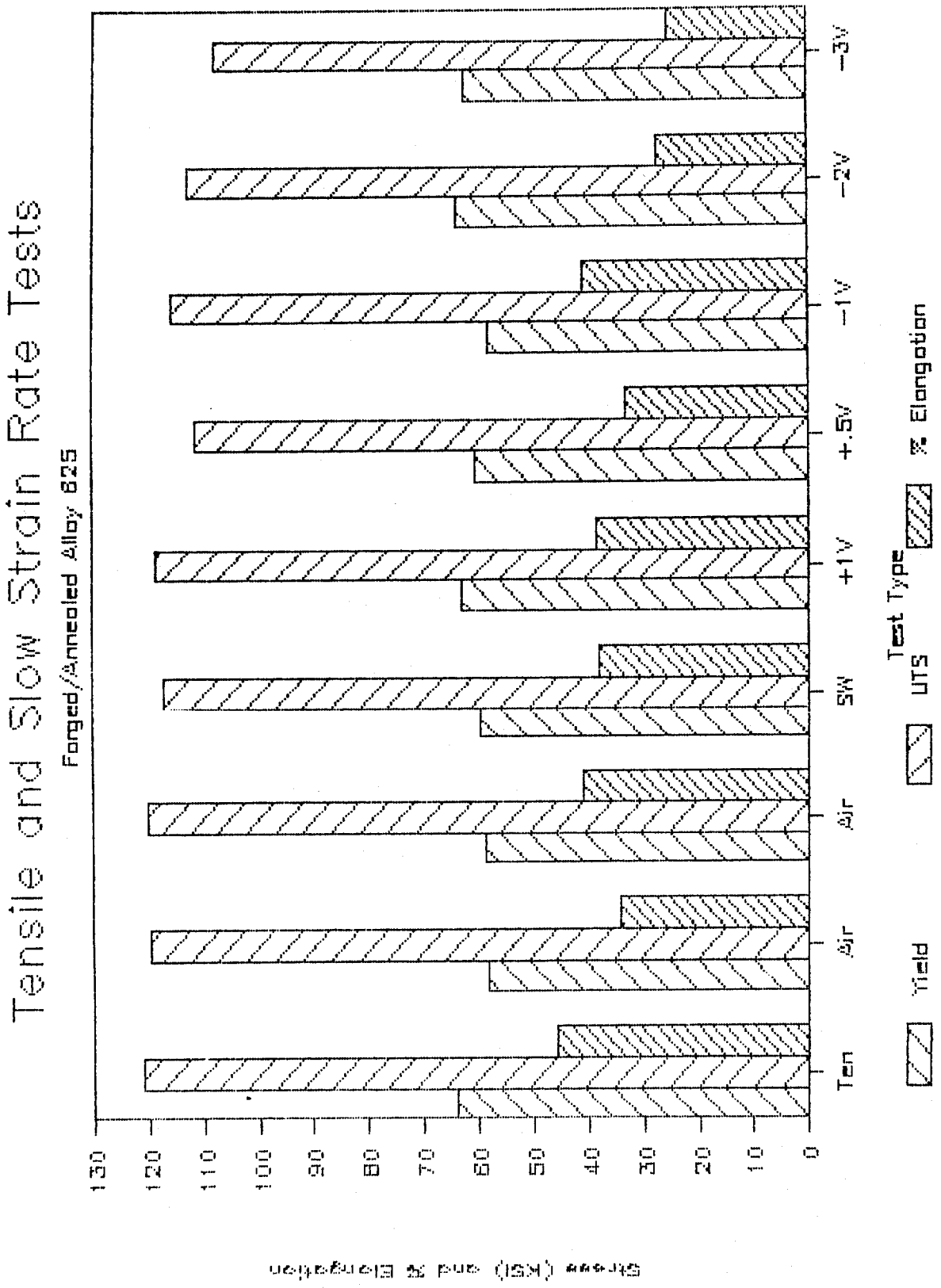

Figure 42 Graph of Tensile and Slow Strain Rate Tests for "Forged/Heat Treated" Alloy 625 - Test Type versus Yield Stress, Ultimate Stress, and Percent Elongation

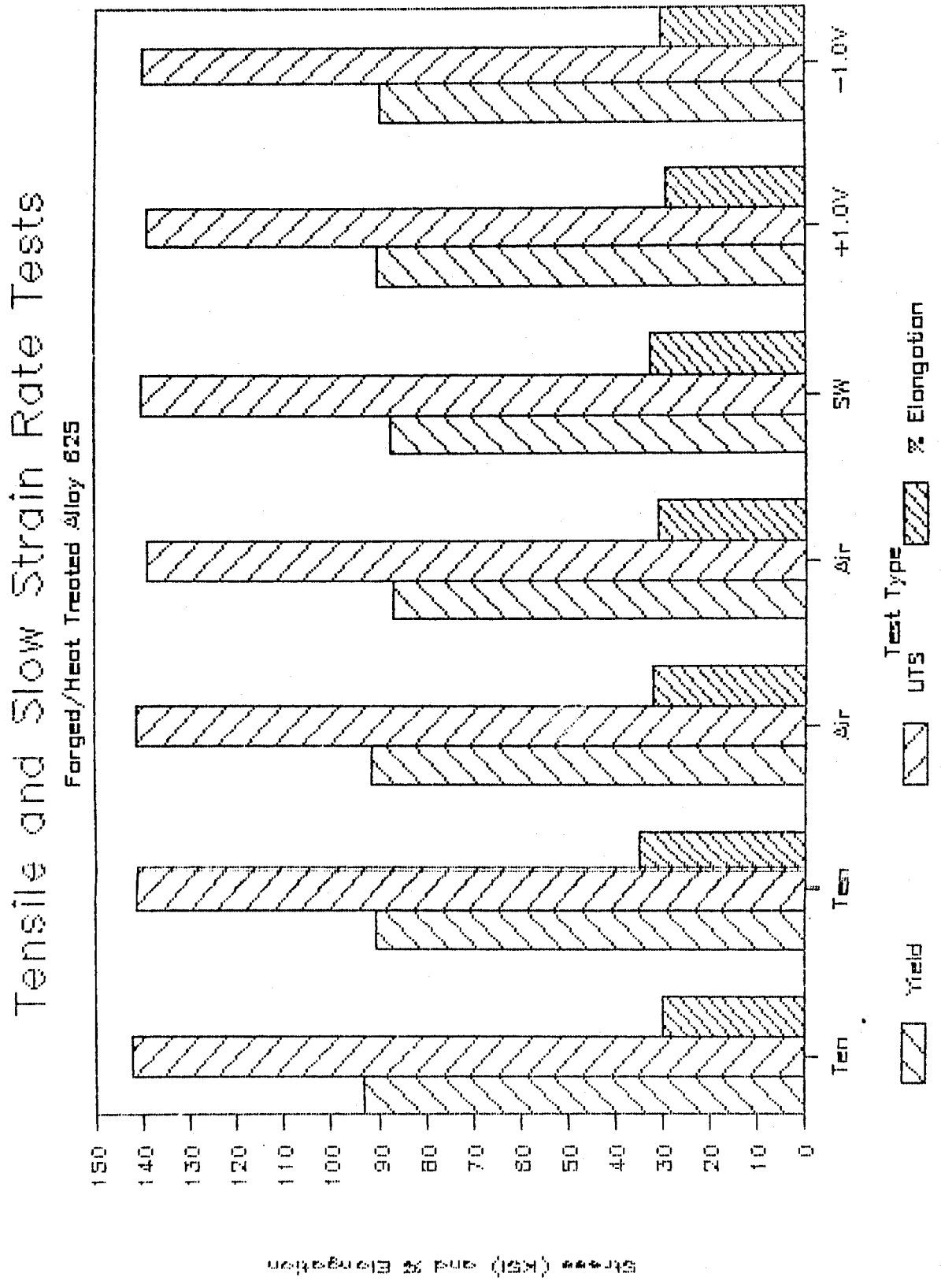

9. DISCUSSION OF RESULTS

The four microstructures that were tested had consistent behavior under all conditions except at cathodic potentials where hydrogen was produced. The deviations in the test results for this latter condition were a reduction in elongation and a reduction in yield work energy. These two effects indicate how far a material will stretch under load and how much energy is needed to cause this stretching.

Examination of the load-displacement curves explains why the UTS levels did not significantly drop along with the other two indicators above. This was due to the extreme elongation of Alloy 625 and the low slope of the load-displacement curve in the work hardening range. Loss of 40 percent of the top end of the curve is only a few percent decrease in UTS.

Fracture load percentage of UTS is an important consideration since it portrays the behavior of the material in the post UTS range. It indicates whether the alloy can hold itself together while necking or planer slippage is occurring, or whether it fractures immediately. These tests were run at a continuous, constant displacement of the tension machine crosshead. Therefore, a low fracture load does not mean the material did not hold together after UTS, but rather it did hold together, even if most of the cross section was fractured. The photomicrographs of the fracture surfaces indicate there was no percent reduction of area that matched the percent drop that occurred from UTS load to

fracture load. Thus, cross sectional fracture was on going while some parts of the cross section still clung together.

Actual reduction of area measurements were not taken due to; the degree of non-uniformity in the cross section at the fractures (see Figures 31 through 34), the angle many of the fractures were to the direction of elongation, and the consistency of other similar research tests in the literature where elongation and reduction of area react together.

The slow strain rate tests were conducted at a strain rate that should have shown susceptibility to anodic stress corrosion under the environmental conditions tested. However, none of the indicators showed any variations that would support susceptibility.

The -1.0 volt cathodic tests produced a higher percentage of surface cracks, but still did not give any indication of damaging susceptibility through the normal parameters. This potential is on the edge of what is possible to achieve in a sea water system through bimetallic couplings. Possibly there actually is a susceptibility at this potential from low hydrogen levels, but the slow strain rate test may not allow enough time for hydrogen to build up to a high enough level to be damaging. Another possibility is that the hydrogen may react with some of constituents in the alloy leaving cumulative permanent damage in the form of hydrides.

The -2.0 and -3.0 volt tests distinctively show that Alloy 625 is susceptible to hydrogen embrittlement by the decrease in elongation and yield work energy and the formation of intergranular cracks where there are no large carbides to act as nucleation sites. The SEM work on the fracture surfaces and sectioned specimens verified this. Whether a shipboard system can produce the same level of hydrogen remains to be seen.

The number and size of carbides both intergranular and as inclusions in the matrix were very large. These carbides can also be formed with nitrogen, i.e. [Cb,Mo][N] nitrides. Carbides are beneficial to high temperature service applications. When Alloy 625 is to be used in sea water applications the carbon content should be reduced and nitrogen exposure controlled during processing.

10. CONCLUSIONS

The following conclusions have been made as a result of the above experimental research and associated literature research.

1. Based on the conditions under which the testing was conducted, Alloy 625 does not appear susceptible to stress corrosion cracking in the normal sea water system environment.

2. Alloy 625 is susceptible to hydrogen embrittlement when subjected to conditions that cause hydrogen evolution while the surface of the metal is in a tensile state of stress. This is also called hydrogen induced stress corrosion cracking or hydrogen cracking.

3. The slow strain rate tensile test is a good test for the rapid evaluation of the effects of different environments and the stress corrosion cracking susceptibility of an alloy. The main limitation of the test is that it does not give quantitative results. Passivation and penetration (or diffusivity) as functions of time are overridden enabling a fast response to the subjected conditions.

4. The small gage diameter used for these slow strain rate tests caused undesirable data scatter for the cast material tests. This was due to the grain size in the "as cast" samples being on the same order as the gage diameter, and even larger in the "cast/homogenized" samples.

5. The microstructure of Alloy 625 material that will be used to meet mechanical design requirements must be known

and carefully controlled throughout the processing history of the alloy.

6. The carbon content of Alloy 625 should be carefully controlled for applications other than high temperature structures. It will be important to reduce the carbon content to minimize the number of fracture sites at MC carbides, (Cb,Mo)(C,N). Processing history should also be monitored to refine the carbide distribution.

11. FUTURE WORK

The preceding testing program left many questions unanswered. The matrix of tests conducted was not inclusive of what could and should be learned about Alloy 625. It is recommended that the following be investigated:

a. Does heat treating the cast and forged material cause the same reaction to hydrogen as was found in the other phases?

b. How does the degree of hydrogen assisted cracking vary with strain rate in this alloy?

c. How does passivity vary with strain rate? This may affect the hydrogen diffusivity during testing.

d. What is the loss of metal rate in sea water at +1.0 volts anodic potential? The above testing showed thick general surface corrosion, but this was aggravated by the constant elongation of the specimen cracking the film.

e. Does the chlorine driven from the sea water have any contribution to the observed cracking found at cathodic potentials? Slow strain rate testing should be conducted in a hydrogen environment that is free of chlorine.

f. Does the hydrogen react/interact with the materials in the alloy to form hydrides that cause permanent damage, or will the hydrogen diffuse back out?

g. Sea water service will result in environments that are somewhat warmer, up to around the 130°F range, and could have a brine density 50 percent higher than what these tests were conducted at. Slow strain rate testing should also be accomplished under these conditions.

12. REFERENCES

1. INCONEL alloy 625, Huntington Alloys, Inc., Huntington, West Virginia, 1978.

2. Sims, C. T., Hagel, W. C., The Superalloys, John Wiley and Sons, New York, New York, 1972.

3. Tapping, R. L., "Surface Studies of Austenitic Alloys Subjected to Crevice Corrosion in Sea Water", Corrosion Science, Vol 25, No. 6 PP. 363-376, Pergamon Press, New York, New York, 1985.

4. Masubuchi, K., Analysis of Welded Structures, Pergamon Press, New York, New York, 1980.

5. Fontana, M. G., Greene, N. D., Corrosion Engineering, McGraw-Hill, New York, New York, 1978.

6. Latanision, R> M>, Gastine, O. H., Compeau, C. R., "Stress Corrosion Cracking and Hydrogen Embrittlement: Differences and Similarities", Environment-Sensitive Fracture of Engineering Materials, Foroulis, Z. A., ed., TMS-AIME, Chicago, Illinois, 1977.

7. Thompson, A. W., Bernstein, I. M., "The Influence of Hydrogen on Plastic Fracture Processes", Second International Congress on Hydrogen in Metals, Paris, France, 1977.

8. Hayes, S. C., Heat Treatment Parameters for the Aging of Alloy 625, Knolls Atomic Power Laboratory, Schenectady, New York, 1981.

9. Wilhelm, S. M., Results of Slow Strain Rate Testing of Inconel 625, Cortest, Cypess, Texas, 1986.

The following references were used/reviewed during the literature search and throughout this research program. In alphabetical order by author:

10. ASM, Metals Handbook, Ninth Edition, Vol 10, American Society for Metals, 1986.

11. ASM, Metals Reference Book, American Society for Metals, 1981.

12. Bieber, B. L., Lake,B. L., Smith, D. F., "A Hot-Work-Hardening Coefficient for Nickel-Base Alloys", Metals Engineering Quarterly, May, 1976.

13. Bohm, H., Ehrlich, N. K., Kramer, K. H., "Das Ausscheidungsverhalten der Nickellegierung Inconel 625", Metall 24, Jan-Feb, 1970.

14. Bodner, S. R., Plasticity, Lecture Note, Sep. 1985.

15. Boyd, W. K., Berry, W. E., "Stress Corrosion Cracking Behavior of Nickel and Nickel Alloys", Stress Corrosion Cracking of Metals - A State of the Art, ASTM STP 518, American Society For Testing and Materials, pp. 58-78, 1972.

16. Bond, B. J., Inconel 625: Evaluation of Large ESR Ingot Conversion, Wyman Gordon, North Grafton, Massachusetts, 1985.

17. Bond, B. J., Inconel 625: VAR Ingot Conversion, Wyman Gordon, North Grafton, Massachusetts, 1985.

18. Brown, M. H., Kirchner, R. W., "Sensitization of Wrought High Nickel Alloys", Corrosion NACE,pp. 470-473, Feb. 1973.

19. Byner, T. G., Forging Handbook, Forging Industry Association, American Society for Metals, 1985.

20. Carter, J. P., McCawley, F. X., "Corrosion Tests in Brine and Steam from the Salton Sea KGRA", Journal of Materials for Energy Systems, Vol. 3, No. 4, Mar. 1982.

21. Carter, J. P., McCawley, F. X., "In Situ Corrosion Tests in Salton Sea Geothermal Brine Environments", Journal of Metals, pp. 10-15, Mar. 1978.

22. Conaway, H. R., Mesick, J. H., "A Report on New Matrix-Stiffened Nickel-Chromium Welding Products", Welding Journal, Jan. 1970.

23. Davis, J. A., Gehring, G. A., "Corrosion Behavior Variations with Time and Velocity in Sea Water", Corrosion 75, The International Corrosion Form, Apr. 1975.

24. Davis, R. V. V., "Inconel Alloy 625 Weld Overlaying for Corrosion Resistance", U.K. National Corrosion Conference, London, Nov. 1982.

25. Deel, O. L., Mindlin, H., Engineering Data on New Aerospace Structural Materials, Battelle Columbus Laboratories, Dec. 1971.

26. Delaney, G. L., Lemke, T. F., "Corrosion Resistance of Nickel Alloys in Aqueous Environments", Corrosion Australasia, Vol. 6, Iss. 3, pp. 4-6, 1981.

27. Eddy, N. S., Evaluation of ESR - Melted Alloy 625 Forged in WG 15858 Dies, Wyman Gordon, North Grafton, Massachusetts, 1986.

28. Eddy, N. S., Evaluation of VAR - Melted Alloy 625 Forged in WG 15858 Dies, Wyman Gordon, North Grafton, Massachusetts, 1986.

29. Hammand, J. P., Patriarca, P., Slaughter, G. M., Maxwell, W. A., "Comparative Results on Chloride Stress Corrosion Cracking of Steam Generators in Cyclic Steam Environments", Materials Performance, pp. 41-52, Nov. 1975.

30. Hammond, J. P., Ductility Minimum and its Reversal with Prolonged Aging in Cobalt- and Nickel-Base Superalloys, Oak Ridge National Laboratory, 1978.

31. Hammond, . P., Effects of Long-Term Aging at 815°C on the Tensile Properties and Microstructural Stability of Four Cobalt- and Nickel-Based Superalloys, Oak Ridge National Laboratory, 1976.

32. Harris, J. A., "Effect of Metallurgical Reactions in Inconel Nickel-Chromium-Molybdenum Alloy 625 on Corrosion Resistance in Nitric Acid", Journal of Metals, Sep. 1971.

33. Hasson, D. F., Zanis, C., Aprigliano, L., Fraser, C., "Corrosion and Corrosion-Fatigue Behavior of IN625 Weld Surface 3.25 Nickel Steel", Journal of Materials for Energy Systems, Vol. 7, No. 3, Dec. 1985.

34. Hasson, D. F., Zanis, C., Aprigliano, L., Fraser, C., "Surfacing of 3.25% Nickel Steel with Inconel 625 by the Gas Arc Welding-Pulsed Arc Process", Welding Journal Research Supplement, Jan. 1978.

35. Hayes, R. W., Age Hardening of Inconel 625 Alloy After Prior Hot and Cold Work, Metals Technology Inc., 1981.

36. Hayes, S. C., Heat Treatment Parameters for the Aging of Alloy 625, Knolls Atomic Power Laboratory, Schenectady, New York, 1981.

37. Heady, R. B., "Evaluation of Sulfide Corrosion Cracking Resistance in Low Alloy Steels", Corrosion NACE, Apr. 1975.

38. Hertzberg, R. W., Deformation and Fracture Mechanics of Engineering Materials, John Wiley and Sons, New York, New York, 1976.

39. Jones, R. H., Grain Boundary Segregation and Environmentally-Induced Fracture of Materials, Pacific Northwest Laboratory, Richland, Washington, 1985.

40. Kain, R. M., "Crevice Corrosion Resistance of Several Iron and Nickel Base Cast Alloys in Sea Water", Corrosion 82, 1982.

41. Kain, R. M., Lee, T. S., Oldfield, J. W., "Use of Electrochemical Techniques for the Study of Crevice Corrosion in Natural Sea Water", Corrosion 85, 1985.

42. Kane, R. D., Corrosion of Stainless Alloys in Oilfield Production Environments, Cortest Laboratories.

43. Kane, R. D., Watkins, M., Jacobs, D. F., Hancock, G. L., "Factors Influencing the Embrittlement of Cold Worked High Alloy Materials in H_2S Environments", Corrosion NACE, Vol.33, No.9, Sep. 1977.

44. Kehl, G. L., Metallographic Laboratory Practice, McGraw-Hill, New York, New York, 1949.

45. Kohl, H. K., Peng, K., "Thermal Stability of the Superalloys Inconel 625 and Nimonic 86", Journal of Nuclear Materials, 101, pp. 243-250, 1981.

46. Jorden, D. E., Richards, E. G., Heat Treatment Aspects of Welded Nickel-Based Superalloys, International Nickel Ltd., 1972.

47. Lemke, T. F., Harris, J. A., High-Alloy Materials for Offshore Applications, Huntington Alloys Inc., 1983.

48. Loutham, M. R., Cashey, G. R., Donovan, J. A., Rawl, D. E., "Hydrogen Embrittlement of Metals", Material Science and Engineering, Jun. 1982.

49. MacGregor, C. W., "Mechanical Properties of Materials", Handbook of Experimental Stress Analysis, Hetenyi, M., ed., John Wiley and Sons, New York, New York, 1950.

50. Maylor, "Corrosion Resistance of High Nickel Alloys in Sea Water", AntiCorrosion Methods Material, Vol. 25, Iss. 7, pp. 3-9, Jul. 1978.

51. Meyers, M. A., Chawla, K. K., Mechanical Metallurgy Principles and Application, Prentice-Hall, Englewood Cliffs, New Jersey, 1984.

52. Nassif, N., "Influence of Impurities in Phosphoric Acid on the Corrosion Resistance of Some Commercially Produced Alloys", Surface Technology, 26, pp. 189-198, 1985.

53. Pourbaix, M., "Corrosion", Atlas of Electrochemical Equilibra in Aqueous Solution.

54. Price, C. E., Traylor, L. B., "A Comparison of Microvoid Sizes in Nickel Base Alloys Tested in Air and in the Presence of Hydrogen", Scripta Metallurgica, Vol. 17, pp. 901-904, 1983.

55. Purohit, A., Thiele, U., O'Donnell, J. E., Fatigue Strength and Evaluation of Creep Damage During Fatigue Cycling of Inconel Alloy 625, Argonne National Laboratory, Argonne, Illinois, 1983.
56. Sparks, R. B.,Heat Treatment of INCO 625, Wyman Gordon, North Grafton, Massachusetts, 1985.

57. Sundararaman, M., Mukhopadhyay, P., "Heterogeneous Precipitation of the Gamma Double Prime Phase in Inconel 625", Materials Science Forum, Vol. 3, pp. 273-280, 1985.

58. Theus, G. J., Staehle, R. W., "Review of Stress Corrosion /cracking and Hydrogen Embrittlement in the Austenitic Fe-Cr-Ni Alloys", Conference- Stress Corrosion Cracking and Hydrogen Embrittlement of Iron Base Alloys, Unieux-Firminy, France, pp. 845-892, 1977.

59. Tjong, S. C., "Localized Corrosion Behavior of Ni-Base Superalloys", Metals Forum, Vol. 7 No. 4, pp. 251-253, 1984.

60. Ugiansky, G. M., Stress Corrosion Cracking--The Slow Strain-Rate Technique, ASTM STP 665, Philadelphia, Pennsylvania, 1979.

61. Vonk, S. J., Characterization and Processing of Large Diameter U-625 Material, Special Metals Corp., Utica, New York, 1984.